NUREG/CR-5430
Vol. 1

FLAC (Fast Lagrangian Analysis of Continua) Version 2.20

Software Summary

Prepared by Mark Board

Itasca Consulting Group, Inc.

Prepared for
U.S. Nuclear Regulatory Commission

8911080378 891031
PDR NUREG
CR5430 R PDR

AVAILABILITY NOTICE

Availability of Reference Materials Cited in NRC Publications

Most documents cited in NRC publications will be available from one of the following sources:

1. The NRC Public Document Room, 2120 L Street, NW, Lower Level, Washington, DC 20555

2. The Superintendent of Documents, U.S. Government Printing Office, P.O. Box 37082, Washington, DC 20013-7082

3. The National Technical Information Service, Springfield, VA 22161

Although the listing that follows represents the majority of documents cited in NRC publications, it is not intended to be exhaustive.

Referenced documents available for inspection and copying for a fee from the NRC Public Document Room include NRC correspondence and internal NRC memoranda; NRC Office of Inspection and Enforcement bulletins, circulars, information notices, inspection and investigation notices; Licensee Event Reports; vendor reports and correspondence; Commission papers; and applicant and licensee documents and correspondence.

The following documents in the NUREG series are available for purchase from the GPO Sales Program: formal NRC staff and contractor reports, NRC-sponsored conference proceedings, and NRC booklets and brochures. Also available are Regulatory Guides, NRC regulations in the *Code of Federal Regulations*, and *Nuclear Regulatory Commission Issuances*.

Documents available from the National Technical Information Service include NUREG series reports and technical reports prepared by other federal agencies and reports prepared by the Atomic Energy Commission, forerunner agency to the Nuclear Regulatory Commission.

Documents available from public and special technical libraries include all open literature items, such as books, journal and periodical articles, and transactions. *Federal Register* notices, federal and state legislation, and congressional reports can usually be obtained from these libraries.

Documents such as theses, dissertations, foreign reports and translations, and non-NRC conference proceedings are available for purchase from the organization sponsoring the publication cited.

Single copies of NRC draft reports are available free, to the extent of supply, upon written request to the Office of Information Resources Management, Distribution Section, U.S. Nuclear Regulatory Commission, Washington, DC 20555.

Copies of industry codes and standards used in a substantive manner in the NRC regulatory process are maintained at the NRC Library, 7920 Norfolk Avenue, Bethesda, Maryland, and are available there for reference use by the public. Codes and standards are usually copyrighted and may be purchased from the originating organization or, if they are American National Standards, from the American National Standards Institute, 1430 Broadway, New York, NY 10018.

DISCLAIMER NOTICE

This report was prepared as an account of work sponsored by an agency of the United States Government. Neither the United States Government nor any agency thereof, or any of their employees, makes any warranty, expressed or implied, or assumes any legal liability of responsibility for any third party's use, or the results of such use, of any information, apparatus, product or process disclosed in this report, or represents that its use by such third party would not infringe privately owned rights.

NUREG/CR-5430
Vol. 1

FLAC (Fast Lagrangian Analysis of Continua) Version 2.20

Software Summary

Manuscript Completed: September 1989
Date Published: October 1989

Prepared by
Mark Board

Itasca Consulting Group, Inc.
1313 5th Street SE, Suite 210
Minneapolis, MN 55414

Prepared for
Division of High-Level Waste Management
Office of Nuclear Material Safety and Safeguards
U.S. Nuclear Regulatory Commission
Washington, DC 20555
NRC FIN D1016

ABSTRACT

FLAC (Fast Lagrangian Analysis of Continua), Version 2.20, is a two-dimensional, large-strain, explicit finite difference code written for analysis of problems in geotechnical engineering. FLAC has the ability to perform static mechanical analyses as well as transient heat transfer and fluid flow simulations. Various constitutive models are available to describe linear and non-linear response of the solid. Coupling can be performed between the thermal and mechanical, as well as the fluid and mechanical, models. The following report presents the documentation specified in NUREG-0856, Documentation of Computer Codes for High Level Waste Management. The documentation is presented in three volumes. Volume 1 contains the mathematical basis for the various aspects of the code; Volume 2 is the code User's Manual, and Volume 3 presents FLAC verification, example and benchmark problems.

TABLE OF CONTENTS

VOLUME 1

SOFTWARE SUMMARY

TABLE OF CONTENTS

TABLE OF CONTENTS
(continued)

TABLE OF CONTENTS
(continued)

TABLE OF CONTENTS
(continued)

TABLE OF CONTENTS
(continued)

TABLE OF CONTENTS
(continued)

TABLE OF CONTENTS
(continued)

TABLE OF CONTENTS
(continued)

LIST OF FIGURES

LIST OF FIGURES
(continued)

LIST OF FIGURES
(continued)

LIST OF FIGURES
(continued)

LIST OF TABLES

1.1 STATEMENT AND DESCRIPTION OF THE PROBLEM

The analysis of problems in geomechanics may involve a number of physical phenomena including mechanical, thermal and hydraulic response of the rock and/or soil. The response may be characterized by non-linear constitutive behavior which exhibits coupling effects between the mechanical, thermal and hydrologic mechanisms. FLAC, Version 2.20, is a large strain, two-dimensional explicit finite different program written specifically to analyze complex, quasi-static and transient non-linear problems in geomechanics. In particular, many of the functions of the program have been written to simplify analysis of problems in soil mechanics, rock mechanics, underground excavation design and assessment of radioactive waste disposal in a variety of rock types. The program logic is not specific to geomechanics, however, and may be used for general stress analysis, heat transfer or hydraulics problems.

The FLAC program contains a word-oriented command interpreter, error-trapping logic and extensive interactive graphics facilities. Although the code is generally distributed in an executable version for the IBM PC and compatibles, it is easily transportable to mini- and mainframe computer systems.

FLAC is a proprietary computer program written and owned by Itasca Consulting Group, Inc. and Peter Cundall. Access to the source code generally is not available, although it can be examined through special arrangement with Itasca Consulting Group, Inc.

Program Capabilities, Version 2.20

FLAC is a finite difference program which uses an explicit solution procedure to solve non-linear thermal, mechanical and hydrologic problems in plane and axisymmetric geometries. The mechanical analysis is quasi-static, but the heat transfer and fluid flow can be transient. Thermomechanical and hydromechanical coupling is possible for all of the available material models. Other features of the program are given below.

1. Geometric Features

   (a) plane strain (can account for out-of-plane stress)
   (b) plane stress
   (c) axisymmetry

2. Motion Calculation

   (a) quasi-static (non-inertial) mechanical

   (b) transient heat transfer (Fourier's Law) and fluid flow (Darcy Flow)

3. Solution Mode/Kinematics

   (a) mechanical — explicit, large or small strain, large displacement

   (b) heat transfer — explicit or implicit

   (c) fluid flow — explicit

4. Constitutive Models

   (a) mechanical

      (i) linear elastic

      (ii) transversely isotropic elastic

      (iii) Mohr-Coulomb plasticity

      (iv) Mohr-Coulomb plasticity with general strain hardening/softening

      (v) ubiquitous joint

      (vi) viscoelastic models (steady-state creep)

         - Kelvin Law
         - WIPP Power Law
         - Norton One- or Two-Component Power Law

      (vii) null elements to represent excavation

(b) thermal

(i) isotropic conductivity
(ii) transversely isotropic conductivity
(iii) temperature-dependent conductivity
(iv) exponentially-decaying heat sources

(c) fluid flow

(i) isotropic Darcy Flow
(ii) transversely isotropic Darcy Flow

5. Boundary Conditions

(a) mechanical

(i) displacement (velocity)
(ii) force
(iii) pressure
(iv) stress (traction)

(b) thermal

(i) temperature
(ii) flux
(iii) adiabatic (insulated)
(iv) volumetric source

(c) fluid flow

(i) pore pressure
(ii) flux
(iii) volumetric flow rate

6. Initial Conditions

(a) initial stress
(b) initial temperature
(c) initial pore pressure distribution
(d) initial velocity

7. Rock/Soil Structure Interaction

   (a) structural elements (beams) to represent interior support systems, surface structures or point anchor rock bolts

   (b) cable elements to represent grouted rock bolts or cable anchors

8. Interfaces

   (a) cohesive frictional interfaces to allow slip/separation

   (b) intersecting interfaces allowed

9. Graphics

   (a) interactive screen graphics, allowing over 50 different types of plots which may be overlayed

   (b) color, intervals, scales, contour types, etc. are all user-controllable

   (c) hard-copy plots may be delivered to a variety of pen, dot matrix and laser printers

10. File Handling

   (a) interactive or batch mode operation
   (b) save and restart files
   (c) screen text diversion to disk file

11. Mesh Generation

   (a) automatic mesh generation

   (b) mesh may be distorted, expanded geometrically, etc.

   (c) automatic mesh adjustment to fit user-defined shapes, including circle, line, arc, and general table of x,y values

12. Other Features

(a) automatic error trapping and recovery (error messages without losing a run)

(b) automated problem solution specifications

(c) assignment of different properties and/or material model for every element possible

(d) assignment of gradients to any property, velocities, forces, stresses, pressures or initial conditions across the mesh

(e) access to DOS system functions

(f) ability to store and plot histories of any variable at any location within the grid

(g) English word-oriented command interpreter

(h) plasticity state history stored for all elements

(i) gravitational loading

(j) logic for tracing boundaries of grid, making application of boundary conditions simple for curved or irregular boundaries

FLAC provides automatic inertia scaling and damping to ensure a stable solution. The mixed discretization technique of Marti and Cundall (1982) is used to ensure numerical stability due to incompressibility in plastic flow and provide accurate solutions to collapse problems. The code itself is written in ANSI standard FORTRAN77. All higher-order graphics functions (i.e., contouring) used in the program are self-contained. Only the primitive graphics functions (pen up/down, text screen write, graphics device open and close) are system-dependent. These routine calls are located in a single file, making the code easily transportable to various computer systems.

Because FLAC is a commercially-supported code, continual development is performed by Itasca staff. Updates are issued approximately every year. The documentation given here refers specifically to Version 2.20 of the code.

1.2 EXPLICIT SOLUTION PROCEDURE

1.2.1 Introduction

The finite difference method is perhaps the oldest numerical technique used for the solution of initial or boundary value problems (see, for example, Desai and Christian, 1977). The variables describing the response of a body may vary in both space and time. To numerically solve such a problem, the body is discretized into a mesh consisting of a number of gridpoints (nodes) which define the corners of zones (elements). The governing equations (e.g., equations of motion, Fourier's Law or Darcy's Law) for a given system can be discretized into spatial and/or time coordinates and solved at the nodes subject to initial and boundary conditions. The governing equations for all nodes in a body give rise to a system of algebraic equations. Two basic options are possible for solving these equations. In an "implicit" approach, quantities at all nodes in the body are interrelated, resulting in a set of simultaneous equations which must be solved for the equilibrium or steady-state solution. In an "explicit" approach, quantities at the nodes are decoupled and, therefore, no system of equations is formed. In the former case, solutions are determined at specific times (e.g., at equilibrium for a static analysis, or at a specific time in a transient heat transfer analysis), whereas, for the explicit approach, the solution at a given node is always given in terms of the known conditions at the previous time. Since no system of equations is solved, it is not necessary to store coefficients, or to make use of equation solvers; however, a number of calculation cycles are necessary for solving for the equilibrium steady-state condition..

The general solution procedure employed by FLAC is shown in Fig. 1.2-1. This solution procedure involves solving the basic equation of motion (i.e., Newton's Second Law) for each gridpoint in the body. Application of the equation of motion provides velocities of the gridpoints which are used to calculate internal element strains. These strains are used through constitutive relations for the zone to provide element stresses, or equivalent gridpoint forces. These forces are the basic input necessary for the implementation of the equation of motion on the next calculation cycle. The procedure in Fig. 1.2-1 is performed once per "timestep" or, more appropriately, calculation cycle.

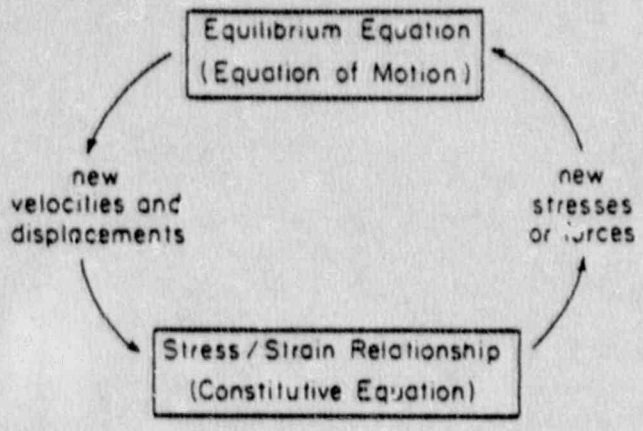

Fig. 1.2-1 Basic Explicit Calculation Cycle

Although FLAC solves the dynamic motion equation, the mechanical solution is limited to equilibrium or steady conditions only through the use of damping to extract vibrational energy from the system. The "timestep" referred to above is therefore used only as a means of arriving at the mechanical steady state. This procedure is valid only if adjacent zones are physically unable to communicate during a calculation cycle. This condition is satisfied if the solution time increment (timestep) is small enough that information cannot pass between neighboring elements even if it travels at the highest possible speed. For mechanical problems, the physical information transfer between zones occurs at the speed of propagation of confined elastic compression waves. For heat transfer, the speed of propagation is governed by the thermal diffusivity and by the permeability in fluid flow.

The explicit procedure has some distinct advantages, as well as disadvantages, over implicit methods as reviewed in Table 1.2-1. Perhaps the most important advantage from the standpoint of analysis of soil and rock behavior is the ability to accurately model non-linear behavior without significant effort over the standard elastic case.

Table 1.2-1

COMPARISON OF EXPLICIT AND IMPLICIT SOLUTION METHODS
[Cundall, 1980]

EXPLICIT	IMPLICIT
Time-step must be smaller than a critical value for stability.	Time-step can be arbitrarily large, with unconditionally stable schemes.
Small amount of computational effort per time-step.	Large amount of computational effort per time-step.
No significant numerical damping introduced.	Numerical damping dependent on time-step present with unconditionally stable schemes.
No iterations necessary to follow nonlinear constitutive law.	Iterative procedure necessary to follow nonlinear constitutive law.
Provided that the time-step criterion is always satisfied, nonlinear laws are always followed in the correct physical way.	Always necessary to demonstrate that the above mentioned iterative procedure is a) stable b) follows the physically correct path (for path-sensitive problems).
Matrices are never formed. Memory requirements are always at a minimum. No bandwidth limitations.	Stiffness matrices must be stored. Ways must be found to overcome associated problems such as bandwidth. Memory requirements tend to be large.
Since matrices are never formed, large displacements and strains are accommodated without additional computing effort.	Additional computing effort needed to follow large displacements and strains.

1.2.2 Program Structure

As described in Section 1.3 of this document, the body to be modeled is subdivided into a series of gridpoints which form the corners of zones (elements). A critical timestep is determined based on the element geometry, properties and phenomena to be modeled. The masses of elements are assumed to be "lumped" at the gridpoints. For numerical convenience and rapid convergence, the critical mechanical timestep is set equal to unity by proper adjustment of the gridpoint inertial masses. The general procedure illustrated in Fig. 1.2-1 is then used to perform calculation "cycles". Since FLAC solves only static (or quasi-static) mechanical problems through viscous damping of the equations of motion, the term "timestep" is somewhat erroneous, as time is problem time, not real time, and velocities are given in terms of displacement/ timestep. Therefore, for mechanical problems, each timestep can be considered a calculation cycle or iteration. For true transient problems such as heat transfer or fluid flow, the timestep has real meaning, and represents an absolute increment

of time in seconds. During each timestep, one calculation cycle is performed for each gridpoint in the entire grid, based on values btained from the previous timestep.

If true transient analysis is performed (heat transfer or fluid flow), timesteps are performed until the desired total time has elapsed; however, histories of the problem solution can be obtained and stored at any desired point from time = 0 to the total time. For linear elastic mechanical analysis, one is concerned only with the equilibrium state of the body. In this case, timestepping is performed until the out-of-balance forces at each gridpoint are sufficiently small. FLAC provides a method for automatically determining the equilibrium state based on pre-set criteria provided by the user. For non-linear mechanical analyses, it is often desirable to examine the deformation and yield history of the body as it progresses toward equilibrium. In fact, many processes such as collapse or steady-state creep will never arrive at an equilibrium state. In these cases, it is imperative that one have the ability to view the progression of the failure (deformation) process. The user may perform as many timesteps as desired, stop, examine the results, and continue.

An incremental approach is used in all constitutive laws. The equations of motion are used to determine velocities (strain rates) of the gridpoints. The strain rates are used to determine an incremental elastic stress. For non-linear constitutive laws, these "trial" elastic increments are compared to yield criteria, and corrections made, if necessary, to conform to the criteria.

A generalized flow chart of the program is given in Fig. 1.2-2. A more detailed flow chart of the mechanical portions of the program is given in Fig. 1.2-3. A command interpreter examines each command line in interactive or batch mode, and calls the proper code section to execute the command. The finite difference grid is set up first, a material model(s) and properties assigned, and boundary conditions applied. As the major functions of the code are executed, error checking and trapping is performed. If an error is detected, an error flag is set, the code halted, and an error message printed. Once the problem has been set up, solution begins by executing timesteps (or, better defined as calculation cycles for non-transient problems). The program loops through all zones in the grid, first performing mechanical calculations, as shown in Fig. 1.2-3. Options of axisymmetry or plane analysis can be made, each calling a different routine for stress determination. A choice of eight (8) constitutive laws, in addition to a null (excavation) model, is possible for the plane geometry, and five (5) for the axisymmetric geometry. These may all be solved in large strain mode, if desired, and are described in detail in Section 1.4, Component Models.

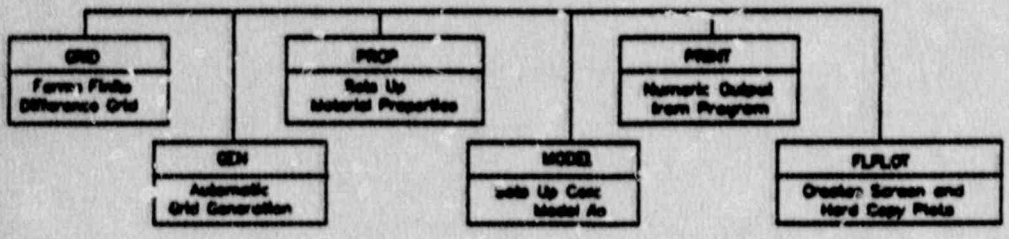

Fig. 1.2-2 Generalized Flow of FLAC Program Showing Greater Detail of Calculation Cycle

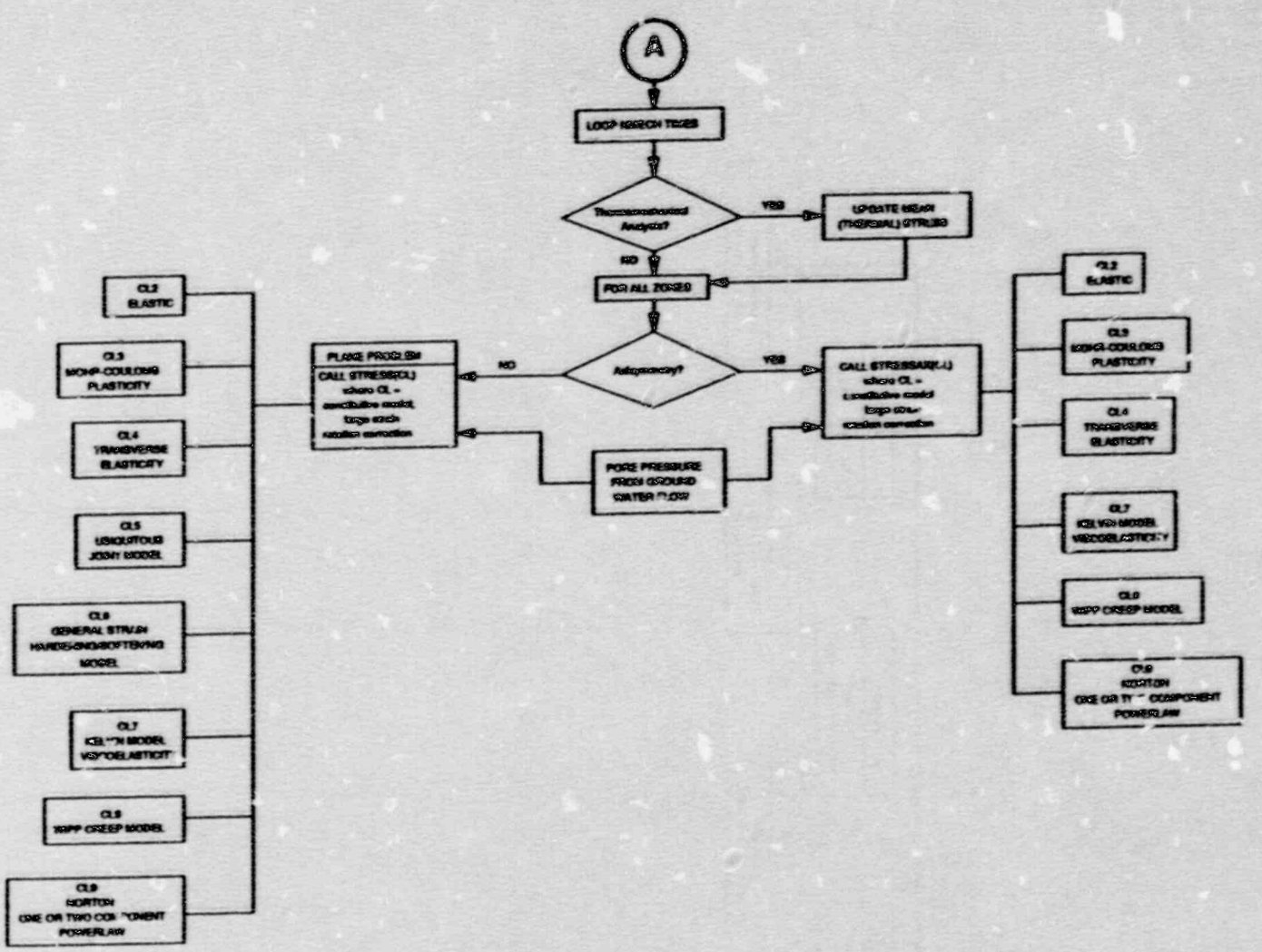

Fig. 1.2-3 Detail of Mechanical Calculations in FLAC
(refers to A from Fig. 1.2-2)

After performing stress calculations for all zones, fluid flow and/or thermal timesteps are performed, updating the pore pressure and temperature distributions in the grid. Thermomechanical coupling is performed by adjusting the mean stress according to the isotropic thermal expansion of the zone. The flow of fluid through the grid results in adjustments to the pore pressures which enter the calculation of total stress increments. The strains are coupled back to the fluid flow through a reduction in element volume. The total zone stresses are used to determine equivalent gridpoint forces. The forces from the interfaces and structural/cable elements are added to arrive at the total gridpoint forces. These forces are used as input to the law of motion from which new gridpoint velocities (and displacements) are derived. This same process continues until a user-defined limit is reached.

1.2.3 Field Equations

The solution of solid body, heat transfer or fluid flow problems in FLAC requires the equations of motion and constitutive relations, Fourier's Law for conductive heat transfer, and Darcy's Law for fluid flow in a porous solid, as well as boundary conditions. The following sections review the basic governing equations; the solution methodology is described in detail in Section 1.3.

1.2.3.1 Motion and Equilibrium Equations

The equations of motion relate the motion of a mass m, subjected to time-varying forces, F. Figure 1.2-4 is a simple illustration showing a mass subjected to a force F, resulting in a velocity, acceleration, and displacement.

In its simplest form, Newton's Law of Motion is given by

$$\frac{\partial \dot{u}}{\partial t} = \frac{F}{m} \qquad \text{(i.e., } F = ma\text{)} \qquad (1.2\text{-}1)$$

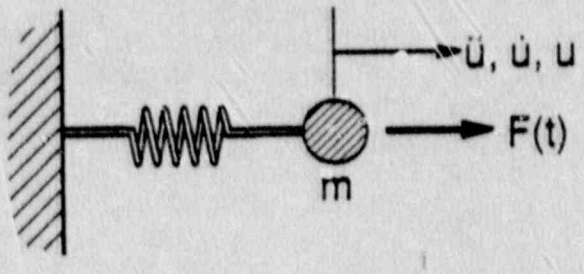

Fig. 1.2-4 Application of a Time-Varying Force to a Mass, Resulting in Acceleration, ü, Velocity, u̇, and Displacement, u

In its general form,

$$\rho \left[\frac{\partial \dot{u}_i}{\partial t} \right] = \frac{\partial \sigma_{ij}}{\partial x_j} + \rho g_i \qquad (1.2\text{-}2)$$

where ρ = mass density,

t = time,

x_j = coordinate direction,

g_i = acceleration of gravity (body force components), and

σ_{ij} = stress tensor.

The relationship of velocity to strain increment is given by

$$\Delta e_{ij} = \frac{1}{2} \left[\frac{\partial \dot{u}_i}{\partial x_j} + \frac{\partial \dot{u}_j}{\partial x_i} \right] \Delta t \qquad (1.2\text{-}3)$$

where Δe_{ij} = strain increment,

$\dot{u}_i$ = velocity, and

Δt = time increment.

Mechanical constitutive laws are of the form

$$\sigma_{ij} = M\ (\sigma_{ij},\ \Delta e_{ij},\ x) \qquad (1.2\text{-}4)$$

where M ( ) is the functional form of the constitutive law, and x is a history parameter(s) which may or may not be present, depending on the particular law.

1.2.3.2 Fourier's Law for Conductive Heat Transfer

Fourier's Law for conductive heat transfer can be written as

$$Q_i = - k_i \frac{\partial T}{\partial x_i} \qquad (1.2\text{-}5)$$

where Q_i = heat flux in the i-direction,

k_i = thermal conductivity in the i-direction, and

$\frac{\partial T}{\partial x_i}$ = thermal gradient in the i-coordinate direction.

The change in temperature of a mass, m, is given by

$$\frac{\partial T}{\partial t} = \frac{Q_{heat}}{C_p m} \qquad (1.2\text{-}6)$$

where t = time,

Q_{net} = sum heat flow into the mass,

C_p = specific heat, and

m = mass.

Combining Eqs. (1.2-5) and (1.2-6) yields the diffusion equation

$$\frac{\partial T}{\partial t} = \frac{1}{\rho C_p} \left[k_x \frac{\partial^2 T}{\partial x^2} + k_y \frac{\partial^2 T}{\partial y^2} \right] \qquad (1.2\text{-}7)$$

The above equation forms the basis of conductive heat transfer in FLAC. The stress change resulting from temperature increase in the body is given by

$$\Delta\sigma_{ij} = - \delta_{ij} \, 3K \, \alpha \, \Delta T \qquad (1.2\text{-}8)$$

where $\Delta\sigma_{ij}$ = stress change due to a temperature increase, ΔT,

α = linear thermal expansion coefficient,

K = bulk modulus of solid, and

δ_{ij} = Kronecker's delta.

1.2.3.3 Darcy's Law for Anisotropic Porous Media

Darcy's Law for an anisotropic porous medium is

$$V_i = K_{ij} \frac{\partial P}{\partial x_j} \qquad (1.2\text{-}9)$$

where V_i is the specific discharge vector,

P is the fluid pressure, and

K_{ij} is the permeability tensor.

The continuity equation is given by

$$\frac{\partial P}{\partial t} = - \frac{K_w}{nV} Q_{net} \qquad (1.2\text{-}10)$$

where Q_{net} is the sum of flows into a node,

n is the porosity,

V is the volume of the area represented by the node, and

K_w is the bulk modulus of the fluid.

Equations (1.2-9) and (1.2-10) are analogous to Eqs. (1.2-5) and (1.2-6) for Fourier's Law. The coupling of fluid flow to the mechanical portion of the code occurs through pore pressure (effective stress) and volume change due to mechanical strain. This is described in detail in Section 1.4, Component Models.

1.2.4 Boundary Conditions

The solution of problems in solid body mechanics and heat transfer of fluid flow requires that initial and boundary conditions be specified. For the mechanical models, the boundary conditions include fixed velocity (i.e., displacement), pressure, force, or traction. Heat Transfer includes fixed temperature, zero heat flux (adiabatic), flux or volume source; fluid flow includes fixed pressure, flux or volume source or sink. Initial conditions for the models include initial stress, initial temperature, and initial pore pressure distribution

1.3 GENERAL NUMERICAL PROCEDURE

1.3.1 Introduction

This section presents the finite difference implementation of the basic state equations presented in the previous section. FLAC uses a form of dynamic relaxation similar to that proposed by Otter et al. (1966), with adaptations for arbitrary grid shapes and large strains. The finite differencing scheme used is derived from Wilkins (1963). The full dynamic equations of motion are solved for mechanical analysis, but used only for solution of quasi-static problems by limiting applied velocities to small values and by use of internal viscous damping.

1.3.2 Basic Mechanical Finite Difference Formulation

1.3.2.1 Introduction

The user develops a finite difference mesh composed of quadrilateral elements. Internally, the code subdivides the element into two sets of overlapping constant-strain triangular elements (Fig. 1.3-1). No higher-order elements are used in the code.

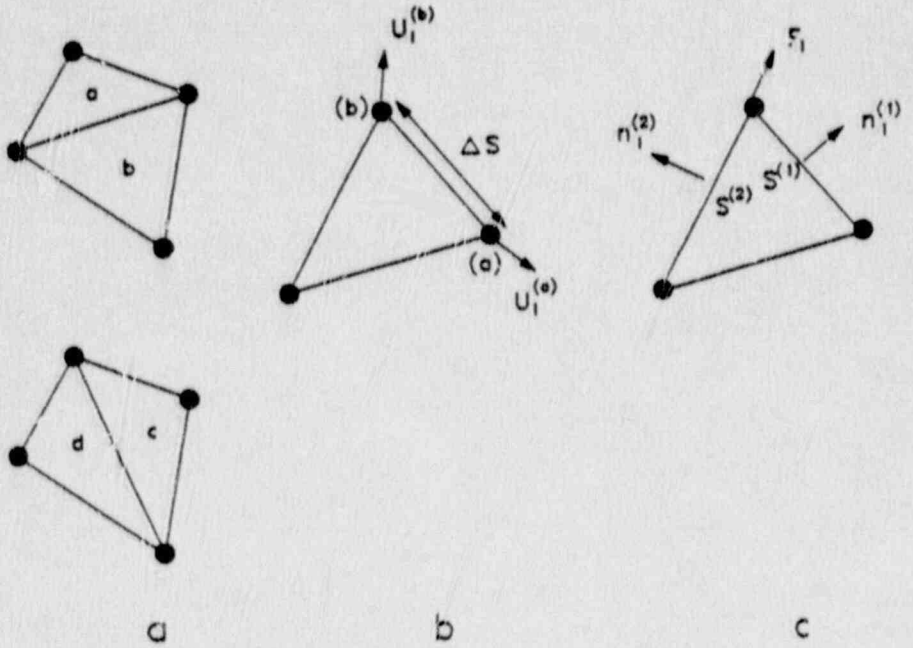

Fig. 1.3-1 (a) Overlayed Quadrilateral Elements used in FLAC;
(b) Typical Triangular Element with Velocity Vectors;
(c) Nodal Force Vector

The four (4) triangular subelements are termed a, b, c and d. The deviatoric stress components of each triangle are maintained independently, requiring twelve (12) stress components to be stored for each element. The forces exerted on each node are taken to be the mean of those exerted by the two overlayed quadrilaterals shown in the figure. The response of the composite element is symmetric in contrast to the response of a single pair of triangles.

1.3.2.2 Difference Equations

The difference equations for a triangle are derived from the generalized form of Gauss' divergence theorem (e.g., Malvern, 1969):

$$\int_s n_i \, f \, ds = \int_A \frac{\partial f}{\partial x_i} \, dA \qquad (1.3\text{-}1)$$

where $\int_s$ is the integral around the boundary of a closed surface,

n_i is the unit normal to the surface, s,

f is a scalar, vector or tensor,

x_i are positive vectors,

ds is an incremental arc length, and

$\int_A$ is the integral over the surface area, A.

Defining the average value of the gradient of f over the area A as

$$< \frac{\partial f}{\partial x_i} > = \frac{1}{A} \int_A \frac{\partial f}{\partial x_i} \, dA \qquad (1.3\text{-}2)$$

one obtains, by substitution into Eq. (1.3-1),

$$< \frac{\partial f}{\partial x_i} > = \frac{1}{A} \int_S n_i \, f \, ds \qquad (1.3\text{-}3)$$

For the triangular subelements, the finite difference form of Eq. (1.3-3) becomes

$$< \frac{\partial f}{\partial x_i} > = \frac{1}{A} \sum_s <f> \, n_i \, \Delta s \qquad (1.3\text{-}4)$$

where Δs is the length of a side of the triangle, and the summation occurs over the three sides of the triangle. The value of <f> is taken to be the average over the side. This formula, suggested by Wilkins (1963), enables strain increments, Δe_{ij}, to be written in terms of nodal velocities for a zone by substituting the velocity vector for f

$$\frac{\partial \dot{u}_i}{\partial x_i} \equiv \frac{1}{2A} \sum_s (\dot{u}_i^{(a)} + \dot{u}_i^{(b)}) \, nj \, \Delta s \qquad (1.3\text{-}5)$$

and

$$\Delta e_{ij} = \frac{1}{2} \left[\frac{\partial \dot{u}_i}{\partial x_j} + \frac{\partial \dot{u}_j}{\partial x_i} \right] \Delta t$$

where Δt is the timestep and (a) and (b) are two consecutive nodes on the triangle boundary.

It is noted here that the use of triangular elements eliminates the problem of hourglass deformations which may occur with constant strain finite difference quadrilaterals. The term "hourglassing" comes from the shape of the deformation pattern of elements within a mesh. For polygons with more than three nodes, combinations of nodal displacements exist which produce no strain and result in no opposing forces. The resulting effect is unopposed deformations of alternating direction.

A common problem which occurs in modeling of materials undergoing active collapse is the incompressibility condition of plastic flow. The use of plane strain or axisymmetric geometries introduces a kinematic restraint in the out-of-plane direction, often giving rise to overprediction of collapse load. This condition is sometimes referred to as "mesh-locking" or "excessively stiff" elements and is discussed in detail by Nagtegaal et al. (1974). The problem arises as a condition of local mesh incompressibility which must be satisfied during flow, resulting in over-constrained elements. To overcome this problem, the isotropic stress and strain components are taken to be constant over the whole quadrilateral element, while the deviatoric components are treated separately for each triangular subelement. This procedure, referred to as mixed-discretization, is described by Marti and Cundall (1982). The term mixed discretization arises from the different discretizations for the isotropic and deviatoric parts of the stress and stain tensors.

The volumetric strain is averaged over each pair of triangles according to the mixed discretization scheme. The strain increments in triangles a and b of Fig. 1.3-1 are adjusted in the following way:

$$\Delta e_m = (\Delta e^a_{11} + \Delta e^a_{22} + \Delta e^b_{11} + \Delta e^b_{22})/2 \qquad (1.3\text{-}6)$$

$$\Delta e^a_d = \Delta e^a_{11} - \Delta e^a_{22}$$
$$\Delta e^b_d = \Delta e^b_{11} - \Delta e^b_{22} \qquad (1.3\text{-}7)$$

$$\Delta e^a_{11} = (\Delta e_m + \Delta e^a_d)/2$$
$$\Delta e^b_{11} = (\Delta e_m + \Delta e^b_d)/2$$
$$\Delta e^a_{22} = (\Delta e_m - \Delta e^a_d)/2 \qquad (1.3\text{-}8)$$
$$\Delta e^b_{22} = (\Delta e_m - \Delta e^b_d)/2$$

Similar adjustments are made for triangles c and d. The component Δe_{12} is unchanged.

In large strain mode, finite rotations of elements produce changes in the stress components referred to a fixed frame of reference. The stresses are adjusted, as follows, prior to invoking the constitutive law.

$$\sigma_{ij} := \sigma_{ij} + (\omega_{ik}\,\sigma_{kj} - \sigma_{ik}\,\omega_{kj})\,\Delta t \qquad (1.3\text{-}9)$$

where $\omega_{ij} = \frac{1}{2}\left[\frac{\partial \dot{u}_i}{\partial x_j} - \frac{\partial \dot{u}_j}{\partial x_i}\right]$, and

:= means replaced by.

The constitutive law is of the form

$$\sigma_{ij} := M\,(\sigma_{ij},\ \Delta e_{ij},\ S_i) \qquad (1.3\text{-}10)$$

where M ( ) is the constitutive law,

Δe_{ij} are the current strain increments, and

S_i are state variables which vary with constitutive models.

The non-elastic constitutive laws require the adjustment of σ_{ij} based on corrective stresses determined from a yield function and flow rule. The various constitutive laws are described in detail in Section 1.4, Component Models.

Mixed discretization is then invoked on the stresses to equalize isotropic stress between the two triangles in a pair:

$$\sigma_o^{(a)} = \sigma_o^{(b)} := \left[\frac{\sigma_o^{(a)}\,A^{(a)} + \sigma_o^{(b)}\,A^{(b)}}{A^{(a)} + A^{(b)}}\right] \qquad (1.3\text{-}11)$$

where $\sigma_o^{(a)}$ is the isotropic stress in triangle (a) and

$A^{(a)}$ is the area of triangle $A^{(a)}$.

This equalization only has an effect for constitutive laws that involve shear-induced dilation.

For the explicit scheme used in FLAC, Eq. (1.3-10) is evaluated once per zone per timestep. As described in Section 1.2 of this document, no iterations are necessary to force all elements to conform to the constitutive law, as the timestep is made small enough that information cannot physically propagate from one zone to the next within one timestep. The calculation of the critical timestep is given later.

Once the stresses in each triangular zone are calculated, the equivalent forces applied to each nodal point are determined [Fig. 1.3-1(c)]:

$$F_i = \frac{1}{2} \sigma_{ij}^{(1)} \left(n_j^{(1)} S^{(1)} + n_j^{(2)} S^{(2)} \right) \qquad (1.3\text{-}12)$$

If the body is at equilibrium, or in steady-state flow (e.g., creep), the net force ΣF_i on the node will be zero; otherwise, the node will be accelerated. If a zone is missing (i.e., excavated or at a boundary), the force summation for an adjacent node simply ignores this term. The forces, and all stresses and coordinates, are known at times t, t + Δt, etc. (whole timesteps).

The gridpoint velocities at the next half timestep are determined by integrating the acceleration using central differences:

$$\dot{u}_i^{(t + \Delta t/2)} = \dot{u}_i^{(t - \Delta t/2)} + \left[\Sigma F_i^{(t)} - \alpha \left| \Sigma F_i^{(t)} \right| \text{sign}(\dot{u}_i) \right] \frac{\Delta t}{m} + g_i \Delta t \qquad (1.3\text{-}13)$$

In Eq. (1.3-13), α is a damping parameter, and m is the lumped mass of the node. The above scheme allows quasi-static problems to be solved by damping the vibrational energy of the nodes. Several damping schemes have been used in dynamic relaxation problems and are discussed in detail below.

For large strain problems, the velocity calculated in Eq. (1.3-13) is used to determine the new coordinate of the gridpoint

$$x_i^{(t + \Delta t)} = x_i^{(t)} + \dot{u}_i^{(t + \Delta t/2)} \Delta t \qquad (1.3\text{-}14)$$

1.3.2.3 Mechanical Damping

The equations of motion must be damped to provide static or quasi-static (non-inertial) solutions. The objective in FLAC is to achieve the steady state (either equilibrium or steady flow) in a numerically stable way with minimal computational effort. The damping used in standard dynamic relaxation methods is velocity-proportional—i.e., the magnitude of the damping force is proportional to the velocity of the nodes. This is commonly viewed as a dashpot fixed to the ground at each nodal point, as shown in the simple degree-of-freedom system given in Fig. 1.3-2.

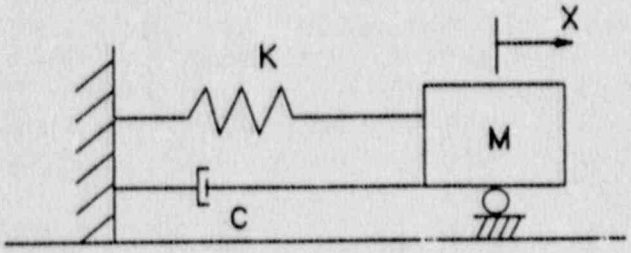

Fig. 1.3-2 Damped, Single Degree-of-Freedom System

The equation of motion for free vibration of the single degree-of-freedom system is given by

$$m \ddot{x} + c \dot{x} + kx = 0 \qquad (1.3\text{-}15)$$

where m is the mass, c is the viscous damping constant, k is the spring stiffness, and x is the coordinate.

It is clear in this illustration that the damping force produced is proportional to the velocity, $\dot{x}$, of the mass.

The following is adapted from Cundall (1987).

The use of velocity-proportional damping in standard dynamic relaxation involves three main difficulties:

(a) The damping introduces body forces, which are erroneous in "flowing" regions, and may influence the mode of failure in some cases.

(b) The optimum proportionality constant depends on the eigenvalues of the matrix, which are unknown unless a complete modal analysis is done. In a linear problem, this analysis needs almost as much computer effort as the dynamic relaxation calculation itself. In a non-linear problem, eigenvalues may be undefined.

(c) In its standard form, velocity-proportional damping is applied equally to all nodes—i.e., a single damping constant is chosen for the whole grid. In many cases a variety of behavior may be observed in different parts of the grid; for example, one region may be failing while another is stable. For these problems, different amounts of damping are appropriate for different regions.

In an effort to overcome one or more of these difficulties, alternative forms of damping may be proposed. In soil and rock, natural damping is mainly hysteretic; if the slope of the unloading curve is higher than that of the loading curve, energy may be lost. The type of damping can be reproduced numerically, but there are at least two difficulties. Firstly, the precise nature of the hysteresis curve is often unknown for complex loading-unloading paths. This is particularly true for soils, which are typically tested with sinusoidal stress histories. Cundall (1976) reports that very different results are obtained when the same energy loss is accounted for by different types of hysteresis loop. Secondly, ratcheting can occur—i.e., each cycle in the oscillation of a body causes irreversible strain to be accumulated. This type of damping has been avoided, since it increases path-dependence and makes the results more difficult to interpret.

Adaptive damping has been described briefly by Cundall (1982). Viscous damping forces are still used, but the viscosity constant is continuously adjusted in such a way that the power absorbed by damping is a constant proportion of the rate of change of kinetic energy in the system. The adjustment to the viscosity constant

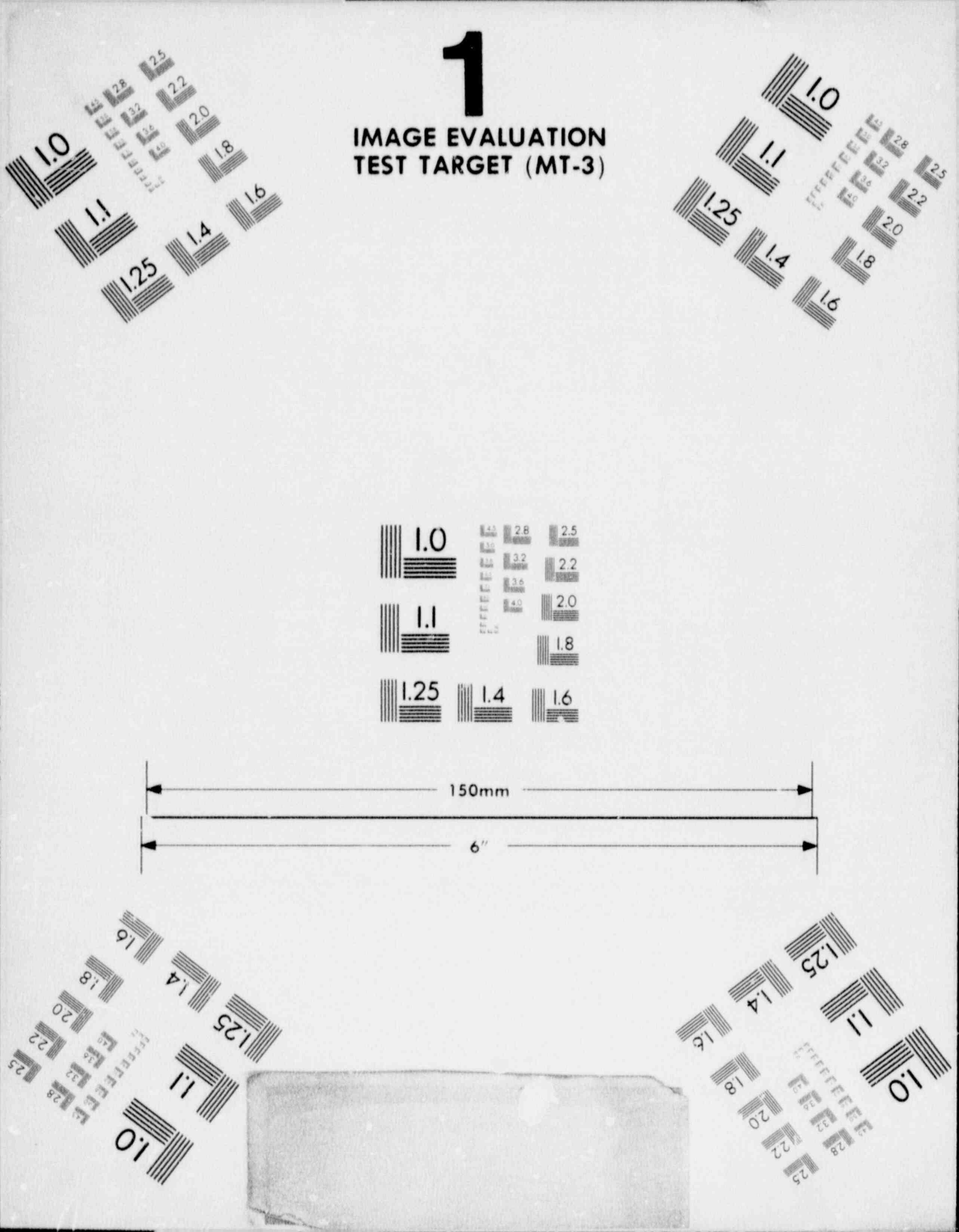
1
IMAGE EVALUATION
TEST TARGET (MT-3)
1.0
1.1
1.25
1.4
1.6
1.8
2.0
2.2
2.5
2.8
3.2
3.6
4.0
150mm
6"

1

IMAGE EVALUATION TEST TARGET (MT-3)

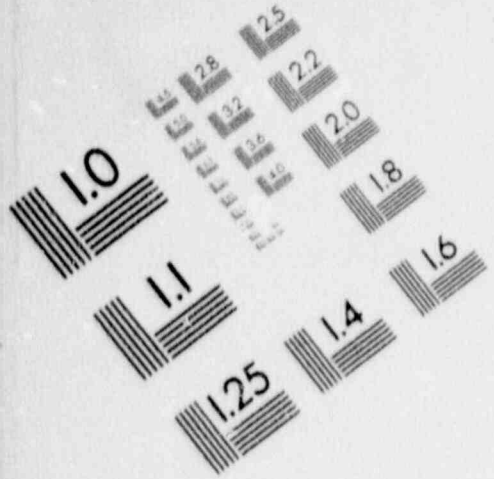

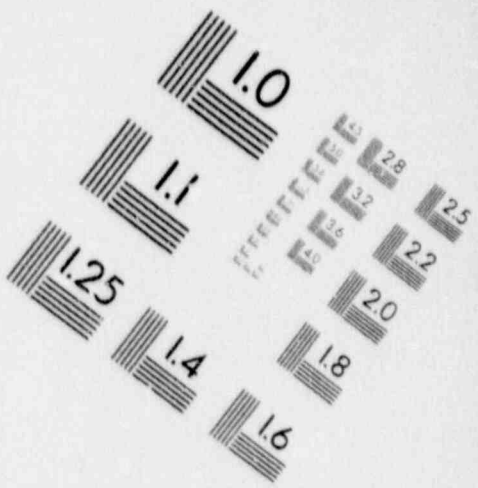

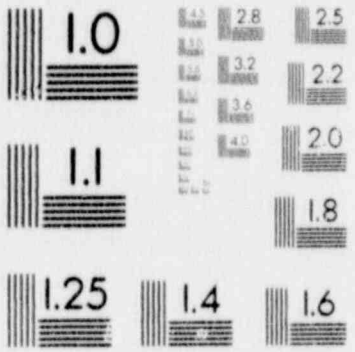

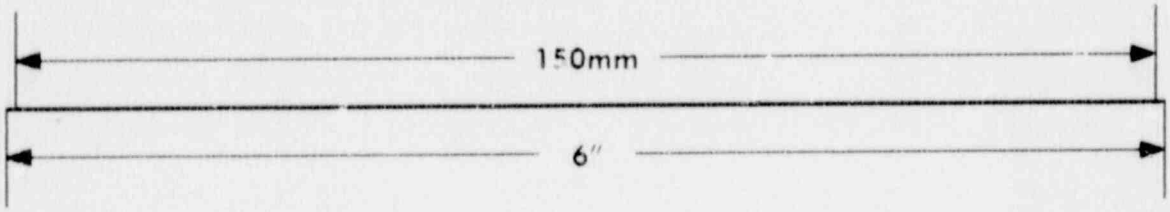

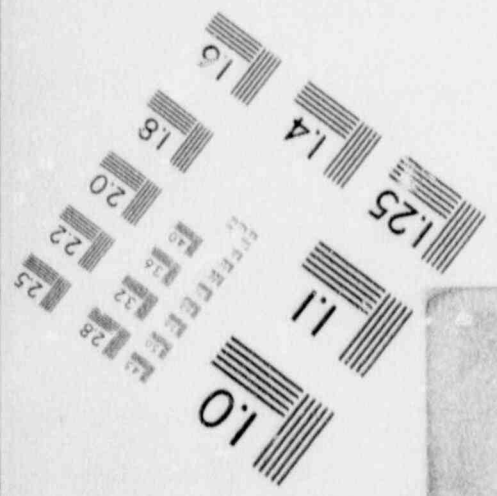

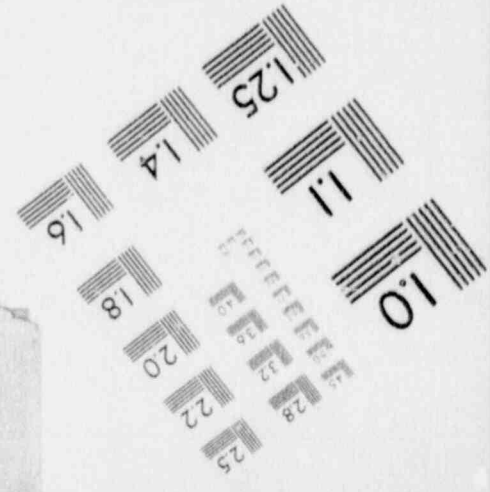

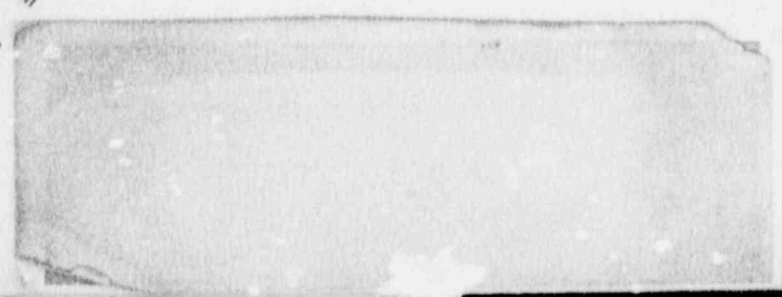

1

IMAGE EVALUATION TEST TARGET (MT-3)

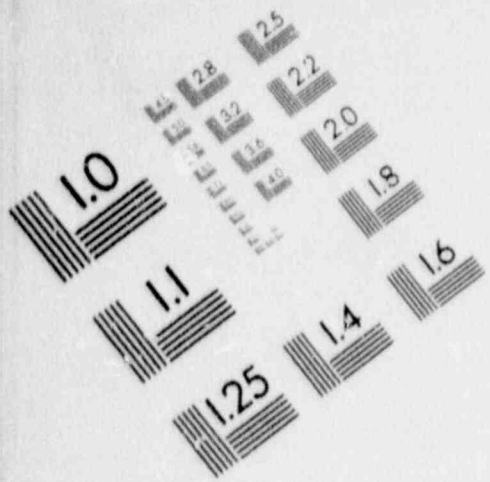

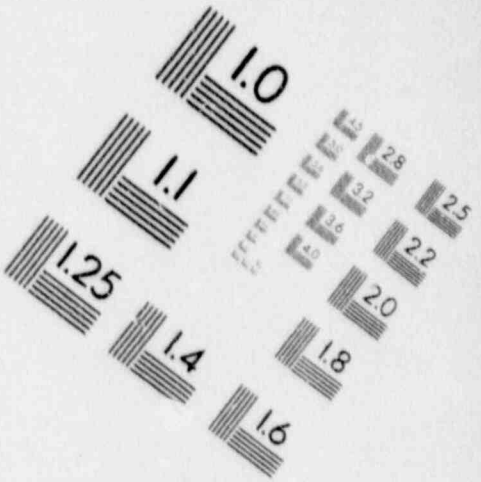

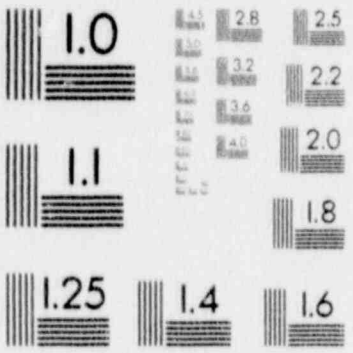

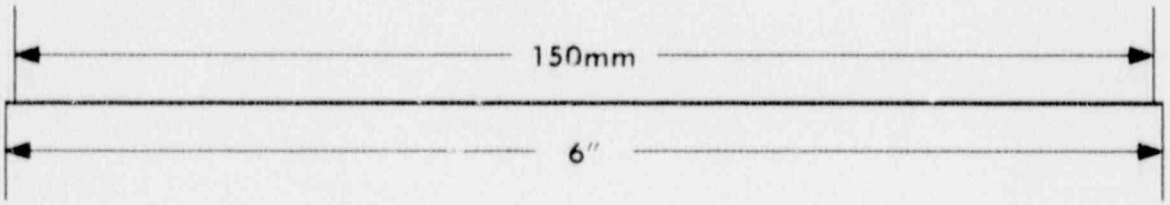

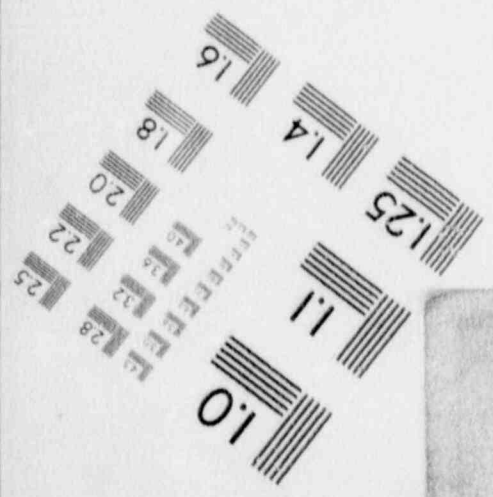

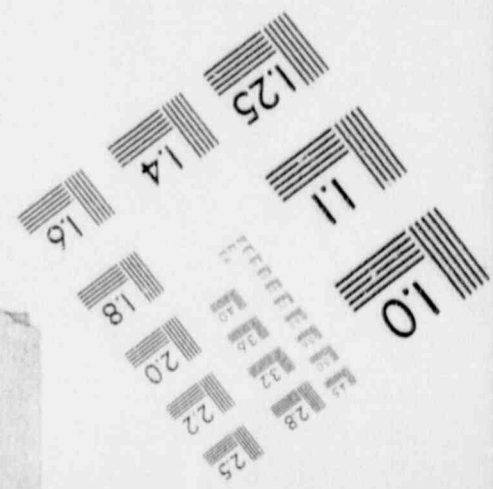

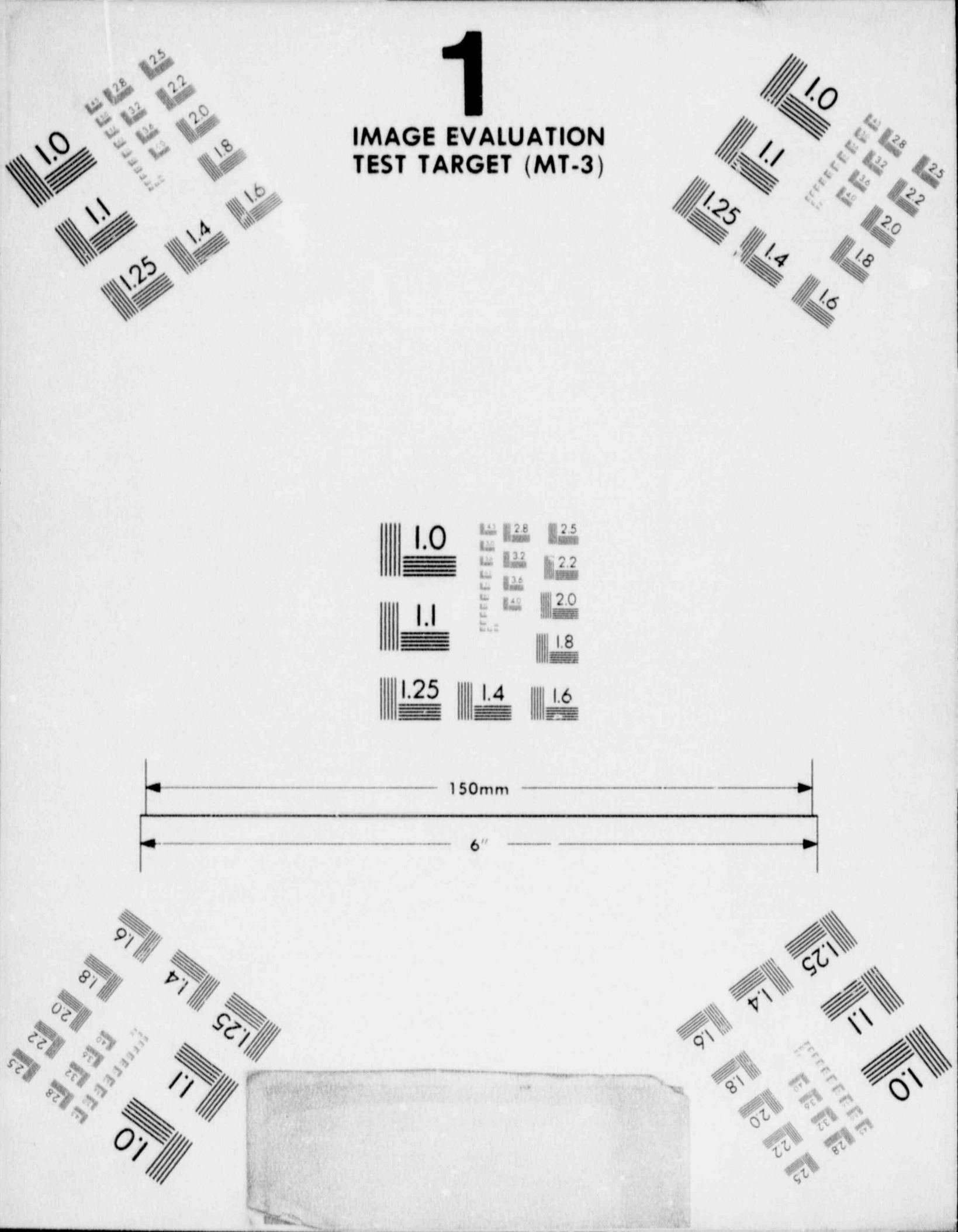
1
IMAGE EVALUATION
TEST TARGET (MT-3)
1.0
1.1
1.25
1.4
1.6
1.8
2.0
2.2
2.5
2.8
3.2
3.6
4.0
150mm
6"

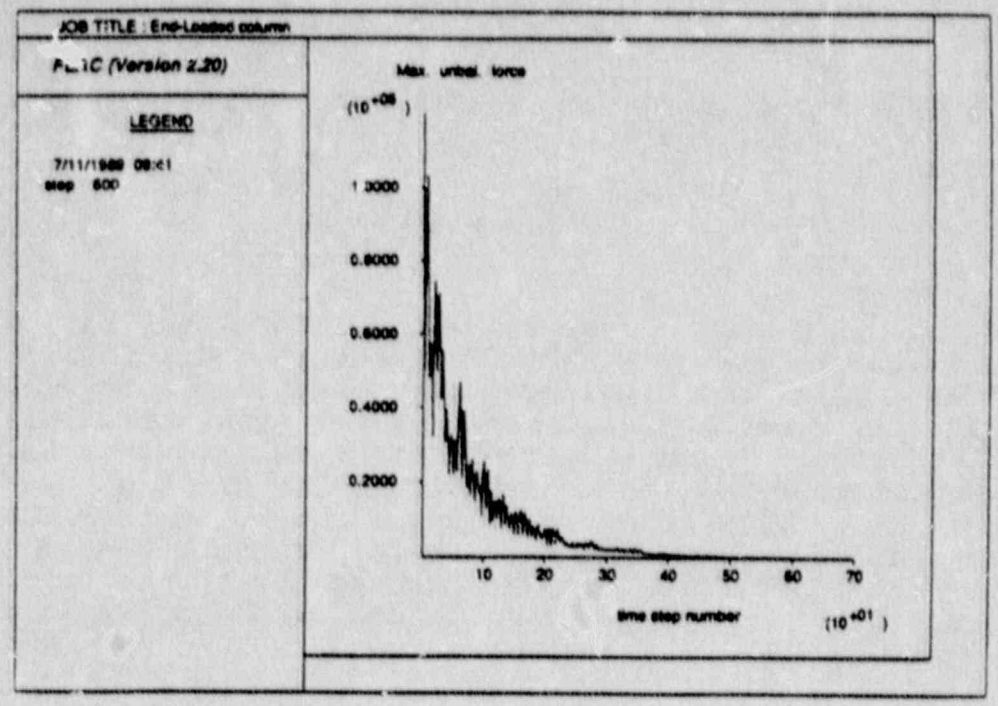

(a)

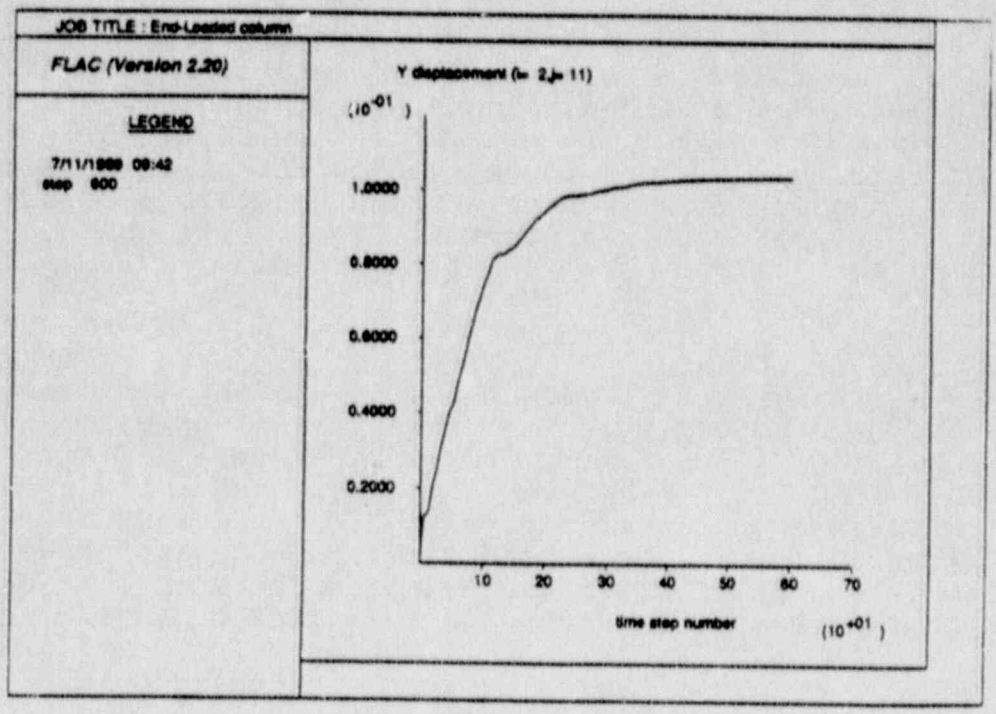

(b)

Fig. 1.3-3 Effect of Damping for the Problem of Sudden End Load Application to a Column

is made by a numerical servomechanism that seeks to keep the following ratio equal to a given ratio:

$$R = \Sigma P / \Sigma \dot{E}_k \qquad (1.3\text{-}16)$$

where P is the damping power for a node, $\dot{E}_k$ is the rate of change of nodal kinetic energy, [and] Σ represents the summation over all nodes. This form of damping overcomes difficulty (b) above, and partially overcomes (a), since as a system approaches steady state (equilibrium or steady flow) the rate of change of kinetic energy approaches zero and consequently the damping power tends to zero. Finally, a new form of damping is used in FLAC in which the damping force on a node is proportional to the magnitude of the out-of-balance force. A sign is applied to the damping form that ensures that energy is dissipated. The damping force is given by:

$$F_d = - |F| \, \text{sign}(\dot{u}) \qquad (1.3\text{-}17)$$

where F is the nodal out-of-balance force [cf, Eq. (1.3-12)]. This type of damping is equivalent to a local form of adaptive damping described above. In principle, the difficulties reported above are addressed: body forces vanish for steady-state conditions; the magnitude of damping constant is dimensionless and is independent of properties or boundary conditions; and the amount of damping varies from point to point (Cundall, 1987, pp. 134-135).

Figure 1.3-3 illustrates the typical results of the damping in FLAC for a problem that involves a suddenly-applied compression on the end of a column which is locked on the opposite end. Figure 1.3-3(a) shows the maximum unbalanced force (ΣF_i) in the model as a function of timestep; Fig. 1.3-3(b) shows the y-displacement at the center of the column, just beneath the applied load. Examination of the unbalanced force history shows the progression toward equilibrium (zero unbalanced force). Small oscillations of the system occur as the solution progresses. The damping effects are less evident in the plot of displacement history, which displays a typical slightly overdamped response.

1.3.2.4 Mechanical Timestep Determination, Convergence and Stability

As described previously, the explicit solution procedure, in general, does not guarantee a convergent solution. The basic premise of the method is that each zone in the grid can essentially be uncoupled from all other zones if the timestep for calculation is small enough to prevent information transfer between neighboring zones during any given timestep. The choice of timestep, therefore, governs the resulting stability of the simulation. FLAC automatically determines a stable mechanical timestep for all models. For the elastic and plasticity models, no user-intervention is typically necessary, as the use of timestepping is only a device to obtain the equilibrium solution. For the steady-state creep constitutive models, however, use of the initial elastic timestep would result in stable, but exceedingly large, solution times. The user must define empirically a timestep adjustment for these models which will produce stable system response while minimizing run time. This is described in detail later.

The timestep, Δt, enters into the motion law for calculation of new gridpoint velocities [see Eq. (1.3-13)]. Since the code still solves the complete dynamic equations of motion, the inertial mass will affect the transient solution obtained, but not the equilibrium or steady state. Because the concern is only with achieving the steady state as rapidly as possible, the inertial masses may be scaled to provide a timestep which optimizes the rate of convergence. This is similar to the use of an overrelaxation factor for more efficient solution of systems of equations by iterative methods. For a single mass-spring system, the critical timestep is

$$\Delta t_c = 2(m/k)^{1/2} \qquad (1.3\text{-}18)$$

where m is the mass, and k is the spring stiffness.

Optimum convergence is obtained when Δt_c is roughly the same for all nodes. In the above equation, the stiffness, k, refers to all stiffnesses connected to a node, including zone stiffness, interface stiffness connections (Section 1.3.5), and structural connections (Section 1.3.6)

$$k_{node} = k_z + k_i + k_s \qquad (1.3\text{-}19)$$

where k_{node} is the total stiffness connected to a node,

k_i is the interface stiffness,

k_s is the structural stiffness, and

k_z is the zone stiffness.

Figure 1.3-4 illustrates the various possible mechanical stiffnesses which can be connected to a node. The zone stiffness, k_z, for a triangular zone is given by

$$k_z = \frac{8}{3} [K + (4/3)G] L \qquad (1.3\text{-}20)$$

where $K + (4/3)G$ = confined modulus of zone material, and

L = the maximum edge length squared divided by the area of the zone.

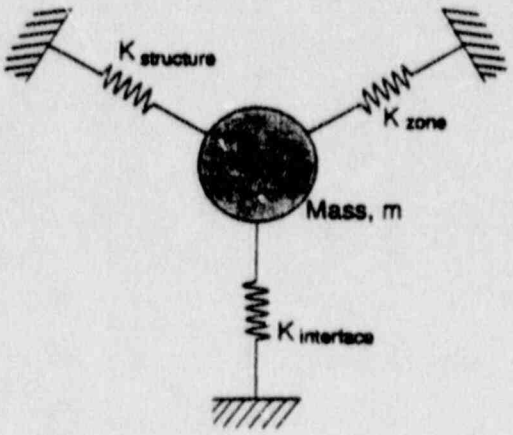

Fig. 1.3-4 Stiffnesses Used in Mechanical Timestep Calculations

Recall that a rectangular element is divided into triangles for the finite difference calculations. The zone stiffness contribution given above is averaged for all triangular zones surrounding a gridpoint as shown in Fig. 1.3-5.

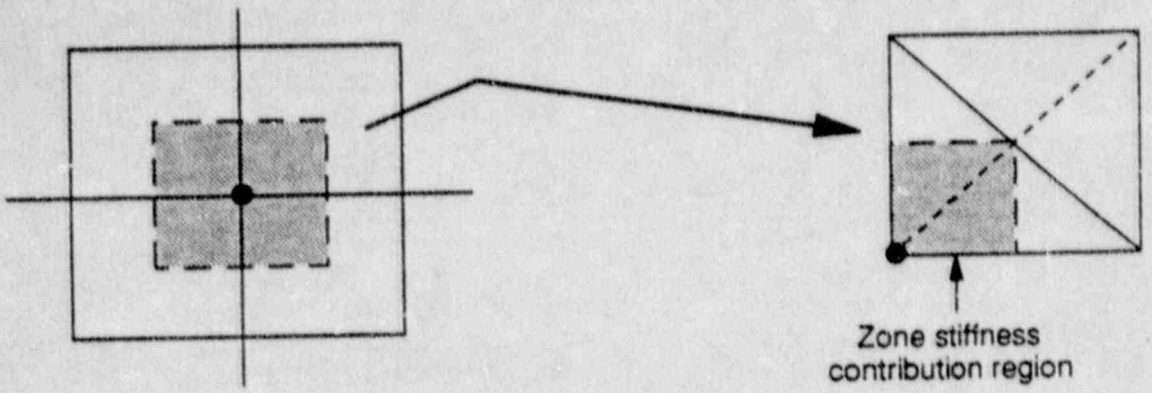

Fig. 1.3-5 Schematic Illustrating Zone Stiffness Contribution from Surrounding Triangular Sublements

To obtain the timestep, the gridpoint mass, m, is treated as a relaxation factor, and adjusted to equal the sum of the stiffnesses connected to the node:

$$m_{node} = k_{node} = \Sigma \text{ weighted stiffness connected to the node} \quad (1.3\text{-}21)$$

Thus, the mass is scaled such that the critical timestep for a node given in Eq. (1.3-18) becomes

$$\Delta t_c := 1.0 \quad (1.3\text{-}22)$$

Optimum convergence is obtained if the timestep is the same for all nodes. The use of Δt of 1.0 simplifies the motion calculation in the code (e.g., the incremental nodal displacement for any given timestep is simply equal to the velocity of the node, since velocity is given in terms of displacement per timestep).

1.3.2.5 Creep Timestep Methodology

The basic critical timestep at a node is the same for the creep as the elastic model, as the elastic timestep must be the minimum zone timestep. However, a physically meaningful value of time is necessary for creep strain calculations, even though the problem is quasi-static. The user is required to define a timestep value in the present version of the code, and has the option of allowing the program to automatically increase this value as a function of the value of the maximum out-of-balance force. In the main body of the code, a timestep (which is inertia scaled to equal 1.0) is used. However, once in the creep constitutive law (subroutines CL7-CL9), the mechanical timestep of 1.0 is multiplied by the user-defined timestep, dt. This value (dt) is then used to calculate increments of creep strain which are, in turn, used to adjust the deviatoric stress components. It is possible, therefore, to obtain instability in this model through a poor choice of the creep timestep, dt. This is discussed in greater detail in Section 1.4, Constitutive Models.

1.3.3 Basic Thermal Finite Difference Equations

1.3.3.1 Introduction

The basic field equations for heat transfer used in FLAC were introduced in Section 1.2. Here, the implementation is described. Two options for the solution procedure for heat transfer problems are allowed in FLAC: explicit and implicit methods. The explicit method used in the mechanical portion of FLAC holds distinct advantages in solution of problems in which non-linearity occur. However, if the response is linear, the explicit method for two-dimensional problems may be slow. For thermal and groundwater flow problems, the explicit solution requires that one determine a critical timestep, Δt, and solve the problem at Δt, $2\Delta t$, . . ., $n\Delta t$, where $n\Delta t$ is the total time frame for the analysis. In other words, the user is forced to determine a solution at times when the results may not be required. Because the timestep is controlled by geometry and thermal properties, examination of problems of small zone dimensions or high thermal diffusivity may result in exceedingly small timesteps, or excessive run times may result if long time analyses are to be performed. For these reasons, implicit temperature and fluid flow logic has been developed in which large timesteps are possible. Both schemes are described here.

1.3.3.2 Difference Equations

The diffusion equation given previously In Eq. (1.2-7) can be re-written as:

$$\rho C_p \frac{\partial T}{\partial t} = k_x \frac{\partial^2 T}{\partial x^2} + k_y \frac{\partial^2 T}{\partial y^2} \qquad (1.3\text{-}23)$$

For a typical finite difference grid, consisting of zones which are Δx wide by Δy in height (Fig. 1.3-6), an energy balance may be performed.

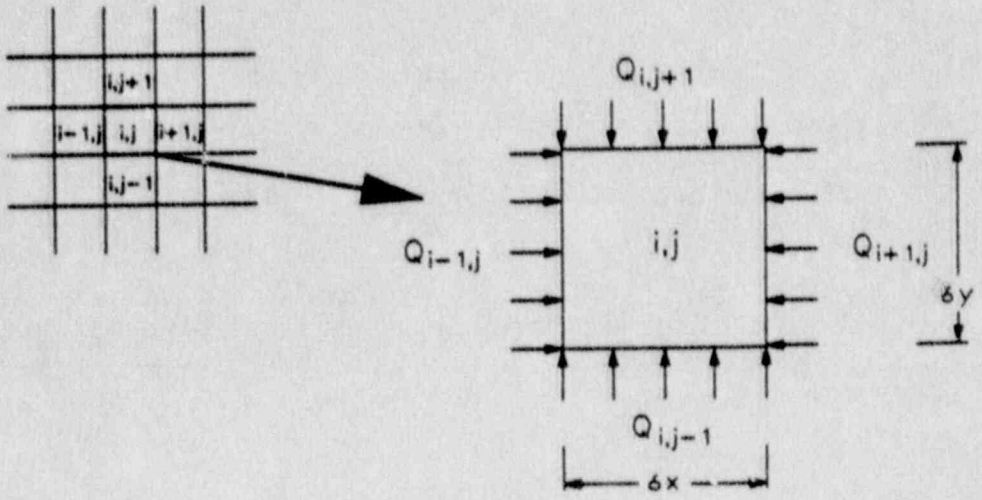

Fig. 1.3-6 Nomenclature for Determination of Energy Balance for a Typical Interior Zone

Conservation of energy requires the sum of heat flowing into element i,j to be zero for steady conditions.

$$\Sigma Q_{ij} = Q_{i-1,j} + Q_{i+1,j} + Q_{i,j-1} + Q_{i,j+1} = 0$$

$$= k_x \Delta y \left[\frac{T^{(t)}_{i-1,j} - T^{(t)}_{i,j}}{\Delta x} \right] + \left[\frac{T^{(t)}_{i+1,j} - T^{(t)}_{i,j}}{\Delta x} \right] +$$

(1.3-24)

$$k_y \Delta x \left[\frac{T^{(t)}_{i,j-1} - T^{(t)}_{i,j}}{\Delta y} \right] + \left[\frac{T^{(t)}_{i,j+1} - T^{(t)}_{i,j}}{\Delta y} \right] +$$

$$= 0$$

where Q = heat flow,

$T^{(t)}$ = temperature at a node at time, t, and

k = thermal conductivity in x- or y-direction.

For transient conduction, Eq. (1.3-24) is equal to the net energy storage in the mass of the zone i,j over a timestep Δt:

$$\rho C_p \Delta x \Delta y \frac{T^{(t+\Delta t)}_{i,j} - T^{(t)}_{i,j}}{\Delta t} = k_x \Delta y \left[\frac{T^{(t)}_{i-1,j} - T^{(t)}_{i,j}}{\Delta x} + \frac{T^{(t)}_{i+1,j} - T^{(t)}_{i,j}}{\Delta x} \right] +$$

(1.3-25)

$$k_y \Delta x \left[\frac{T^{(t)}_{i,j-1} - T^{(t)}_{i,j}}{\Delta y} + \frac{T^{(t)}_{i,j+1} - T^{(t)}_{i,j}}{\Delta y} \right]$$

or, re-arranging,

$$T_{i,j}^{(t+\Delta t)} = \frac{k_x \Delta t}{\rho C_p (\Delta x)^2}\left[T_{i-1,j}^{(t)} - 2T_{i,j}^{(t)} + T_{i+1,j}^{(t)} \right] + \frac{k_y \Delta t}{\rho C_p (\Delta y)^2}\left[T_{i,j-1}^{(t)} - 2T_{i,j}^{(t)} + T_{i,j+1}^{(t)} \right] \quad (1.3\text{-}26)$$

If $k_x = k_y = k$, then $k/\rho C_p = \kappa$, the thermal diffusivity. Expression (1.3-26) is the standard explicit finite difference form of the diffusion equation, since all terms on the right-hand side are known.

Convective, flux, radiation or adiabatic boundaries are easily handled through proper alteration of the heat flow terms in the energy balance equation [Eq. (1.3-24)]. For example, for a convective boundary at i+1,j (where the conduction terms are negligible), the associated $Q_{i-1,j}$ term in Eq. (1.3-24) becomes

$$Q_{i+1,j} = h \Delta y \ (T_\infty - T_{i,j}) \quad (1.3\text{-}27)$$

where h = convective heat transfer coefficient, and

T_∞ = temperature of the fluid to which the solid surface convects.

The radiative and adiabatic boundaries may be handled in a similar fashion.

1.3.3.3 Stability and Accuracy of the Explicit Scheme

The critical timestep for stability, assuming $\Delta x = \Delta y =$ the smallest dimension in the grid (see, for example, Karlekar and Desmond, 1982), determined from Eqs. (1.3-25 and 1.3-27) is:

$$\Delta t \leq \frac{(\Delta x)^2}{4\kappa \left[1 + \frac{h\Delta x}{2k} \right]} \qquad (1.3\text{-}28)$$

where κ = thermal diffusivity,

h = convection coefficient, and

k = thermal conductivity.

The accuracy of the explicit solution scheme is determined by the introduction of errors from several sources. A strict definition of error in the explicit formulation is not obtained simply because error arises from the finite difference approximations used, as well as the grid discretization and timestep. The explicit solution introduces a mixed order of error in the diffusion equation. This is because a forward difference formulation is used in time, the order of which is $O(h^1)$, and a central difference is used in spatial coordinates, the order of which is $O(h^2)$.

1.3.3.4 Implicit Solution Procedure

An implicit solution procedure can be used to solve the diffusion equation. A central difference in time corresponding to the half-timestep can be used, whereas the explicit formulation uses a forward difference in time. The spatial derivatives may also be represented by averaging central differences at t and t + Δt. An an example of this procedure, the diffusion equation in one dimension (x) can be written as

$$\frac{\rho C_p}{k}\left[\frac{T_i^{(t+\Delta t)} - T_i^{(t)}}{\Delta t}\right] = \frac{1}{2}\left[\frac{T_{i+1}^{(t+\Delta t)} - 2T_i^{(t+\Delta t)} + T_{i-1}^{(t+\Delta t)}}{(\Delta x)^2} + \frac{T_{i-1}^{(t)} - 2T_i^{(t)} + T_{i-1}^{(t)}}{(\Delta x)^2}\right] \quad (1.3\text{-}29)$$

This method, known as the Crank-Nicholson method, has the advantage that it provides stable solutions for all values of Δt. The gridpoint temperatures now not only depend simply on the temperatures at the previous timestep, but also on all gridpoint temperatures at the current step. This can be seen by the re-arrangement of Eq. (1.3-29) to give

$$\frac{\rho C_p}{k\Delta t}\Delta T_i = \left[\frac{T_{i+1}+1/2(\Delta T_{i+1})-2(T_i+1/2(\Delta T_i))+T_{i+1}+1/2(\Delta T_{i+1})}{(\Delta x)^2}\right] \quad (1.3\text{-}30)$$

since $T_k(t + \Delta t) = T_k(t) + \Delta T_k$, where ΔT_i are the unknown temperature increments. Because of this dependence, a system of equations must be solved. This requires greater memory, as the temperature coefficients must be stored for each gridpoint. The implicit method requires that a set of equations be solved at each timestep for the ΔT_i.

In matrix notation, the <u>explicit</u> method can be written as

$$\Delta T = \mathbf{C}\,\underline{T} \quad (1.3\text{-}31)$$

where **C** is a coefficient matrix, $\underline{T}$ is a vector of temperature, and $\underline{\Delta T}$ is a vector of the temperature change. Notice that ΔT is a function of $\underline{T}$ only. Similarly, the <u>implicit</u> scheme can be written as

$$\underline{\Delta T} = \mathbf{C}\,[\underline{T} + 1/2(\underline{\Delta T})] \quad (1.3\text{-}32)$$

where $\underline{\Delta T}$ is a function of $\underline{T}$ and $\underline{\Delta T}$. This equation can be rewritten as

$$[I - (1/2)\mathbf{C}]\ \underline{\Delta T} = \mathbf{C}\ \underline{T} \qquad (1.3\text{-}33)$$

where we need to solve for $\underline{\Delta T}$ at each timestep.

The matrix

$$\mathbf{A} = [\mathbf{I} - (1/2)\mathbf{C}] \qquad (1.3\text{-}34)$$

is diagonally dominant and sparse, because only neighboring points contribute non-zero values to **C**.

Thus, this set of equations is efficiently solved by an iterative scheme. For ease of implementation as a simple extension of the explicit method, the Jacobi method is used. For the NxN system $\underline{Ax=b}$, this can be generally written for the n^{th} iteration as

$$x_i^{(n+1)} = \frac{b_i}{a_{ii}} - \sum_{\substack{j=1 \\ j\neq i}}^{N} \left[\frac{a_{ij}}{a_{ii}} x_j^{(n)} \right] \qquad \begin{matrix} i = 1,2,\ldots,N \\ n = 1,2,\ldots, \end{matrix} \qquad (1.3\text{-}35)$$

where a_{ij} are the array elements of **A**, and

b_i are the elements of the right-hand side vector

— that is,

$$x_i^{(n+1)} = \frac{1}{a_{ii}} \left[b_i - \sum_{j=1}^{N} a_{ij}\, x_j^{(n)} \right] + x_i^{(n)} \qquad (1.3\text{-}36)$$

For Eq. (1.3-33), this becomes

$$\Delta T_i^{(n+1)} = \frac{1}{1 - (1/2)C_{ii}} \left[\sum_{j=1}^{N} C_{ij} T_j - \sum_{j=1}^{N} (\delta_{ij} - \frac{1}{2} C_{ij}) \Delta T_j^{(n)} \right]$$

$$+ \Delta T_i^{(n)} \qquad (1.3\text{-}37)$$

where C_{ij} are elements of the C array.

This implicit scheme equation can be compared to the explicit scheme, which can be written as

$$\Delta T_i = \sum_{j=1}^{N} C_{ij} T_j \qquad (1.3\text{-}38)$$

The amount of calculation required for each timestep is approximately n+1 times that required for one timestep in the explicit scheme, where n is the number of iterations per timestep. This extra calculation can be more than offset by the much larger timestep permitted by the implicit method, which makes the implicit scheme advantageous when the temperature change is linear in time.

1.3.3.5 Stability and Accuracy

As described previously, the implicit solution scheme holds the advantage that it is unconditionally stable for all timesteps. However, the differencing scheme presented in Eq. (1.3-29) assumes that the temperature change is a linear function of time in a single timestep. Depending on the problem to be modeled, this assumption may lead to inaccurate results if temperature gradients are very high, or are changing very rapidly— e.g., at early times in a simulation. The code uses a Jacobi iteration method to solve the system of equations at every timestep. From a strictly numerical perspective, convergence of the iteration is achieved if

$$|a_{ii}| > \sum_{\substack{j=1 \\ j \neq i}}^{N} |a_{ij}| \qquad i=1,2,\ldots,N \qquad (1.3\text{-}39)$$

where a_{ij} are the coefficients of the solution matrix **A** described previously.

The above condition simply means that it is possible to obtain a numerical solution to the system of equations, but that solution has no bearing on the accuracy with which the derived solution compares to the true solution.

There is no explicit method for determination of convergence to the true solution as a function of timestep since the convergence depends on many factors, including the properties, grid dimensions and grading, and boundary conditions. In most cases, the critical timestep [from Eq. (1.3-26)]

$$\Delta t \leq \frac{(\Delta x)^2}{4\kappa \left[1 + \frac{h\Delta x}{2k} \right]} \qquad (1.3\text{-}40)$$

provides a lower bound estimate for the implicit timestep. A trial and error procedure is required to set the timestep above this value. Typically, a thermal problem is set up and initialized using the explicit procedure.

1.3.3.6 Thermal Stress Coupling

The heat transfer may be coupled to thermal stress calculations at any time during a transient simulation. The coupling occurs in one direction only—i.e., the temperature may result in stress changes, but mechanical changes in the body resulting from force application do not result in temperature change. This restriction is not felt to be of great significance here since the energy changes for quasi-static mechanical problems is usually negligible. The stress change in a triangular zone is given by [from Eq. (1.2-8)]

$$\Delta\sigma_{ij} = - \Delta\delta_{ij}\, 3K\, \alpha\, \Delta t \qquad (1.3\text{-}41)$$

The above assumes a constant temperature in each triangular zone which is interpolated from the surrounding gridpoints. This stress is added to the zone stress state prior to application of the constitutive law.

1.3.4 Basic Fluid Flow Finite Difference Equations

1.3.4.1 Introduction

FLAC models the full coupling between a deformable, porous solid and a viscous fluid that flows within the pore space of the solid. The fluid obeys the anisotropic form of Darcy's law, and is assumed to be compressible, with a bulk modulus of K_w. Non-steady flow is modeled, with steady flow treated as an asymptotic case. At present, the code only handles fully-saturated flow, with phreatic surfaces represented crudely with a zero-pressure cut-off for pressures that try to become negative.

The interaction between solid and fluid involves two mechanisms. First, changes in pore pressure cause changes in effective stress, which affect the response of the solid constitutive model (for example, a reduction in effective stress may induce plastic flow). Second, changes in the volume of a zone causes changes in the pore pressure within the zone, since the fluid has a non-zero bulk modulus. Both of these effects involve a solid response time that is short compared to the time associated with fluid flow.

It is possible to model several extremes of stress and flow behavior, and all the cases in between. On the one hand, if the solid matrix is very stiff compared to the fluid compressibility, the fluid flow is unaffected by the solid matrix; the diffusion equation is solved by marching in time. At large times, the solution converges to that of the Poisson equation. On the other hand, if the permeability is zero, but the fluid bulk modulus is comparable to that of the solid, mechanical deformation causes pore pressures to change. For example, if a footing on a poro-elastic half-space is suddenly loaded, a pore-pressure distribution will exist when equilibrium is reached. In this case, the fluid will serve to make the solid appear stiffer. If the permeability is then set to some finite value, dissipation occurs, allowing the solid matrix to relax—i.e., some time-dependent movement (consolidation) of the footing occurs.

Because the groundwater flow is modeled as a transient problem, any analysis involving flow occurs in real physical time. In this respect, the fluid flow and heat transfer logic are similar in that flow (fluid or heat) is treated as transient, whereas the mechanical coupling is treated as a quasi-static process.

There are several ways of solving the fully-coupled equations. A review of methods is given in Hart (1981). Common to all methods is the solution of Darcy's law within an element. To avoid "checkerboarding" in the pressure distribution, it is assumed that pressures are located at gridpoints for the purposes of the flow calculation. These are regarded as the "master" pressures. Zone pressures ("slaves") are derived from the master pressures. A matrix can be derived for each zone to relate the unbalanced flows at the four surrounding gridpoints to the pressures at the same four gridpoints since fluid flow is linear according to Darcy's Law. This matrix must be updated if significant geometric changes occur, or if the permeability depends on mean stress. Section 1.3.4.2 contains a derivation of the matrix.

When unbalanced flows exist at gridpoints, the continuity equation is invoked to compute the changes in pore pressure at the gridpoints. The equation also contains source terms from externally-applied flows and from mechanical volume changes. Section 1.3.4.3 presents these equations. The word "node" is used interchangeably with the word "gridpoint" in what follows.

By default, the flow and continuity equations, and the mechanical calculations, are all done at each timestep in FLAC. Hence, the non-steady response of the fluid is masked to some extent by the response of the mechanical system, if the latter is not near to equilibrium. The option exists to switch off either the mechanical or the flow calculation. If the flow calculation is switched off, then the mechanical effect of the fluid is still accounted for. The only fluid solution scheme implemented currently is an explicit one.

1.3.4.2 Difference Equations

1.3.4.2.1 "Stiffness Matrix" for Elements in Fluid Boundary

Darcy's law for an anisotropic porous medium is

$$V_i = K_{ij} \frac{\partial P}{\partial x_j} \qquad (1.3\text{-}42)$$

where V_i is the specific discharge vector,

P is the pressure, and

K_{ij} is the permeability tensor.

Each quadrilateral element is divided into two pairs of triangles in two different ways [see Fig. 1.3-1(a)]. The specific discharge vector can be derived for the generic triangle of Fig. 1.3-7.

By Gauss' theorem,

$$\frac{\partial P}{\partial x_i} = \frac{1}{A} \int_s P n_i \, ds \qquad (1.3\text{-}43)$$

Hence, Eq. (1.3-42) becomes

$$V_i \cong \frac{K_{ij}}{A} \Sigma \, P n_i \, s \qquad (1.3\text{-}44)$$

where Σ is the summation over the three sides of the triangle.

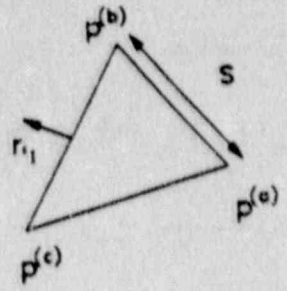

Fig. 1.3-7 Nomenclature for Determination of Specific Discharge Vectors from Gridpoint Pressures

For the x-component of V_i,

$$V_1 = \frac{1}{A}\left[K_{11} \Sigma Pn_1 s + K_{12} \Sigma Pn_2 s \right] \qquad (1.3\text{-}45)$$

The contribution of side (ab) of the triangle to the summation is

$$V_1^{(ab)} = \frac{1}{2A}\left[-K_{11}(P^{(b)}+P^{(a)})(x_2^{(b)}-x_2^{(a)}) + K_{12}(P^{(b)}+P^{(a)})(x_1^{(b)}-x_1^{(a)}) \right] \qquad (1.3\text{-}46)$$

Similarly, the y-component of V_i from side (ab) is:

$$V_2^{(ab)} = \frac{1}{2A}\left[-K_{21}(P^{(b)}+P^{(a)})(x_2^{(b)}-x_2^{(a)}) + K_{22}(P^{(b)}+P^{(a)})(x_1^{(b)}-x_1^{(a)}) \right] \qquad (1.3\text{-}47)$$

The other two sides, bc and ca, provide similar contributions to V_i. This specific discharge vector is then converted to scalar volumetric flow-rates at the nodes by making dot products with the normals to the three sides of the triangle. The general expression for nodal flow rates is

$$Q = \frac{V_i \; n_i \; s}{2} \qquad (1.3\text{-}48)$$

where the factor of 2 accounts for the fact that we take the average of the contribution from the two triangle pairs that make up the quadrilateral element.

In particular, the flow-rate into node (a) in terms of coordinates is then

$$Q^{(a)} = \frac{\left[- V_1 (x_2^{(b)} - x_2^{(c)}) + V_2 (x_1^{(b)} - x_1^{(c)}) \right]}{2} \qquad (1.3\text{-}49)$$

Similar expressions apply to nodes (b) and (c). Nodal flow rates are added from the other three triangles shown in Fig. 1.3-1(a). A stiffness matrix, **M**, for the whole quadrilateral element can be defined in terms of the relation between the pressures at the four nodes and the four nodal flow rates by combining Eqs. (1.3-44) and (1.3-48). The matrix representation is:

$$\{Q\} = [\mathbf{M}] \; \{P\} \qquad (1.3\text{-}50)$$

The effect of gravity is incorporated as follows. If the grid-point pressures around a zone conform to the hydrostatic gradient $\partial P / \partial x_i = g_i \rho_w$, where g_i is the vector of gravitational acceleration, then the nodal flow rates $\{Q\}$ should be zero. Hence, Eq. (1.3-50) is modified as follows

$$\{Q\} = [\mathbf{M}] \; \{P - (x_i - x_i^{(1)}) \; g_i \; \rho_w\} \qquad (1.3\text{-}51)$$

$$= 0$$

where $x_i^{(1)}$ is the x-coordinate of one of the corners.

1.3.4.2.2 Continuity Equation

The flow imbalance between quadrilateral elements, ΣQ, at a node causes a change in pore pressure as follows:

$$\frac{\partial P}{\partial t} = - \frac{K_w}{nV} \Sigma Q \qquad (1.3\text{-}52)$$

where nV is the pore volume associated with the node (n is the porosity and V is the total volume). The term ΣQ is the net flow at the node and includes contributions from the four surrounding zones and any sources that are specified by the user (e.g., inflow from a well). In finite difference form, Eq. (1.3-52) becomes

$$p(t + \Delta t) = p(t) - \frac{K_w \Sigma Q \Delta t}{nV} \qquad (1.3\text{-}53)$$

The term nV is computed as the sum of the contributions from all triangular subzones connected to the node. Each subzone triangle contributes a third of its volume-porosity product. The resulting sum is divided by two, to account for the double overlay scheme in FLAC.

Tensile pore pressures at nodes are prevented by setting P = 0 if the calculated pore pressure is negative. Zone pore pressures are then derived by taking the arithmetic average of the pressures of the four surrounding gridpoints.

1.3.4.3 Stability and Convergence

There are two aspects of numerical stability associated with the pore-fluid scheme: first, an explicit solution of the fluid flow equations requires that the timestep is less than a critical value; and, second, the bulk modulus of the fluid increases the mechanical stiffness. The effect of increased mechanical stiffness is incorporated into the density-scaling scheme already described—that is, the apparent mechanical bulk modulus of a zone is increased as follows: $K := K + K_w/n$, where := means replaced by, K is the solid bulk modulus, and n is the porosity of the zone.

The explicit fluid timestep can be derived by imagining that one node at the center of four zones is given a pressure of P_0. The resulting nodal flow is then given by the summation of Eq. (1.3-50) for each zone, which can be written as $Q = P_0 \Sigma M_{kk}$, where ΣM_{kk} is the sum over the four zones of the diagonal terms corresponding to the selected node. The excess nodal flow gives rise to an increment in pressure ΔP, according to Eq. (1.3-53):

$$\Delta P = - \frac{K_w Q \Delta t}{nV} \qquad (1.3\text{-}54)$$

The new pressure at the node, $P^{(t + \Delta t)}$ is then

$$P^{(t + \Delta t)} = P_0 + \Delta P = P_0 \left[1 - \frac{K_w \Sigma M_{kk} \Delta t}{nV} \right] \qquad (1.3\text{-}55)$$

This relation is stable and monotonic if

$$\Delta t < \frac{nV}{K_w \Sigma M_{kk}} \qquad (1.3\text{-}56)$$

The value of Δt used in FLAC is that given by this equation, multiplied by a safety factor (0.8).

1.3.5 Interfaces

1.3.5.1 Introduction

FLAC provides logic for frictional and cohesive interfaces to exist between portions of the continuum grid. Unlike interface elements or "slidelines" in many implicit-based codes [e.g., Fossum (1984), Morgan (1981)], FLAC allows slip, separation and recontact between bodies across frictional and cohesive interfaces which may have a tensile strength. Because FLAC is a large strain code, large deformations may occur along interfaces. Interfaces are defined through specification of nodes which may potentially interact. The code checks for contact between the

gridpoints on one side of the interface with zone edges on the other side of the interface, and sets up reaction forces to the nodes based on the stiffness of the interface in shear and normal directions. A Mohr-Coulomb slip condition is used to define the elastic limit in shear.

1.3.5.2 Numerical Implementation

An interface is represented as a normal and shear stiffness between two planes which may contact one another (Fig. 1.3-8).

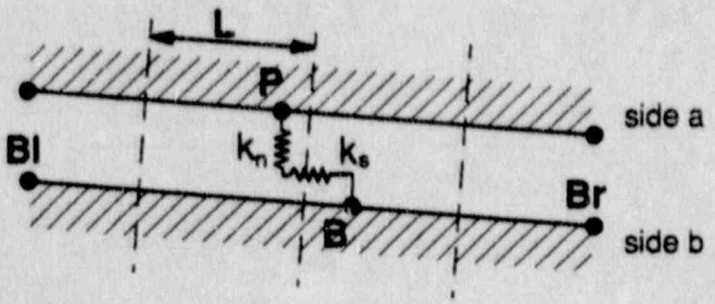

Fig. 1.3-8 An Interface Represented by Sides a and b, Connected by Shear (k_s) and Normal (k_n) Stiffness

FLAC uses a contact logic for either side of the interface which is similar in nature to that employed in the distinct element method [e.g., Itasca (1989)]. Figure 3-9 presents a simple flow chart of the contact detection logic.

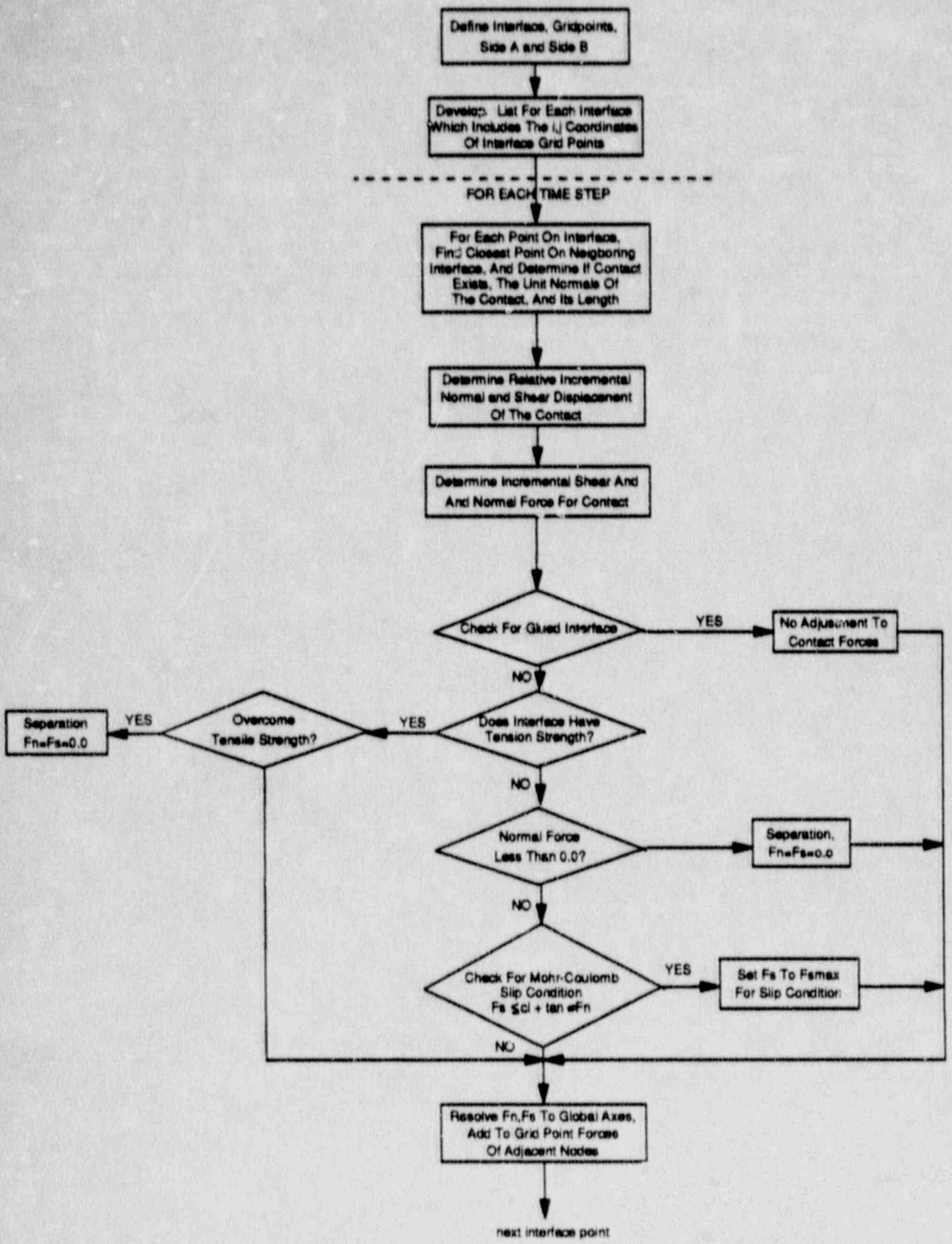

Fig. 1.3-9 Contact Detection and Interface Force Calculation Flow Diagram

The code keeps a list of the gridpoints (i,j) which lie on each side of any particular interface. Each point is taken, in turn, and checked for contact with its closest neighboring point on the opposite side of the interface. Referring to Fig. 1.3-8, gridpoint P is checked for four contact conditions: (1) no contact; (2) contact on segment between B and B_r; (3) contact on segment between B and B_l; and (4) contact, centered at B. Based on these conditions, the normal, n, to the contact, P, and the "length", L, of the contact along the interface belonging to node P are calculated. The length associated with P is equal to half the distance to the nearest gridpoint to the left plus half the distance to the nearest gridpoint to the right, irrespective of whether the neighboring gridpoint is on the same side of the interface or on the opposite side.

During each timestep, the velocity, $\dot{u}_i$, of each gridpoint is determined. Since the units of velocity are displacement per timestep, and the timestep has been density-scaled to unity to speed convergence, then the incremental displacement for any given timestep is

$$\Delta u_i = \dot{u}_i \tag{1.3-57}$$

The total normal and shear forces are determined by

$$F_n^{(t+\Delta t)} = F_n^{(t)} - k_n \Delta u_n^{(t+(1/2)\Delta t)} L$$

$$F_s^{(t+\Delta t)} = F_s^{(t)} - k_s \Delta u_s^{(t+(1/2)\Delta t)} L \tag{1.3-58}$$

Several options are available for specifying the conditions of the interface which may require adjustment of the contact forces.

1. Glued Interfaces — If interfaces are declared glued, no slip is allowed, and no adjustment is made to F_n or F_s (i.e., the grid acts as a continuum).

2. Tension Strength — If tension exists, the Mohr-Coulomb condition is examined for extensional shear, followed by a check for the case of tension strength set to some value. If the tension strength is exceeded, separation occurs and $F_n = F_s = 0$. The default case is zero tensile strength.

3. Mohr-Coulomb Shear Strength — The normal force is input to the Mohr-Coulomb condition and examined for compressional shear.

$$F_{smax} = CL + \tan\phi \, F_n \qquad (1.3\text{-}59)$$

where C = joint cohesion,

L = effective contact length (see Fig. 1.3-8), and

ϕ = friction angle of joint surfaces.

If the criterion is satisfied, i.e., if $|F_s| \geq F_{smax}$, then $F_s = F_{smax}$, with the sign of shear preserved.

The corrected forces are then rotated back to the global x-y reference frame (from the normal and shear directions) and lumped onto the adjacent gridpoints in such a ratio as to preserve moment equilibrium. These are then summed with all the other forces when unbalanced force sums are calculated for each timestep.

1.3.5.3 Stability

The influence of the interfaces must be accounted for in determination of critical timestep, or instability in the solution may result. If the timestep is too large, the gridpoints on either side of the interface may overlap excessively prior to calculation of the opposing reaction forces. The result may be unstable displacements along the interface. The factors controlling the timestep contribution from the interfaces are the normal and shear stiffnesses, and the gridpoint mass of the interface gridpoints.

As described in Section 1.3.4.2, the interface stiffness enters the determination of the critical mechanical timestep for those nodes which lie along the interface. The interface stiffness contribution, k_i, is given by

$$k_i = 4 \bullet k \qquad (1.3\text{-}60)$$

where k is the norm of the shear and normal stiffnesses:

$$k = (k_s^2 + k_n^2)^{1/2} \qquad (1.3\text{-}61)$$

The multiplier 4 relates to the highest oscillation frequency of a set of springs in series (see Fig. 1.3-10). In this mode of oscillation, alternate nodes move in opposite directions. The center of each spring is therefore at rest, by symmetry. A node then "sees" two half-sprirgs in parallel, which accounts for the factor of 4.

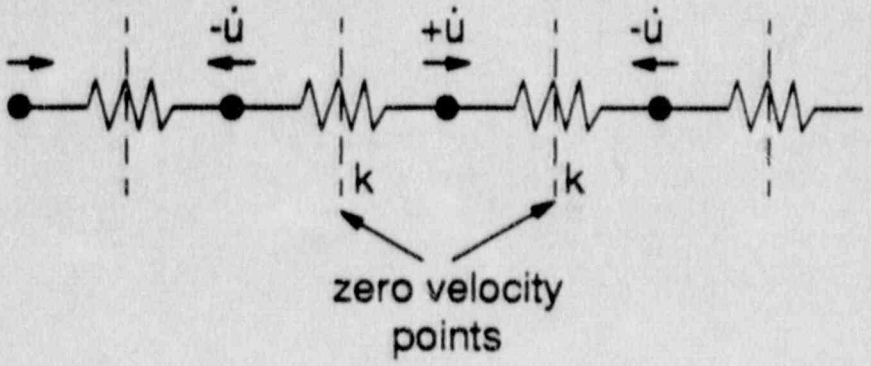

Fig. 1.3-10 Shear and Normal Springs in Series

Experience has shown that FLAC provides stable interface response with the present form of timestep calculation for a majority of problems. There is a practical limit on interface stiffnesses for efficient modeling. If a high (or "infinite") stiffness is required, the stiffness should be limited to ten times the equivalent neighboring zone stiffness.

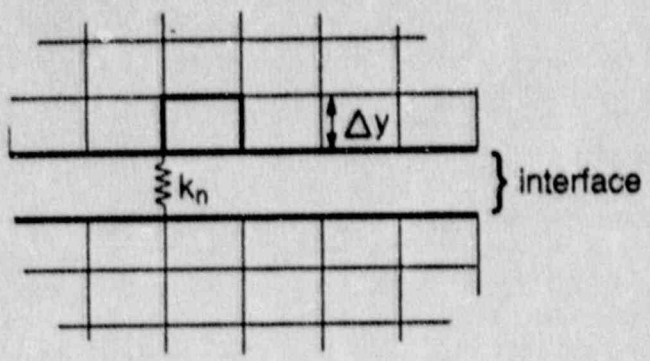

Fig. 1.3-11 Schematic Illustrating Interface Normal Stiffness

For zone compression in the normal direction (see Fig. 1.3-11),

$$\frac{\sigma_n}{e_n} = K + \frac{4}{3} G \tag{1.3-62}$$

$$\frac{\sigma_n}{u_n} = \frac{1}{\Delta y} \left[K + \frac{4}{3} G \right]$$

where e_n is the strain in the normal direction.

Hence, k_n for the interface should be

$$k_n \leq \frac{10}{\Delta y} \left[K + \frac{4}{3} G \right] \tag{1.3-63}$$

This value of k_n gives a good approximation to a "rigid" interface without compromising efficiency.

1.3.6 Structural Elements/Cable Elements

1.3.6.1 Introduction

An important aspect of geotechnical analysis and design is the use of structural support in stabilizing the rock or soil mass. FLAC provides logic for modeling of the interaction of major support types, with the rock or soil mass allowing calculation of support loads and moments.

Two major forms of support are used: structural elements and cables (or bolts). The cables may be anchored at a specific point in the rock (point-anchored) or may be grouted along their length. Additionally, the cable may be pre-tensioned or left untensioned. In the latter case, forces in the bolt develop as the rock undergoes deformation. The structural elements are two-dimensional beams with three degrees-of-freedom (dof) at each end node. These can be used for modeling interior support for tunnels (e.g., shotcrete, concrete arches, etc.) and structures such as sheet piles or surface frame structures. The elements use the same basic lumped mass formulation as in the continuous portion of the FLAC code, and are therefore subject to the dynamic equations of motion. The equilibrium solution is obtained through damping of the motion equation. Structures may undergo large deformations similar to the rest of the code. Two restrictions are made regarding the structural elements: (1) the self-weight of the structure is not included when applying gravity (although external forces may be applied to simulate self-weight); and (2) the structures behave linearly elastically with no failure limit.

1.3.6.2 Structural Element Formulation

The structural elements in FLAC are standard two-dimensional beam elements with rectangular cross-section with 3 degrees-of-freedom (two displacements and one moment) at each end node (Fig. 1.3-12). A typical beam element is defined by its material and geometric properties. The beam is assumed to behave as a linear-elastic material with no failure limit. The beam can be considered to have a cross-section (Fig. 1.3-13) with area A, and second moment of area, I, and is defined by its endpoints, a and b, with length L.

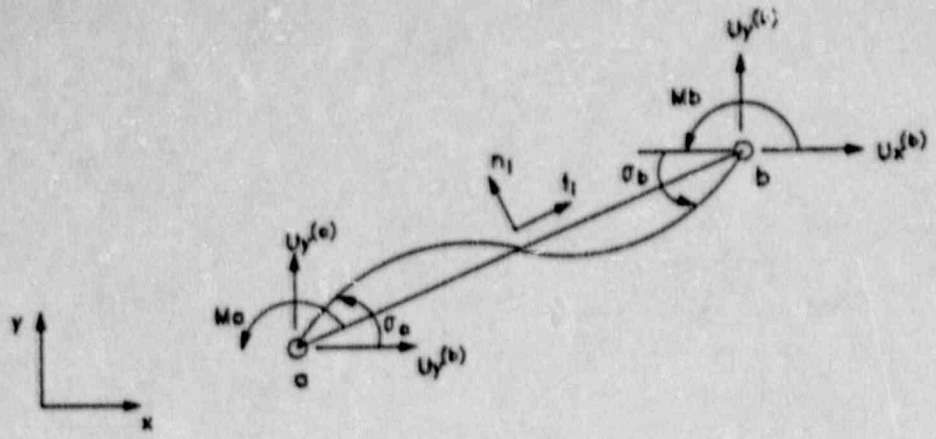

Fig. 1.3-12 Beam Element Illustrating Nomenclature

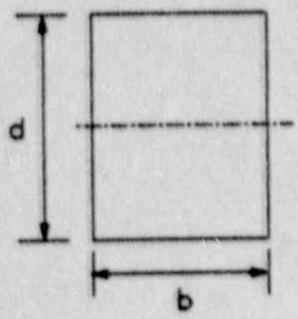

$$I_1 = \frac{1}{12} bd^3$$

$$A = bd$$

Fig. 1.3-13 Rectangular Beam Cross-Section with Second Moment of Area, I, and Cross-Sectional Area, A

The orientation of the beam in two-dimensional space is defined by its direction cosines, n_i, t_i, where (Fig. 1.3-14)

$$t_1 = \frac{x_b - x_a}{z} = \frac{\Delta x}{z} = \cos\theta, \qquad z = (\Delta x^2 + \Delta y^2)^{1/2}$$

$$t_2 = \frac{y_b - y_a}{z} = \frac{\Delta y}{z} = \sin\theta, \qquad z = (\Delta x^2 + \Delta y^2)^{1/2} \tag{1.3-64}$$

$$n_1 = - t_2 = - \cos\theta$$

$$n_2 = t_1 = \sin\theta$$

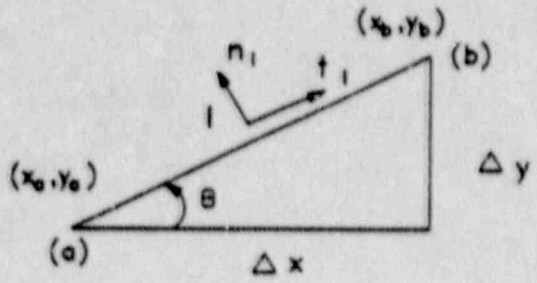

Fig. 1.3-14 Direction Cosines for a Beam Element

The x- and y-forces at each node are given by

$$F_i^{(a)} = F_a^{(a)}\, t_i + F_a^{(n)}\, n_i$$

$$F_i^{(b)} = F_b^{(a)}\, t_i + F_b^{(n)}\, n_i \qquad (1.3\text{-}65)$$

where $F_i^{(a)}$ = force in the i-direction at node (a),

$F_a^{(a)}$ = force at a in axial direction,

$F_a^{(n)}$ = force at a in normal direction,

$F_i^{(b)}$ = force in the i-direction at node (b),

$F_b^{(a)}$ = force at b in axial direction,

$F_b^{(n)}$ = force at b in normal direction,

t_i, n_i = direction cosines,

the superscript (n) refers to normal direction, and

the superscript (a) refers to axial direction.

The component axial and shear forces and moments at each node are given by the stiffness matrix for a flexural element (see, for example, Chajes, 1983):

$$\begin{bmatrix} F_a^{(a)} \\ F_a^{(n)} \\ M_a \\ F_b^{(a)} \\ F_b^{(n)} \\ M_b \end{bmatrix} = \mathbf{K} \begin{bmatrix} u_a^{(a)} \\ u_a^{(n)} \\ \theta_a \\ u_b^{(a)} \\ u_b^{(n)} \\ \theta_b \end{bmatrix} \qquad (1.3\text{-}66)$$

where $u_a^{(a)}$ = axial displacement at a,

$u_a^{(n)}$ = normal (shear) displacement at a,

$u_b^{(a)}$ = axial displacement at b,

$u_b^{(n)}$ = normal (shear) displacement at b,

θ_a = rotation at a,

θ_b = rotation at b, and

$$K = \frac{E}{L}\begin{bmatrix} A & & & & \text{SYM.} \\ 0 & \frac{12I}{L^2} & & & \\ 0 & \frac{6I}{L} & 4I & & \\ -A & 0 & 0 & A & \\ 0 & -\frac{12I}{L^2} & -\frac{6I}{L} & 0 & \frac{12I}{L^2} \\ 0 & -\frac{6I}{L} & 2I & 0 & \frac{6I}{L} \quad 4I \end{bmatrix} \qquad (1.3\text{-}67)$$

Various moment release conditions (i.e., pinned joints) may be applied at each end node. These conditions are:

(1) $M_a = 0$;

(2) $M_b = 0$; and

(3) $M_a = M_b = 0$.

If $M_a = 0$,

$$\theta_a = \frac{1}{2}\left[(3/L)\left[u_b^{(n)} - u_a^{(n)} \right] - \theta_b \right] \qquad (1.3\text{-}68)$$

If $M_b = 0$,

$$\theta_b = \frac{1}{2}\left[(3/L)\left[u_b^{(n)} - u_a^{(n)} \right] - \theta_a \right] \qquad (1.3\text{-}69)$$

If $M_a = M_b = 0$,

$$\theta_a = \theta_b = 0 \qquad (1.3\text{-}70)$$

Numerical Implementation

The structural elements use the same explicit logic for numerical implementation as described in Section 1.3.3.2. Displacements of the rock mass (u_a,u_b) result in incremental forces and moments in the structure which are added to the unbalanced force sum at the respective node points. The structural elements may operate in large strain mode, if desired. The coordinates are updated by:

$$x_i := x_i + \Delta\dot{u}_i \qquad (1.3\text{-}71)$$

(Note: $\Delta u_i = \Delta\dot{u}_i$ since $\Delta t = 1.0$ via mass scaling.)

1.3.6.3 Cable Elements

Cable and bolt reinforcements in rock have two somewhat different functions. In hard rock subjected to low magnitude in-situ stress fields, failure may be localized to wedges of rock directly adjacent to the openings. The effect of the rockbolt reinforcement here is to provide a local stiffness at the joint surfaces to resist their deformation. The bending, as well as the axial stiffness of the reinforcement, may be important in resisting shear deformations. In FLAC, this type of bolt action may be modeled using beam elements which have a flexural rigidity. The beams, however, do not allow the modeling of a shearing resistance along their length, as provided by grout. In many instances, it is necessary to consider more than just the local effect of the reinforcement—its presence in resisting deformation must be accounted for along its entire length. Such situations arise in modeling inelastic deformations associated with failed rock and/or reinforcement systems (e.g., cable bolts) in which the bonding agent (grout) may fail in shear over some length of the reinforcement. The numerical formulation for rock reinforcement which accounts for inelastic deformation of the intact rock and shear behavior of the grout annulus is described here.

The cable length is divided into a number of elements of length L, with nodal points located at each end. The mass of each element is lumped at the nodal points, as in the continuum portion of FLAC.

1.3.6.3.1 Axial Behavior

The axial behavior of conventional reinforcement systems may be assumed to be governed entirely by the reinforcing element itself. The reinforcing element is usually steel and may be either a bar or cable. Because the reinforcing element is slender, it offers little bending resistance (particularly in the case of cable), and is treated as a one-dimensional member subject to uniaxial tension (compression not allowed). A one-dimensional constitutive model is adequate for describing the axial behavior of the reinforcing element. In the present formulation, the axial stiffness is described in terms of the reinforcement cross-sectional area, A, and Young's modulus, E.

The incremental axial force is calculated (using the same nomenclature as beam elements) by

$$\Delta F^{(a)} = - \frac{EA}{L} \Delta u^{(a)} \qquad (1.3\text{-}72)$$

where $\Delta u^{(a)} = (u_b^{(1)} - u_a^{(1)})\, t_1 + (u_b^{(2)} - u_b^{(2)})\, t_2$,

the superscript refers to the x(1) or y(2) directions,

the superscripts (b),(a) refer to the nodes of the element, referring to its axial direction.

At present, a yield strength can be assigned to the cable. If a cable force is greater than the yield value, the forces remain at a constant level.

In evaluating the axial forces developed in the reinforcement, displacements are computed at nodal points along the axis of the reinforcement as shown in Fig. 1.3-15. Out-of-balance forces at each nodal point are computed from axial forces in the reinforcement as well as shear forces contributed through the grout annulus. Axial displacements are computed based on accelerations from integration of the law of motion using the computed out-of-balance axial force and a mass lumped at each nodal point.

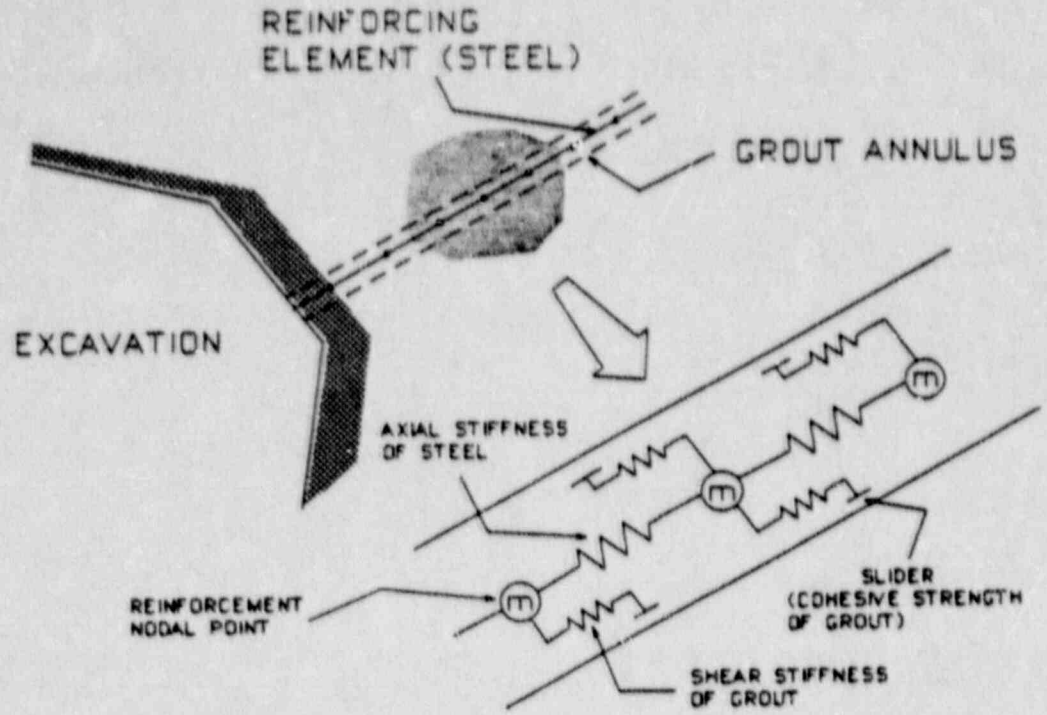

Fig. 1.3-15 Conceptual Mechanical Representation of Fully-Bonded Reinforcement Which Accounts for Shear Behavior of the Grout Annulus

1.3.6.3.2 Shear Behavior of Grout Annulus

The shear behavior of the grout annulus is represented as a spring slider system located at the nodal points shown in Fig. 1.3-15. The shear behavior of the grout annulus during relative displacement between the reinforcing/grout interface and the grout/rock interface is described numerically by the grout shear stiffness (Fig. 1.3-16). Numerical estimates for the shear stress can be derived from an equation describing the shear stress at the grout/rock interface (St. John and Van Dillen, 1983):

$$\tau_G = \frac{G_g}{(D/2+t)} \cdot \frac{u_b - u_r}{\ln(1+2t/D)} \qquad (1.3\text{-}73)$$

where u_b = axial displacement of the bolt,

u_r = axial displacement of the grout/rock interface,

G_g = grout shear modulus,

D = bolt diameter, and

t = annulus thickness.

Consequently, the required grout shear stiffness K_{bond} per unit problem thickness is simply given by

$$K_{bond} = \frac{2\pi\ G_g}{\ln\ (1+2t/D)} \qquad (1.3\text{-}74)$$

In computing the displacement of the grout/rock interface, the following interpolation scheme is used. Consider reinforcement passing through a constant strain-finite difference quadrilateral making up part of the intact rock as shown in Fig. 3-17(a). The incremental x-component of displacement (Δu_{xp}) at the nodal point is given by

$$\Delta u_{xp} = W_1\Delta u_{x1} + W_2\Delta u_{x2} + W_3\Delta u_{x3} + W_4\Delta u_{x4} \qquad (1.3\text{-}75)$$

where Δu_{x1}, Δu_{x2}, Δu_{x3}, Δ_{x4} are the incremental gridpoint x-component displacements, and

W_1, W_2, W_3, W_4 are weighting factors.

The determination of weighting factors is based on satisfying moment equilibrium and involves computation of contributions from subelements.

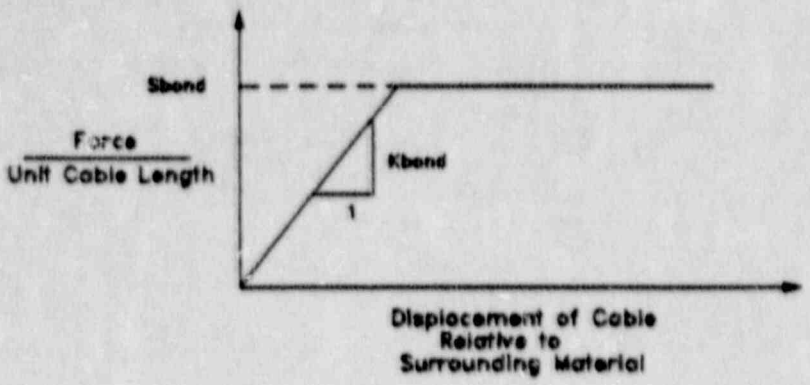

(a)

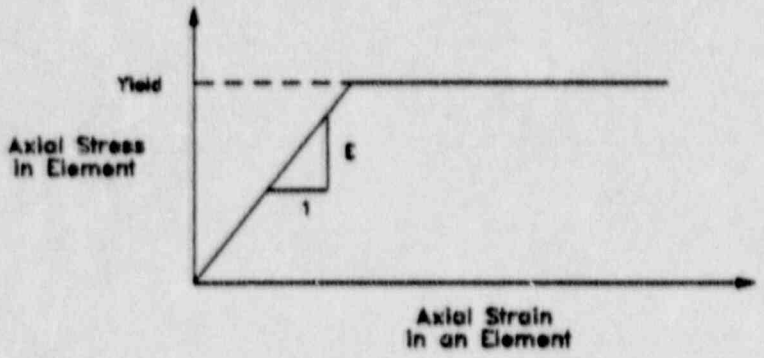

(b)

Fig. 1.3-16 Shear (a) and Axial (b) Behavior of Grouted Cable Elements

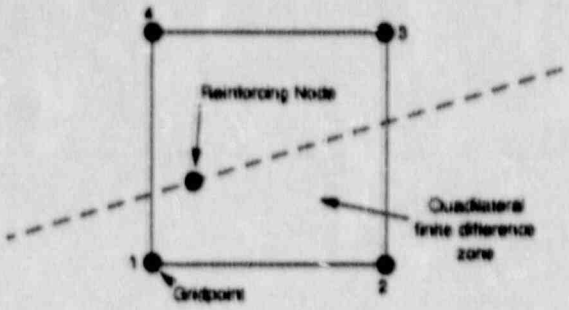

(a) typical reinforcing element passing through a quadrilateral zone

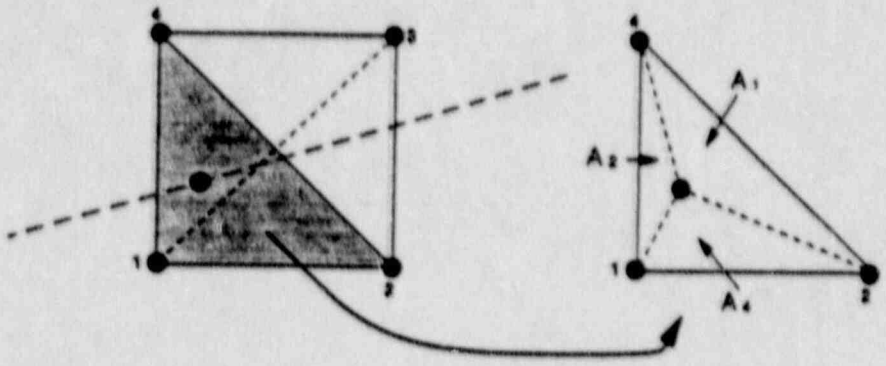

(b) areas from a given subelement used in determining weighting factors for computation of displacement of grout/rock interface

Fig. 1.3-17 Geometry of Quadrilateral Finite Difference Zone and Transgressing Reinforcement Used in FLAC

A similar expression is used for y-component displacements. The weighting factors W_1, W_2, W_3, W_4 are computed from the position of the nodal point within any triangular subelement as follows:

$$W_1 = A_1/A_T \tag{1.3-76}$$

where A_T is the total area of the finite-difference subelement, and

A_1 is the area of the weighting triangle in Fig. 3-17(b).

The final weighting is found by summing the contributions of all triangular subelements and dividing by two, to account for superimposed zoning used in FLAC.

At each timestep, the old gridpoint displacements are used in Eq. (1.3-73) to determine the axial displacement of the grout/rock interface, u_r. Using this displacement and the old cable force, the axial displacement of the bolts due to shearing is determined from Eqs. (1.3-71) and (1.3-72). These new displacements are then proportioned back to the quadrilateral gridpoints using Eq. (1.3-73).

In the present formulation, the maximum amount of shear force per unit length in the grout annulus is limited to a value S_{bond}. The peak shear strength used may be estimated from the results of pull-out tests or, should such results not be available, the peak strength may be estimated as (St. John and Van Dillen, 1983):

$$S_{bond} = \pi\ (D + 2t)\ \tau_I\ Q_B \tag{1.3-77}$$

where τ_I is approximately one-half of the uniaxial strength of the weaker of the rock and grout, and

Q_B is the quality of the bond between the grout and rock (Q_B = 1 for perfect bonding).

The maximum shear force, F_{max}, per unit problem thickness is, therefore, given by

$$F_{max} = S_{bond} \tag{1.3-78}$$

Forces generated at the grout/rock interface (F_{xp}, F_{yp}) are distributed back to gridpoints according to the same weighting factors used previously—i.e.,

$$F_{x1} = W_1 \bullet F_{xp}$$
$$F_{x2} = W_2 \bullet F_{xp} \qquad (1.3\text{-}79)$$
$$F_{x3} = W_3 \bullet F_{xp}$$
$$F_{x4} = W_4 \bullet F_{xp}$$

where F_{x1}, F_{x2}, F_{x3} and F_{x4} are forces applied to the gridpoints.

1.3.6.3.3 2-D/3-D Equivalence

Reducing 3-D problems with regularly-spaced reinforcement to 2-D problems involves averaging the reinforcement effect in 3-D over the distance between the bolts. Donovan et al. (1984) suggest that linear scaling of material properties is a simple and convenient way of distributing the discrete effect of reinforcement over the distance between bolts in a regularly-spaced pattern.

In the present formulation, a scaling factor (f), defined as the ratio of unit problem width (W) to reinforcing spacing (S) perpendicular to the plane of analysis—i.e., $f = W/S$ should be used to scale input material properties E, G_g, and τ_I. For example, if the reinforcing spacing, S, is 2 meters and the unit problem width is 1 meter, the material properties E, G_g and τ_I should all be reduced by a factor of 2.

1.3.6.3.4 Failure at Grout/Reinforcing Interface

Failure of reinforcing systems does not always occur at the grout/rock interface. Failure may occur at the reinforcing/grout interface, as is often true for cable reinforcing. In such cases, the shear stress should be evaluated at this interface. This suggests that the expressions (D+2t) be replaced by (D) in Eqs. (1.3-72) and (1.3-75).

1.3.6.4 Stability and Convergence

The stability of the structural element solution depends on the structural timestep determined automatically by the FLAC code. As done previously for the finite difference zones, structural inertial masses are set equal to the effective stiffness connected to the node in the coordinate directions. The stiffness (i.e., inertial masses) in the x, y and rotational directions are required for timestep calculation, as well as the application of the equation of motion to the structural masses. The stiffness is found by the unit displacement method by alternately fixing $\Delta u_y^{(a)}$ and $\Delta u_y^{(b)}$ and calculating the values of the stiffnesses k_x and k_y.

At end (a) of the beam, for example, let

$$\Delta u_y = 0,$$

$$|\Delta F_x| = \Delta F^{(a)}\ t_1 + \Delta F^{(n)}\ n_1 \qquad (1.3\text{-}80)$$

$$|\Delta F^{(a)}| = \frac{EA}{L}\,\Delta u^{(a)} \quad \text{and} \quad |\Delta F^{(n)}| = \frac{12EI}{L^3} \qquad (1.3\text{-}81)$$

$$\text{where } |\Delta u^{(a)}| = \Delta u_x\ t_1 \text{ , and} \qquad (1.3\text{-}82)$$

$$|\Delta u^{(n)}| = \Delta u_x\ n_1$$

Substituting Eq. (1.3-82) into Eq. (1.3-81) to obtain $|\Delta F^{(a)}|$ and $|\Delta F^{(n)}|$ in terms of Δu_x, the following is obtained:

$$|\Delta F_x| = \frac{EA}{L}\,t_1^2\,\Delta u_x + \frac{12EI}{L^3}\,n_1^2\,\Delta u_x \qquad (1.3\text{-}83)$$

or

$$k_x = \frac{|\Delta F_x|}{|\Delta u_x|} = \frac{EA}{L} t_1^2 + \frac{12EI}{L^3} n_1^2$$

Similarly,

$$k_y = \frac{|\Delta F_y|}{|\Delta u_y|} = \frac{EA}{L} t_2^2 + \frac{12EI}{L^3} n_2^2 \qquad (1.3\text{-}84)$$

and, for rotation,

$$k_r = \left| \frac{\Delta M}{\Delta \theta} \right| = \frac{4EI}{L}$$

The above values k_x, k_y and k_r are local stiffness values for the beam elements which are connected to gridpoints of the finite difference zone. The cable bolt stiffness, k_c, is taken to be

$$k_{bond} \cdot L$$

where L is the effective length of the cable element.

The weighted inertial mass is set equal to the sum of stiffnesses for each node (recall that $\Delta t_c = 1.0$). For the case of a structural node connected to a gridpoint, the inertial mass becomes

$$m_i = m_g + 4.0\ (k_i + k_c)$$
$$m_r = 4.0\ (k_r) \qquad (1.3\text{-}85)$$

where $i = 1,2 = x,y$, and m_g = gridpoint mass.

The multiplier of 4.0 is derived as described previously.

If a structural node is not connected to the grid, then

$$m_i = k_i$$
$$m_r = k_r \qquad (3\text{-}86)$$

where k_i is the sum of the stiffness contributions from each connected beam.

These masses are now used in the motion equation for the beams and cables. Additionally, these stiffnesses effect the calculation of timestep.

Experience with FLAC has shown the structural element formulation to be stable and converge to the quasi-steady state adequately with the present formulation for nearly all cases. Numerical instability has been observed in the case of an end-loaded column with lower pin joint subjected to a velocity load on the free end. This is equivalent to Euler buckling under dynamic loading. It is always possible to modify the code to allow manual reduction of the timestep until stability is obtained; however, the limitations of the structural elements for rapid loading needs to be recognized.

1.3.7 Axisymmetry

1.3.7.1 Introduction

Many common problems in solid body mechanics involve geometries which are symmetric about some axis of rotation. An axisymmetric geometry allows for accurate modeling of the out-of-plane stress component, thereby providing the ability to examine some typical three-dimensional geometries which often occur in geotechnical analysis. Some of these geometries include pillars or laboratory samples, advancing shafts or boreholes, bins, and perhaps some open pit geometries.

1.3.7.2 Formulation of the Axisymmetric Difference Equations

1.3.7.2.1 Basic Assumptions

The axisymmetric problem in FLAC is treated as a three-dimensional problem in which roller boundaries are used in the x-z plane, radiating from x = 0 (Fig. 1.3-18). As the angle θ approaches 0, the solution approaches the case of axisymmetry. Because θ cancels from all equations, this condition is always met, and the equations can be expressed in terms of rectangular, rather than polar, coordinates. Stresses can therefore be expressed in terms of σ_{11}, σ_{12}, σ_{22} and σ_{33}, where σ_{33} is the out-of-plane component.

It is assumed that x = 0 is the axis of symmetry and any gridpoints that have x = 0 (within a tolerance) are fixed in x. For large strains, any gridpoints which move to x = 0 are also fixed.

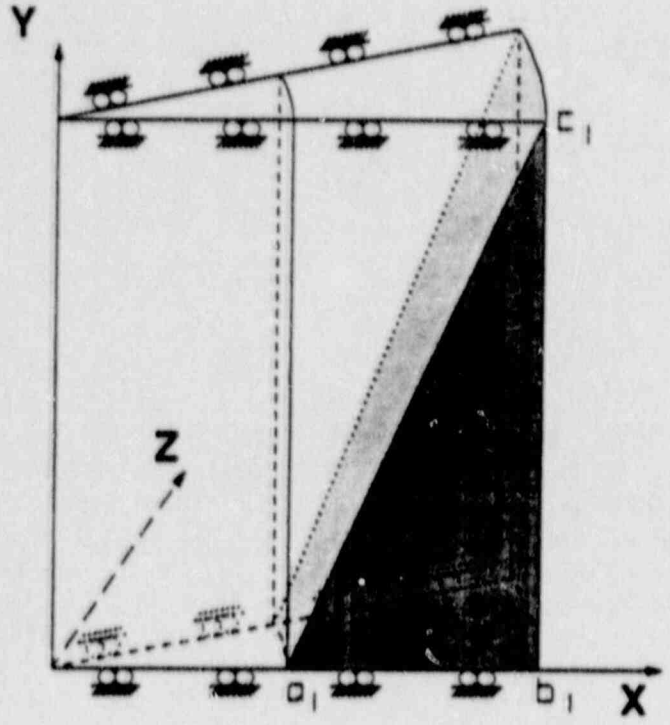

Fig. 1.3-18 Axisymmetry Treated As a Special Three-Dimensional Case

1.3.7.2.2 Strain Increments from Gridpoint Velocities

The Gauss divergence formula in three dimensions is given by

$$\left\langle \frac{\partial f}{\partial x_i} \right\rangle = \frac{1}{V} \sum_{\text{faces}} \langle f \rangle \, n_i \, \Delta A \qquad (1.3\text{-}87)$$

where faces = the five faces of a triangular zone,

ΔA = area of a face,

V = volume of a zone, and

f = a scalar, vector or tensor.

A typical triangular wedge element is shown in Fig. 1.3-19, and is defined by its five faces. Edge face (b_1, b_2, a_2, a_1) is shown in this figure. Note that edges (a_1-a_2, b_1-b_2, c_1-c_2) have a radius of curvature but are assumed to be straight. The top surface of the wedge (face a,b,c) is in the x-z plane. The outward normals of the edge faces are given by

$$\begin{aligned} n_1 &= S_2/s \\ n_2 &= -S_1/s \\ n_3 &= 0 \end{aligned} \qquad (1.3\text{-}88)$$

where n_1,n_2 are the x and y normals to the face, s, in the x-y plane,

$S_1 = (x_1^b - x_1^a)$, and

$S_2 = (x_2^b - x_2^a)$.

For the triangular faces, $n_1 = 0$, $n_2 = 0$, and $n_3 = 1$ for the a_1,b_1,c_1 side, and $n_1 = -\sin\theta$, $n_3 = \cos\theta$ for the a_2,b_2,c_2 side.

For any given edge face, <f> is determined by

$$\langle f \rangle = \frac{1}{A} \int f \, dA = \frac{1}{A} \int\int f \, dx_1 \, ds \qquad (1.3\text{-}89)$$

where, from Fig. 1.3-19(b), $A = |s| \, \theta \, \frac{x_1^a + x_1^b}{2}$.

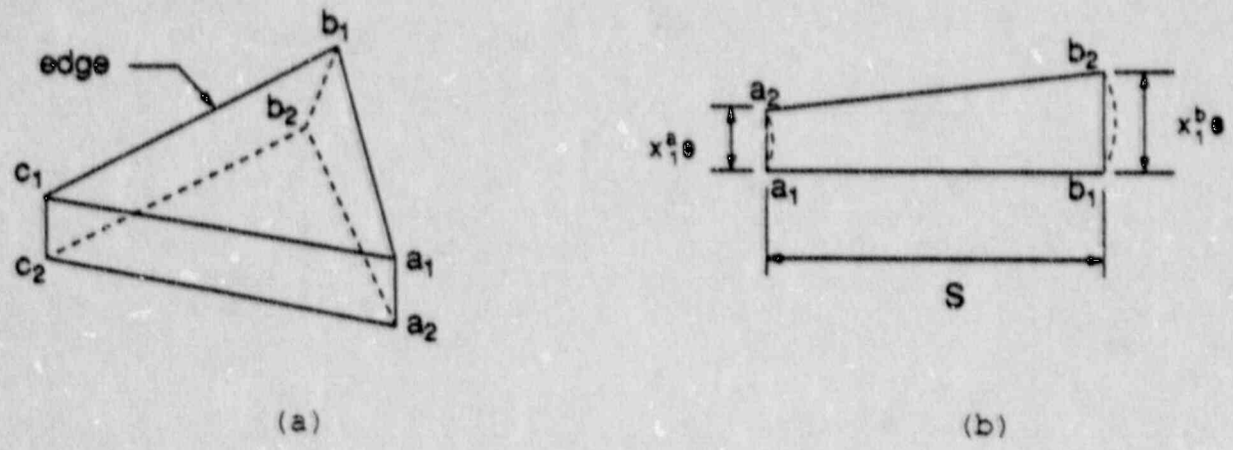

Fig. 1.3-19 (a) Wedge Element and (b) View of Edge a-b

Through a transformation to local coordinates, Eq. (1.3-89) becomes

$$\langle f \rangle = \frac{\theta}{A} \int_0^1 f x_1 \, |s| \, d\xi \qquad (1.3\text{-}90)$$

where $f = f_a \, \xi + (1 - \xi) \, f_b$, and

$$x_1 = x_1^a \, \xi + (1 - \xi) \, x_1^b.$$

Substituting expressions for A, f and x, and solving:

$$\langle f \rangle = \frac{1}{3}\left[f_a + f_b + \frac{x_1^a f_a + x_1^b f_b}{x_1^a + x_1^b} \right] \qquad (1.3\text{-}91)$$

The volume, V, of the wedge element in Fig. 1.3-19(a) may be found from the Gauss divergence formula for the gradient of x_i along x_i:

$$\frac{\partial x_i}{\partial x_i} = \frac{1}{V_{faces}} \Sigma \langle x_i \rangle n_i \Delta A \qquad (1.3\text{-}92)$$

and, since the left-hand side is the sum of the gradients in each of the three directions, the volume is

$$V = \frac{1}{3}\left[\sum_{5 \text{ faces}} (x_1 n_1 + x_2 n_2 + x_3 n_3) \Delta A \right] \qquad (1.3\text{-}93)$$

By substitution from Eq. (1.3-89) and the normals,

$$V = \frac{1}{3}\left[\sum_{3\ \text{sides}}\left[\left[\langle x_1\rangle\,(x_2^b - x_2)\,\frac{(x_1^a + x_1^b)}{2}\right]\theta + \left[-\langle x_2\rangle\,(x_1^b - x_1^a)\,\frac{(x_1^b + x_1^a)}{2}\,\theta\right]\right] + \left[-\sin\theta\ \bar{x}_1\ A_\Delta + \cos\theta\ \bar{x}_3\ A_\Delta\right]\right] \tag{1.3-94}$$

where A_Δ is the area of the triangular face,

$$\bar{x}_1 = (x_1^a + x_1^b + x_1^c)/3\ , \text{ and}$$

$$\bar{x}_3 = \theta\ \bar{x}_1 .$$

Since, as $\theta \to 0$, $\sin\theta \to \theta$, and $\cos\theta \to 1$, the last two terms cancel. Substituting for $\langle x_1\rangle$ and $\langle x_2\rangle$ from Eq. (1.3-89) Eq. (1.3-94) reduces to

$$V = \theta\ \bar{x}_1\ A_\Delta \tag{1.3-95}$$

The volume term can be calculated for the four triangular subelements in FLAC (a,b,c,d), where A_Δ for a,b,c,d are the same as in the 2-D version.

Knowing <f> and V, expressions for the difference formulas for the gradients of <f> can be derived:

$$\frac{\partial f}{\partial x_1} = \frac{1}{V} \Sigma \langle f \rangle n_1 \Delta A$$

$$= \frac{1}{2A_\Delta} [x_2^a (f_c - f_b) + x_2^b (f_a - f_c) + x_2^c (f_b - f_a)] \qquad (1.3\text{-}96)$$

and

$$\frac{\partial f}{\partial x_2} = - \frac{1}{2A_\Delta} [x_1^a (f_c - f_b) + x_1^b (f_a - f_c) + x_1^c (f_b - f_a) \qquad (1.3\text{-}97)$$

The above expressions can be used to determine the gridpoint velocity, gradients and, hence, the strain components from the standard expression,

$$\Delta e_{ij} = \frac{1}{2} \left[\frac{\partial \dot{u}_i}{\partial x_j} + \frac{\partial \dot{u}_j}{\partial x_i} \right] \Delta t \qquad (1.3\text{-}98)$$

The out-of-plane strain component, e_{33}, can be found from

$$\frac{\partial \dot{u}_3}{\partial x_3} = \dot{e}_{33} = \frac{\dot{u}_3}{\theta r} = \frac{\overline{\dot{u}}}{\overline{x}} = \left[\frac{\dot{u}_1^a + \dot{u}_1^b + \dot{u}_1^c}{x_1^a + x_1^b + x_1^c} \right] \qquad (1.3\text{-}99)$$

since $x_3 = \theta x_1$, and

$\dot{u}_3 = \theta \dot{u}_1$.

1.3.7.2.3 Mixed Discretization

The mixed discretization procedure, described previously, is again used in the axisymmetry to ensure accurate solutions for plasticity. Recall that each quadrilateral is divided into two sets of triangular elements: A and B; and C and D. A similar procedure is used for both sets. A and B are used here as an example of the mixed discretization procedure.

Prior to calling the constitutive laws, the strains (calculated in the subroutine STRESAX) are averaged using the mixed discretization procedure. For a quadrilateral, the normal strain increments are averaged by

$$\dot{e}_{kk}^{AB} = \frac{\dot{e}_{kk}^{A} V^{A} + \dot{e}_{kk}^{B} V^{B}}{V^{A} + V^{B}} \qquad (1.3\text{-}100)$$

where $\dot{e}_{kk}^{AB}$ = averaged strain increments,

$\dot{e}_{kk}^{A}$, $\dot{e}_{kk}^{B}$ = strain increments from triangles A and B, and

V^{A}, V^{B} = volume of triangles A and B (see Fig. 1.3-1).

The strain increments from A and B are given by

$$\dot{e}_{kk}^{A} = \frac{\partial \dot{u}_1^{(A)}}{\partial x_1} + \frac{\partial \dot{u}_2^{(A)}}{\partial x_2} + \frac{\partial \dot{u}_3^{(A)}}{\partial x_3} \qquad (1.3\text{-}101)$$

Strain increments are determined separately; then, the average normal strain increment is determined. From the average, the individual increments are determined.

For example, the strain increments for triangle A are:

$$\dot{e}_{11}^{A} = \frac{1}{3}\,\dot{e}_{kk}^{AB} + \dot{e}_{11}^{A\,(dev)}$$

where $\dot{e}_{11}^{A\,(dev)} = \dfrac{\partial \dot{u}_1^{(A)}}{\partial x_1} - \dfrac{1}{3}\,\dot{e}_v^{(A)}$, and (1.3-102)

$$\dot{e}_v^{(A)} = \frac{\partial \dot{u}_1^{(A)}}{\partial x_1} + \frac{\partial \dot{u}_2^{(A)}}{\partial x_2} + \frac{\partial \dot{u}_3^{(A)}}{\partial x_3}$$

There is no correction necessary for shear strains, as they are decoupled from normal strains and are given by

$$\dot{e}_{12}^{A} = \frac{1}{2}\left[\frac{\partial \dot{u}_1}{\partial x_2} + \frac{\partial \dot{u}_2}{\partial x_1}\right]$$

1.3.7.2.4 Averaging of Pressure Terms

After calling the constitutive law, and prior to determination of equivalent gridpoint forces, the pressures in triangular zones are averaged using the mixed discretization procedure. Again, for the A-B triangle pair:

$$\overline{\sigma_0}^{AB} = \frac{\sigma_0{}^{A}\, v^{A} + \sigma_0{}^{B}\, v^{B}}{v^{A} + v^{B}} \qquad (1.3\text{-}103)$$

where $\sigma_0^A = \frac{1}{3} (\sigma_{11}^A + \sigma_{22}^A + \sigma_{33}^A)$, and

$$\sigma_0^B = \frac{1}{3} (\sigma_{11}^B + \sigma_{22}^B + \sigma_{33}^B).$$

The stresses, adjusted for the pressure term, are

$$\sigma_{11}'^A = \sigma_{11}^{A\,(dev)} + \bar{\sigma}_0^{AB}, \text{ etc., for normal stresses} \qquad (1.3\text{-}104)$$

where $\sigma_{11}^{A\,(dev)} = \sigma_{11}^A - \sigma_0^A$, etc.

σ_{12} is unaffected by correction.

1.3.7.2.5 Determination of Gridpoint Forces From Stresses

In the 2-D version of the code, x- and y-component stresses within each zone are assumed to act over a line segment which connects the centroids of the zone surrounding any specific gridpoint. The stresses are transformed to equivalent x- and y-oriented forces using the length of these line segments and are applied to the gridpoint. In the axisymmetric case, the stresses are applied over an area of the triangle subelement rather than a line segment.

The area over which σ_{11} acts for gridpoint calculation for point a is shown in Fig. 1.3-20. The area of the region, A_r, is $(A_{de} + A_{ef})$, which is given by:

$$A_r = \theta \frac{x_1^c + x_1^e}{2} (x_2^d - x_2^e) + \theta \frac{(x_1^e + x_1^f)}{2} (x_2^e - x_2^f) \qquad (1.3\text{-}105)$$

where the coordinates at d, e and f are assumed to be the averaged coordinates of the corner points. In terms of the corner coordinates, Eq. (1.3-105) reduces to

$$A_r = \frac{\theta}{24} \left[- 2A_\Delta + 3 \left(2x_1^a + x_1^b + x_1^c\right) \left(x_2^b - x_2^c\right) \right] \qquad (1.3\text{-}106)$$

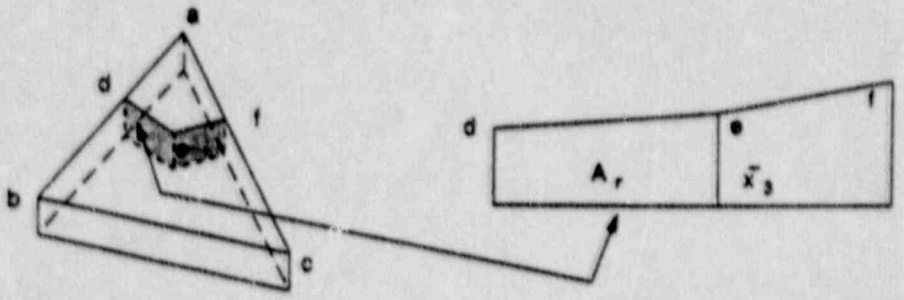

Fig. 1.3-20 Triangular Subelement Showing Area for Gridpoint Force Calculation at Gridpoint a

In the axisymmetry model, the gridpoint masses are determined in the same way as in the 2-D case—that is, no regard is given to the out-of-plane direction. Therefore, the masses are scaled by a factor of the order of the thickness of the wedge element, θx_1. The θ term in the above equation may therefore be replaced by $(1/x_1)$ to scale forces to account for the mass in the third direction.

The force contribution from the z-direction can be found by examining the area upon which the force acts. The projection of the area of the triangular subregion representing gridpoint a (area a,f,e,d of Fig. 1.3-20) perpendicular to x is given by:

$$A = - n_x \frac{A_\Delta}{3} \qquad (1.3\text{-}107)$$

where $\frac{A_\Delta}{3}$ is 1/3 the area of the triangular element, and

$$n_x = -\sin\theta. \tag{1.3-108}$$

The out-of-plane force component will be

$$F_3 = -\sigma_{zz} \sin\theta \frac{A_\Delta}{3} \tag{1.3-109}$$

or, normalizing by the scaling factor $1/(x_1^a\theta)$,

$$F_3 = \frac{1}{3} \sigma_{zz} \frac{A_\Delta}{x_1^a} \tag{1.3-110}$$

This completes the major changes in the differencing logic necessary for axisymmetry. The changes necessary in the constitutive models to account for axisymmetry are described in Section 1.4, Constitutive Models.

Other sections in the code concerning force application must also be modified for axisymmetry. These include applied external forces and gravitational forces.

1.3.7.2.6 Equivalent Applied Forces

Similar logic is used for the conversion of stress to gridpoint force, as previously described. Figure 1.3-21 shows an edge of the triangular zone.

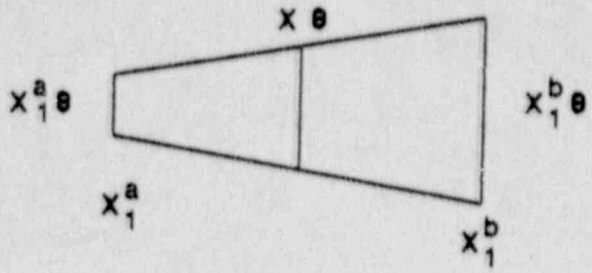

Fig. 1.3-21 Nomenclature for Gridpoint Force Calculation in Axisymmetry, Typical "Edge" Shown

For example, the x-force for gridpoint a is found from

$$F_x^{(a)} = F_x \left[\frac{\bar{x} + x_1^a}{2} \left[\frac{x_1^b + x_1^a}{2} - x_1^a \right] \right] \qquad (1.3\text{-}111)$$

or

$$= F_x \frac{3x_1^a + x_1^b}{4x_1^a}$$

where use has again been made of the scaling factor $1/(x_1^a)$.

1.3.7.2.7 Equivalent Gravitational Forces

The gravitational force component must consider the volume of an element for calculation of equivalent gridpoint forces. Figure 1.3-22 shows an element, as before.

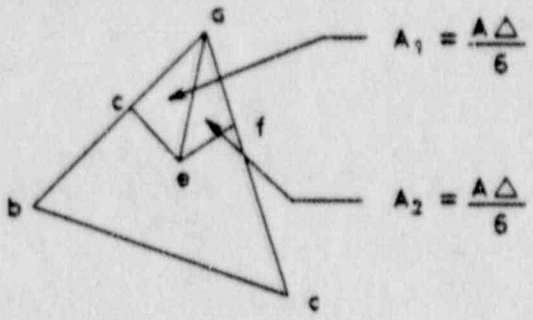

Fig. 1.3-22 Triangular Element Subdivided for Gravity Force Calculation

The volume of the triangular subelements A_1 and A_2 are found from

$$V = \theta \bar{x} \Sigma A_i \qquad (1.3\text{-}112)$$

where $\bar{x}$ is the average coordinate of the triangle.

The applied gravitational force is

$$F_g = \rho g V \qquad (1.3\text{-}113)$$

1.3.7.3 Stability and Convergence

The stability and convergence of the axisymmetric model is subject to the same constraints as described in previous sections.

1.3.7.4 Limitations

It is not reasonable to run all constitutive models in axisymmetric mode due to symmetry considerations. The models not included in the axisymmetric logic are transversely isotopic, ubiquitous joint, and strain softening.

1.4 COMPONENT MODELS

1.4.1 General

1.4.1.1 Methodology for Coupling of Mechanical Models for Transient Problems

This section of the document describes the component mechanical constitutive models available in FLAC. All of the laws are non-transient in nature (i.e., quasi-static), but may be solved in combination with either the thermal or groundwater transient logic. The type of coupling between these models is illustrated in Fig. 1.4-1. The mechanical and thermal models, although both available within the FLAC program, act essentially as uncoupled codes. The thermal model provides temperatures and thermal stresses to the mechanical model. Only the WIPP creep law given here has temperature-dependent mechanical properties. The mechanical model does not provide any "feedback" response to the thermal model. As discussed in Section 1.3, this is not considered to be a restrictive assumption for geotechnical purposes.

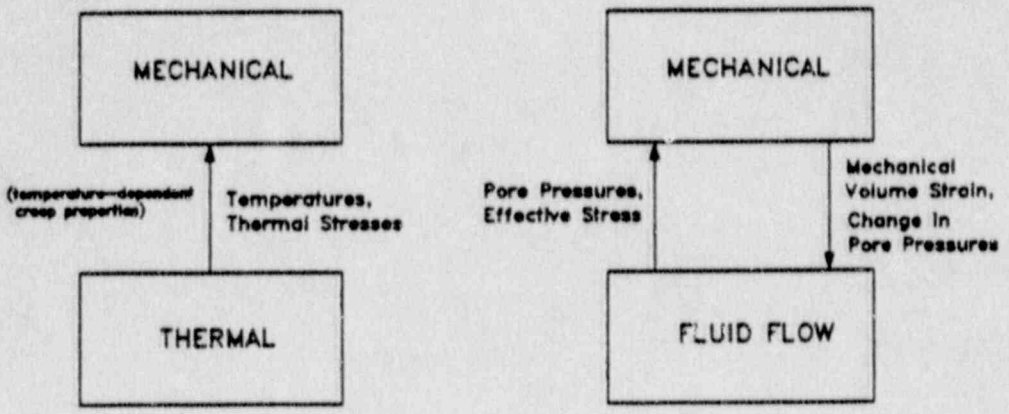

Fig. 1.4-1 Means of Coupling Transient and Mechanical Models in FLAC

A typical thermomechanical problem is conducted in the following fashion. First, the thermal problem is run to a given time t, at which the mechanical state of the body is required. The thermal portion of the code is decoupled, or not solved, and mechanical timesteps are conducted until the body reaches equilibrium or a steady state. The thermal stresses are merely treated as additional out-of-balance forces at the gridpoints. The thermal stresses may result in stress failure for models which allow thermal behavior. This procedure is valid as long as:

(1) for non-linear mechanical models, the temperature should not rise and fall prior to conducting mechanical steps since this process may be load-path dependent;

(2) for creep models, the coupling between thermal and mechanical models needs to be performed with great caution. The creep timestep must be set manually, but must be performed compatibly with the thermal timestep. Since the creep timestep is set manually, stability in the solution is not insured if not chosen correctly.

The fluid flow model can be operated with mechanical behavior decoupled or in a coupled fashion. The coupling methodology is shown in Fig. 1.4-2.

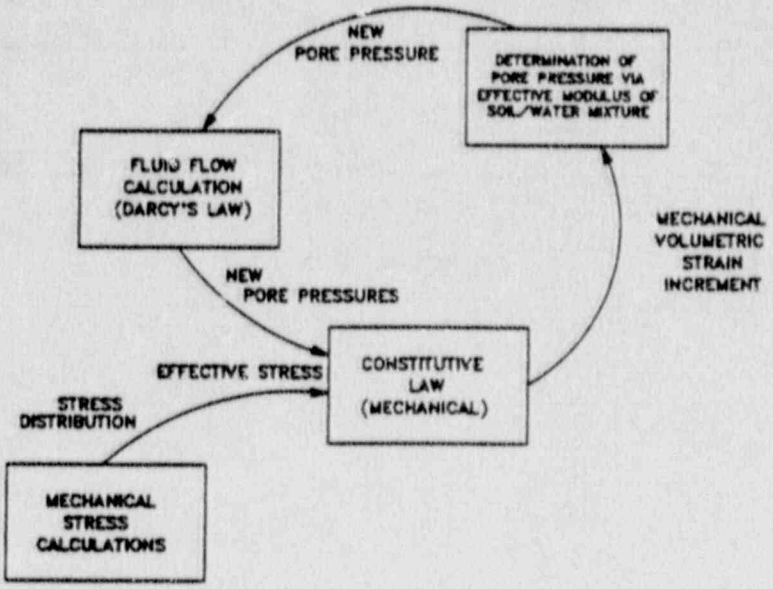

Fig. 1.4-2 Method of Fluid/Mechanical Coupling

During the timestepping procedure, Darcy's Law is invoked, and fluid flow timesteps are conducted. The number of fluid timesteps prior to mechanical steps is controlled by the user. The sequence shown in Fig. 1.4-2 is conducted once per timestep (i.e., one fluid timestep per one mechanical timestep), as the default. The fluid flow calculations result in an updated pore pressure distribution. These pore pressures are added to the total mechanical normal stress components determined from the nodal force balance. The effective stress for a zone is given by $\sigma'_{kk} = \sigma^T_{kk} - P$. The effective stresses are then used in the constitutive law for determination of stress increments. Volumetric strain increments are applied to the fluid/solid mixture to determine pore pressure increments. The coupling here is performed via the bulk modulus of the mixture, $K_m := K + K_w/n$. The mean stress increment due to fluid pressure change from the volume strain is given by

$$\Delta\sigma_0 = \Delta e_v \frac{K_w}{n} \qquad (1.4\text{-}1)$$

Figure 1.4-3 illustrates the conceptual representation of the fluid stiffness effects on the overall stiffness of the system.

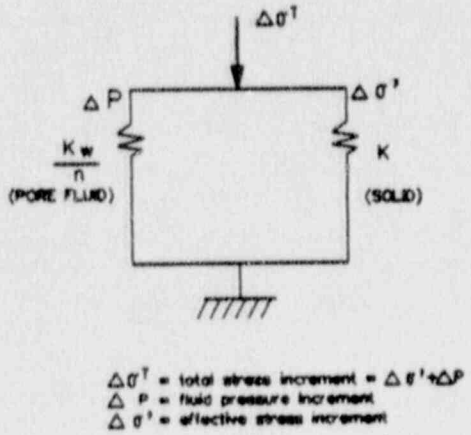

Fig. 1.4-3 Schematic of the Effect of Pore Fluid Stiffness on the Total System Stiffness for Fluid-Solid Coupling

These new pore pressures are then used to drive fluid flow via Eq. (1.3-55). The pore pressure effects can result in non-linear material behavior for the plasticity constitutive laws. For example, yield may occur in a Mohr-Coulomb material as fluid pressure is increased, as the effect of pore pressure is to translate the Mohr's circle toward the origin along the normal stress axis (see Fig. 1.4-4).

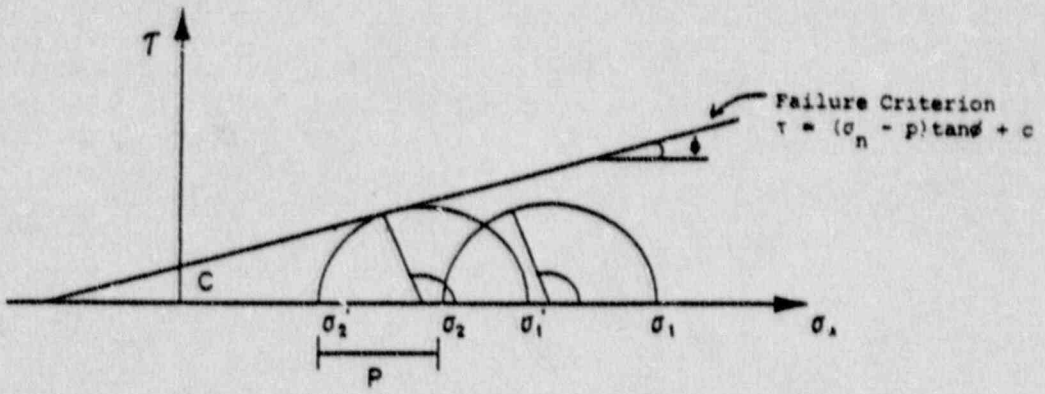

Fig. 1.4-4 Effects of Pore Pressure on the Stress State

The fluid/mechanical coupling may also result in the transient consolidation of the solid—for example, fluid flow as a result of poro-elastic/plastic aquifer compaction beneath a footing.

1.4.1.2 General Methodology for Implementation of Constitutive Laws

All constitutive laws in FLAC use the same general numerical procedure. Rather than repeat this discussion in the following sections, it is given once here, and simply referred to in each section concerning derivation of the numerical model. Figure 1.4-5 shows the basic calculation procedure employed by FLAC for a given zone for a single timestep. At the beginning of a timestep, the following quantities are available to FLAC (calculated from the previous timestep): (1) total stresses in each zone; (2) gridpoint velocities; (3) pore pressures at each gridpoint (if applicable); (4) temperatures at each gridpoint (if applicable); and (5) total plastic strain (if using the strain-hardening/softening model).

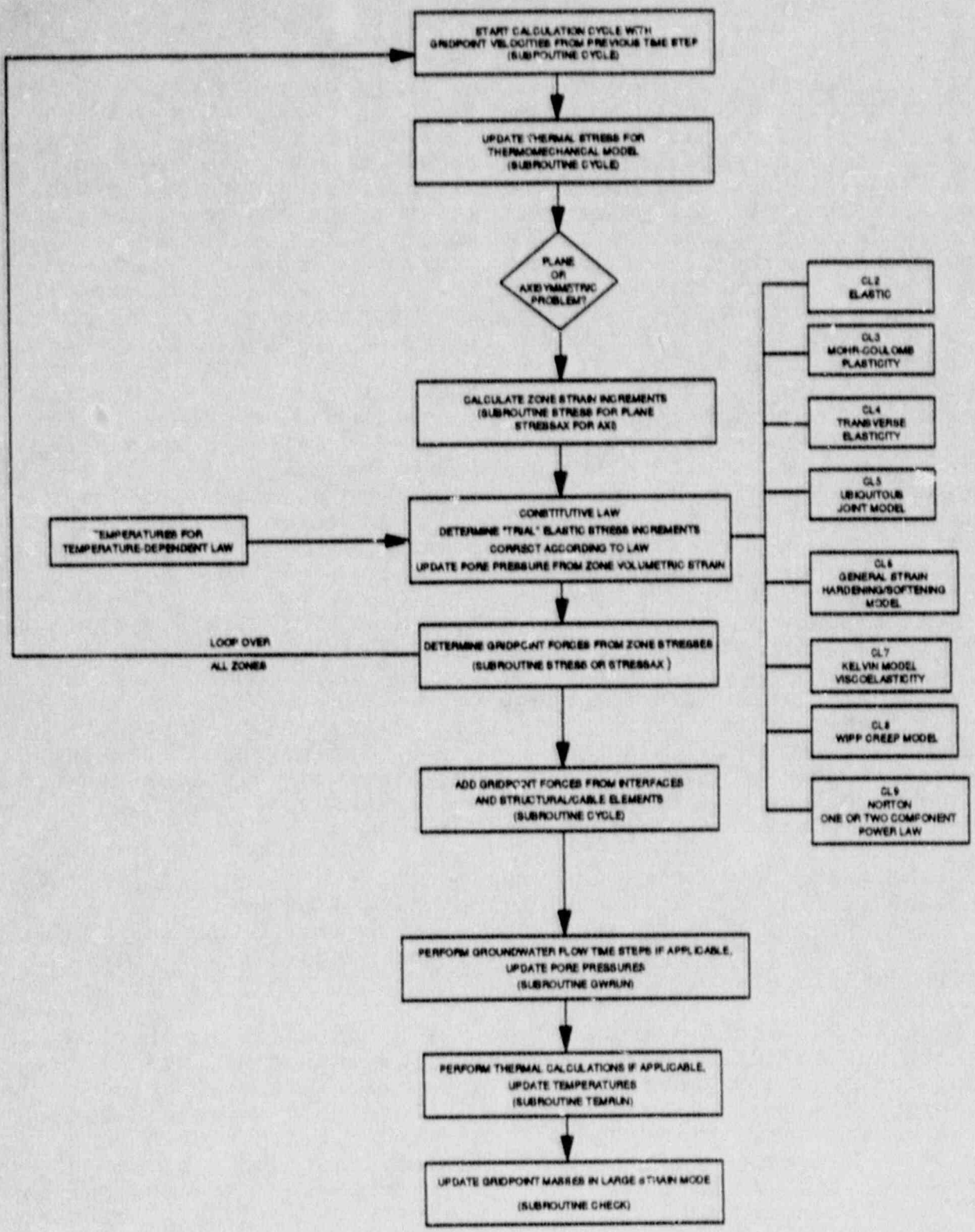

Fig. 1.4-5 Methodology for Constitutive Law Implementation (one timestep loop shown)

The main timestepping routine, CYCLE, loops over the total number of timesteps specified by the user for all zones in the grid. Mechanical timesteps are first conducted. If a thermomechanical analysis is being performed, the thermal stresses are updated through a call to subroutine TSTRES. The strain increments are calculated from the gridpoint velocities (from the previous timestep) by calling subroutine STRESS or STRESAX—the former for plane problems, the latter for axisymmetric problems. Here, the existing pore pressures (from the previous timestep) are used, if applicable, to convert stresses to effective stresses. The constitutive law, with the exception of the creep model, first determines trial elastic stress increments from the strain increments determined in STRESS. For elastic or transversely-elastic models, no correction is necessary, and the code continues. However, if a non-elastic model is used, the effective stresses are used as input to a failure criteria or creep law. If yield is occurring, correction to the stresses are made, via a non-associated flow rule, so that they are not in violation of the yield function. For the creep models, the incremental strains are used to determine new stress increments.

The new stresses are returned to subroutine STRESS, where the zone stresses are averaged by the mixed discretization method. The stresses are then converted to equivalent gridpoint forces and returned to the main timestepping routine, CYCLE. Here, the gridpoint force contribution from the interfaces and structural elements are added in to determine the out-of-balance force sums at each gridpoint. The gridpoint pore pressures are also updated via the mechanical volumetric strain increments for each zone. This is done prior to fluid flow timesteps.

Next, thermal and fluid flow timesteps are conducted, if applicable. Routines TEMRUN and GWRUN are called for thermal and fluid flow steps, respectively. Finally, prior to application of the equation of motion, the gridpoint lumped masses are updated if large strain mode is invoked.

The equations of motion (subroutine MOTION) are implemented to complete the calculation cycle. Using the out-of-balance forces and gridpoint masses, this routine determines the velocities of the gridpoints and the updated coordinates in large-strain mode. This ends the calculation cycle. Non-linear constitutive laws require no iteration to a system of equations. The stresses are determined corresponding to the failure criteria or stress-strain law. Also, the explicit procedure allows no additional computation if differing constitutive laws or properties are used for each zone. There is also very little additional computation necessary for non-linear constitutive laws. The timestepping

procedure described here is conducted until the out-of-balance force approaches a small value. This occurs when the problem approaches equilibrium or a steady flow condition. A typical problem may require 500 to 2000 timesteps to arrive at this condition, depending on constitutive model, number of zones, and gradients of stress.

1.4.2 Elastic, Isotropic Model

1.4.2.1 Purpose

The elastic model describes the simplest form of material behavior. The purpose is to provide for thermoelastic and elastic calculations where linear elastic assumptions are reasonable.

1.4.2.2 Assumptions and Limitations

The elastic model is valid for homogeneous, isotropic, continuous materials which exhibit linear stress-strain behavior with no hysteresis on unloading. The model may be applicable under certain loading regimes and where hysteretic behavior is unimportant, or of limited extent. Also, no material rupture is provided. FLAC assumes that the heat transfer is decoupled from the elastic-mechanical analysis. This, in turn, assumes that there is no mechanical coupling to the energy equation, and that the inertia term in the motion equation can be ignored. These assumptions mean that mechanical strain does not liberate heat, and that stress changes caused by acceleration during heating are small. These effects are negligible for non-dynamic problems.

The primary limitation of this model is that rock often exhibits non-linear material behavior, particularly in an environment of low confining stress (see, for example, Brady and Brown, 1985). Also, deriving elastic properties for this model often involves empirical reduction factors applied to laboratory measurements.

1.4.2.3 Notation

Table 1.4-1 gives the notation used in FLAC for the elastic model. The elastic constitutive law is found in subroutine CL2; the thermal stress calculation is performed in subroutine TSTRES.

Table 1.4-1

ELASTIC MODEL NOTATION

Variable Notation			
Algebraic	Computer	Comment	Where Found
K	zx(kk)	bulk modulus	zx( ) is a material properties array contained in the main common block FLACOM.
G	zx(kg)	shear modulus	
σ_{11}	s11	xx-stress component	passed through common block /STATE/
σ_{22}	s22	yy-stress component	
σ_{12}	s12	xy-stress component	
Δe_{11}	de11	xx-strain increment	
Δe_{22}	de22	yy-strain increment	
Δe_{12}	de12	xy-strain increment	
k^*	stark	maximum confined modulus	

1.4.2.4 Derivation

Hooke's Law in incremental form is given by the following equations.

Plane Strain:

$$\Delta\sigma_{11} = \alpha_1 \Delta e_{11} + \alpha_2 \Delta e_{22}$$

$$\Delta\sigma_{22} = \alpha_2 \Delta e_{11} + \alpha_1 \Delta e_{22} \qquad (1.4\text{-}2)$$

$$\Delta\sigma_{12} = 2G \Delta e_{12}$$

$$\Delta\sigma_{21} = \Delta\sigma_{12}$$

where $\alpha_1 = K + (4/3)G$,

$\alpha_2 = K - (2/3)G$,

K = bulk modulus, and

G = shear modulus.

$$\Delta e_{ij} = \frac{1}{2}\left[\frac{\partial \dot{u}_i}{\partial x_j} + \frac{\partial \dot{u}_j}{\partial x_i}\right]\Delta t \qquad (1.4\text{-}3)$$

where Δe_{ij} = the incremental strain tensor,

$\dot{u}_i$ = the displacement rate, and

Δt = time step.

In plane stress, these equations become

$$\begin{aligned}\Delta\sigma_{11} &= \beta_1 \Delta e_{11} + \beta_2 \Delta e_{22}\\ \Delta\sigma_{22} &= \beta_2 \Delta e_{11} + \beta_1 \Delta e_{22}\\ \Delta\sigma_{12} &= 2G \Delta e_{12}\\ \Delta\sigma_{21} &= \Delta\sigma_{12}\end{aligned} \qquad (1.4\text{-}4)$$

where $\beta_1 = \alpha_1 - (\alpha_2^2/\alpha_1)$, and

$\beta_2 = \alpha_2 - (\alpha_2^2/\alpha_1)$

For axisymmetric geometry, the third stress component is given by

$$\Delta\sigma_{33} = \alpha_2 \Delta e_{11} + \alpha_2 \Delta e_{22} + \alpha_1 \Delta e_{33} \qquad (1.4\text{-}5)$$

The incremental thermal stress components are given by

$$\Delta\sigma_{ij} = - \delta_{ij}\, 3K\, \alpha\, \Delta T \qquad (1.4\text{-}6)$$

where $\Delta\sigma_{ij}$ = stress increment,

K = bulk modulus,

α = linear isotropic thermal expansion coefficient,

ΔT = temperature change in a zone, and

δ_{ij} = Kronecker's delta.

1.4.2.5 Application

This model is applicable to any problem within the assumptions and limitations given in Section 1.4.2.2. This is particularly true in hard rock masses which exhibit little yield for the given stress conditions.

1.4.2.6 Numerical Method Type

No new or unique numerical models are used.

1.4.2.7 Derivation of Numerical Model

FLAC uses the general logic illustrated in Fig. 1.4-5 for solution of the elastic problem. Because the solution is elastic, no constitutive corrections to the stresses are required. By default, the code assumes plane strain; however, plane stress conditions can be used at the discretion of the user Fig. 1.4-5 illustrates the calculation cycle for one zone per timestep. The code loops over all zones, using the velocities and total stresses calculated at the previous timestep to determine incremental strains for the present timestep. At the completion of the calculation loop for each zone, the new stresses are converted to equivalent gridpoint forces. The out-of-balance forces tend to converge to zero at equilibrium or steady flow conditions. The number of timesteps required to reach this state varies from problem to problem, and must be determined by the user. A typical elastic problem may require around 500 timesteps to converge to equilibrium.

1.4.2.8 Location

The major subroutine used in the elastic model (in addition to those given in Section 1.4.1.2) is CL2, which contains the constitutive law logic. This subroutine is called by STRESS.

1.4.2.9 Numerical Stability and Accuracy

The numerical stability of the elastic model is determined by the timestep used for calculation. As described previously, the critical mechanical timestep is defined for each gridpoint using the sum of the stiffnesses attached to the given gridpoint. The program uses a safety factor of 2.0 for the mechanical timestep, to ensure stability. The thermal and fluid flow timesteps are similarly formulated to ensure stability. The damping scheme used can provide slightly overdamped solutions which generally approach the true solution from below. This is not always the case, as some problems involving creep or plastic flow have shown slightly underdamped solutions. Experience with the program shows that the timestep and damping schemes provide stable solutions for all mechanical models, with the possible exception of the creep models if the timestep variation is not chosen carefully.

It is impossible to develop a rigorous assessment of accuracy for any problem, as it depends on many factors, including mesh discretization and application of boundary conditions. It is generally accepted that creation of a finer mesh discretization, as well as location of infinite boundaries at great distance from the excavations (greater than 10 radii), will provide acceptably accurate solutions.

1.4.2.10 Alternatives

Other alternatives provided include a variety of constitutive models for representation of anisotropic elastic or non-linear behavior.

1.4.3 Elastic, Transversely-Isotropic Model

1.4.3.1 Purpose

The purpose of this model is to provide for the ability to model layered elastic media which exhibit elastic behavior, but moduli which are different in the direction perpendicular and parallel to the direction of anisotropy.

1.4.3.2 Assumptions and Limitations

This model has primarily the same limitations as the isotropic elastic model, with the exception that transverse isotropy is allowed in the elastic properties. This means that layered media which may have distinctly different moduli in two directions may be modeled.

There are limitations to which the elastic properties may be varied. Wardle (1980) gives these restrictions based on the restriction that strain energy must be positive:

$$E_1 > 0;\ E_2 > 0;\ F_2 > 0;\ 1 > \nu_1 > -1;\ 1 - \nu_1 - 2\nu_{12}\,\nu_{21} > 0$$

where E_1 = modulus of elasticity in plane of isotropy,

E_2 = modulus of elasticity in plane perpendicular to isotropy,

ν_1 = Poisson's ratio, effect of normal strain in 1 direction on complementary strain in 1 direction,

ν_{12} = Poisson's ratio, effect of 1 direction strain on 2 direction,

ν_{21} = Poisson's ratio, effect of 2 direction strain on 1 direction, and

$F_2 = E_2/(1 + \nu_2)$.

1.4.3.3 Notation

Table 1.4-2 gives the notation used in the elastic, transversely-isotropic model.

Table 1.4-2

ELASTIC, TRANSVERSELY-ISOTROPIC MODEL NOTATION

Variable Notation			
Algebraic	Computer	Comment	Where Found
ϕ	zx(kang)	angle of anisotropy anti-clockwise from x axis	zx( ) is a properties array in the main program common block FLACOM.
G_{11}	zx(kg)	cross shear modulus	
E_1	zx(kxmod)	modulus parallel to anisotropy	
E_2	zx(kymod)	modulus perpendicular to anisotropy	
ν_{12}	zx(knuyx)	Poisson's ratio relating to yx	
ν_{31}	zx(knuzx)	Poisson's ratio relating to zx	
		Stress and strain increments are as noted in Table 1.4-1.	

1.4.3.4 Derivation

For a transversely-isotropic body, FLAC assumes that the plane of isotropy lies within the x-z plane (Fig. 1.4-6).

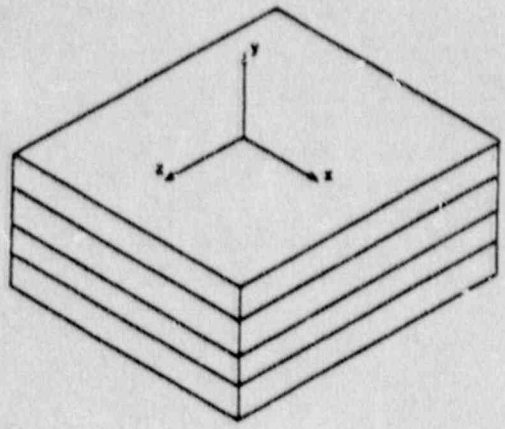

Fig. 1.4-6 Transverse Isotropy Coordinate Axes Convention (x-z direction is plane of isotropy)

For a general orthotropic elastic body, the stress-strain equations are given by Lekhnitskii (1981):

$$\begin{aligned}
\Delta e_{11} &= S_{11}\Delta\sigma_{11} + S_{12}\Delta\sigma_{22} + S_{13}\Delta\sigma_{33} \\
\Delta e_{22} &= S_{21}\Delta\sigma_{11} + S_{22}\Delta\sigma_{22} + S_{23}\Delta\sigma_{33} \\
\Delta e_{33} &= S_{31}\Delta\sigma_{11} + S_{32}\Delta\sigma_{22} + S_{33}\Delta\sigma_{33} \\
\Delta e_{23} &= (1/2)S_{44}\Delta\sigma_{23} \\
\Delta e_{13} &= (1/2)S_{55}\Delta\sigma_{13} \\
\Delta e_{12} &= (1/2)S_{66}\Delta\sigma_{12}
\end{aligned} \qquad (1.4\text{-}7)$$

where: $S_{11} = \cos^4\phi/E_1 + (1/G_{12} - 2\nu_{12}/E_1)\sin^2\phi\cos^2\phi + \sin^4\phi/E_2$,

$S_{22} = \sin^4\phi/E_1 + (1/G_{12} - 2\nu_{12}/E_1)\sin^2\phi\cos^2\phi + \cos^4\phi/E_2$,

$S_{12} = (1/E_1 + 1/E_2 + 2\nu_{12}/E_1 - 1/G_{12})\sin^2\phi\cos^2\phi - \nu_{12}/E_1$,

$S_{13} = -[(\nu_{23}/E_2)\sin^2\phi + (\nu_{13}/E_1)\cos^2\phi]$,

$S_{23} = -[(\nu_{23}/E_2)\cos^2\phi + (\nu_{13}/E_1)\cos^2\phi]$,

$S_{33} = 1/E_3$,

$S_{44} = (\cos^2\phi/G_{23}) + (\sin^2\phi/G_{13})$,

$S_{55} = (\sin^2\phi/G_{23})/(\cos^2\phi/G_{13})$,

$S_{66} = 4(1/E_1 + 1/E_2 + 2\nu_{12}/E_1 - 1/G_{12})\sin^2\phi\cos^2\phi + 1/G_{12}$,

ϕ = angle of anisotropy anti-clockwise from the x-axis (Fig. 1.4-7),

E_1 = modulus of elasticity parallel to x′ axis,

E_2 = modulus of elasticity parallel to y′ axis,

ν_{12} = Poisson's ratio relating normal strain in y′ direction to normal strain in x′ direction,

ν_{31} = Poisson's ratio relating normal strain in x′ direction to normal strain in z direction, and

G_{ij} = cross-shear modulus.

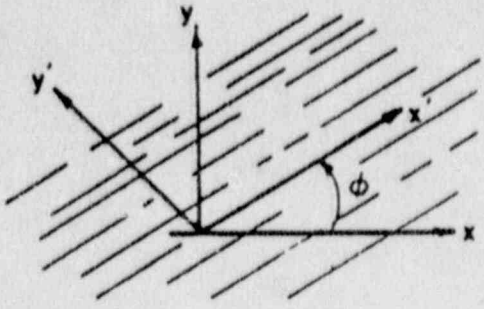

Fig. 1.4-7 Planes of Elastic Anisotropy Oriented at an Angle ϕ From the x-Axis

A state of plane stress with respect to the x-y plane is obtained by setting $\Delta\sigma_{33}=\Delta\sigma_{13}=\Delta\sigma_{23} = 0$ in Eqs. (1.4-7). This gives:

$$\begin{aligned}\Delta e_{11} &= S_{11}\Delta\sigma_{11} + S_{12}\Delta\sigma_{22}\\ \Delta e_{22} &= S_{12}\Delta\sigma_{11} + S_{22}\Delta\sigma_{22}\\ \Delta e_{12} &= 1/2\ S_{66}\Delta\sigma_{12}\end{aligned} \qquad (1.4\text{-}8)$$

The inverse form of these equations are:

$$\begin{aligned}\Delta\sigma_{11} &= (S_{22}\Delta e_{11} - S_{12}\Delta e_{22})/(S_{11}S_{22} - S_{12}^2)\\ \Delta\sigma_{22} &= (-S_{12}\Delta e_{11} + S_{11}\Delta e_{22})/(S_{11}S_{22} - S_{12}^2)\\ \Delta\sigma_{12} &= 2\Delta e_{12}/S_{66}\end{aligned} \qquad (1.4\text{-}9)$$

For a state of plane strain in the x-y plane is obtained from Eqs. (1.4-7) by setting

$$\Delta e_{33} = \Delta e_{13} = \Delta e_{23} = 0 \qquad (1.4\text{-}10)$$

This results in:

$$\begin{aligned}&\Delta\sigma_{13} = \Delta\sigma_{23} = 0,\\ &\Delta\sigma_{33} = -(S_{13}\Delta\sigma_{11} + S_{23}\Delta\sigma_{22})/S_{33}, \text{ and}\\ &\Delta e_{11} = (S_{11} - S^2{}_{13}/S_{33})\Delta\sigma_{11} + (S_{12} - S_{13}S_{23}/S_{33})\Delta\sigma_{22},\\ &\Delta e_{22} = (S_{12} - S_{13}S_{23}/S_{33})\Delta\sigma_{11} + (S_{22} - S^2{}_{23}/S_{33})\Delta\sigma_{22},\\ &\Delta e_{12} = 1/2\ S_{66}\Delta\sigma_{12}.\end{aligned} \qquad (1.4\text{-}11)$$

The inverse form of these equations is:

$$\Delta\sigma_{11} = C_{11}\Delta e_{11} + C_{12}\Delta e_{22}$$

$$\Delta\sigma_{22} = C_{22}\Delta e_{11} + C_{22}\Delta e_{22} \qquad (1.4\text{-}12)$$

$$\Delta\sigma_{12} = 2\, C_{66}\Delta e_{12}$$

where: $C_{11} = (S_{22} - S^2{}_{23}/S_{33})So^2$,

$C_{12} = -(S_{12} - S_{13}S_{23}/S_{33})/So^2$,

$C_{22} = (S_{11} - S_{13}{}^2/S_{33})/So^2$,

$C_{66} = 1/S_{66}$, and

$So^2 = S_{11}S_{22} - S_{12}{}^2 + (2S_{12}S_{13}S_{23} - S_{11}S_{23}{}^2 - S_{22}S_{13}{}^2)/S_{33}$

For the case of transverse isotropy with the plane of isotropy in the x-z plane,

$$E_1 = E_3$$

$$\nu_{12} = \nu_{32} \qquad (1.4\text{-}13)$$

Thermal stress changes are determined from

$$\Delta\sigma_{ij} = \delta_{ij}\, 3K\, \alpha\, \Delta T \qquad (1.4\text{-}14)$$

where $K = \dfrac{E_1\, E_2}{E_2\, 2(1 - \nu_{31}) + E_1\, (1 - 4\, \nu_{21})}$.

1.4.3.5 Application

The elastic, transversely-isotropic model is applicable to any material which exhibits elastic behavior with directionally-dependent response, but with isotropy in one plane. This model may be applicable to layered or jointed hard rock in which the joint surfaces introduce a decrease in the modulus perpendicular to the bedding direction. The restriction here is that the slip between beds may be non-linear, but continuous. Large-scale simulations such as the thermoelastic response of the far-field of a nuclear waste repository in bedded rock may be applicable to this model.

1.4.3.6 Numerical Method Type

No new or unique numerical methods are used in this model.

1.4.3.7 Derivation of Numerical Model

The numerical application of the stress-strain law is conducted identically to the elastic formulation described previously. The total stresses are determined directly from the incremental strain components which have been calculated from gridpoint velocities. These stresses, in turn, are used to determine equivalent gridpoint force components.

1.4.3.8 Location

The elastic, transversely-isotropic model is found in subroutine CL4 and is called from STRESS. Thermal stress change calculation is also found in this subroutine, but called from subroutine TSTRES.

1.4.3.9 Numerical Stability and Accuracy

The previous discussion for the elastic model (Section 1.4.2.9) applies here. Again, the mechanical timestep controls the numerical stability. The maximum modulus term which follows is used in determination of the confined modulus for sound wave speed for timestep calculation (as described in Section 1.3.1):

$$E_1(\max) = E_1 \left[\frac{(1.0 - \nu_{31})}{(1.0 - 2\nu_{13})\ (1 + \nu_{13})} \right]$$

$$E_2(\sigma\max) = E_2 \left[\frac{(1.0 - \nu_{21})}{(1.0 - 2\nu_{12})\ (1 + \nu_{12})} \right] \qquad (1.4\text{-}15)$$

The stability of the solution is also a function of the material properties. As described in Section 1.4.3.2, limits on the material properties are required to enforce strain energy dissipation.

1.4.3.10 Alternatives

The elastic, transversely-isotropic model is restricted in the ratio and magnitude of deformations which can be produced in the plane of isotropy, and the plane perpendicular to it. This restriction is a result of the elastic assumptions as well as the maximum differential moduli required for stability. The ubiquitous joint (anisotropic plasticity) model described in Section 1.4.5 provides an alternative description where interbed slip in closely bedded materials requires a non-linear representation of transverse isotropic behavior.

1.4.4 Mohr-Coulomb Plasticity Model

1.4.4.1 Purpose

The jointed nature of rock masses often results in non-linear material behavior. This behavior (if not time-dependent) is often represented using plasticity theory. One of the most popular representations of plastic material behavior for rock, as well as soil, is the Mohr-Coulomb model.

A large number of investigators have applied this model under a variety of rock and soil conditions. For further discussion on various plasticity failure criteria and application in rock and soil mechanics, see Desai and Christian (1977).

1.4.4.2 Assumptions and Limitations

The assumptions of the Mohr-Coulomb model are:

(1) the material is isotropic; and

(2) there is perfect (ideal) plasticity after the elastic limit is reached.

This model assumes that the material response is elastoplastic. That is, elastic behavior is followed by perfectly-plastic response thereafter, as illustrated in Fig. 1.4-8. Laboratory testing of most rocks and soils shows that yield occurs after load is applied, followed by more-or-less linear response to some peak load at which shear failure of the sample occurs. Load then drops to some residual value where the capacity is approximately constant with continued loading. Depending on the brittleness of the response, and the loading stiffness, this residual strength may be at or near zero. There is some debate as to the existence of "softening" constitutive response as opposed to softening being strictly a geometric effect resulting from failure of the rock.

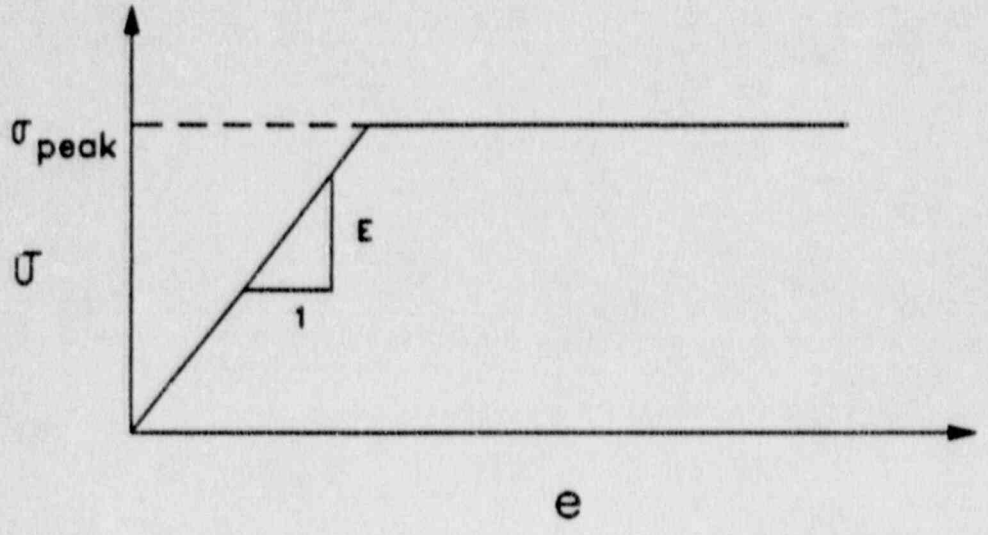

Fig. 1.4-8 Elastoplastic Response

1.4.4.3 Notation

Notation for the Mohr-Coulomb model is given in Table 1.4-3.

Table 1.4-3

MOHR-COULOMB MODEL NOTATION

Variable Notation			
Algebraic	Computer	Comment	Where Found
σ_1	si	maximum principal stress	passed through named common block /state/
σ_2	sii	intermediate principal stress	
σ_3	siii	minimum principal stress	
K	zx(kk)	bulk modulus	zx( ) material properties array located in /FLACOM/
G	zx(kg)	shear modulus	
ϕ	zx(kphi)	friction angle	
ψ	zx(kpsi)	dilation angle	
C	zx(kcoh)	cohesion	
T_0	zx(kten)	tension cutoff strength	
f_{surf}	f	failure criterion	

1.4.4.4 Derivation

1.4.4.4.1 Inclusion of In-Plane Stresses Only

The plasticity formulation in FLAC assumes an elastic, perfectly plastic solid in plane strain or plane stress which conforms to a Mohr-Coulomb yield condition and non-associated flow rule.

The Mohr-Coulomb yield surface is given by:

$$f = \sigma_1 - N_\phi \sigma_2 + 2C\ (N_\phi)^{1/2} \qquad (1.4\text{-}16)$$

and the plastic potential function is given by

$$g = \sigma_1 - N_\psi \sigma_2 + 2C\ (N_\psi)^{1/2} \qquad (1.4\text{-}17)$$

where $N_\xi = (1 + \sin\xi)/(1 - \sin\xi)$ $\quad [\xi = \phi \text{ or } \psi]$,

C = cohesion (positive sign),

ϕ = friction angle,

ψ = dilation angle,

σ_1 = major principal stress

$= 1/2\ ((\sigma_{11} + \sigma_{22}) - [(\sigma_{12}^2 + 1/4)\ (\sigma_{11} - \sigma_{22})^2]^{1/2})$

$= \sigma_p - \sigma_q$, and

σ_2 = minor principal stress

$= 1/2\ ((\sigma_{11} + \sigma_{22}) + [(\sigma_{12}^2 + 1/4)\ (\sigma_{11} - \sigma_{22})^2])$

$= \sigma_p + \sigma_q$.

The yield condition and plastic potential are as shown in Fig. 1.4-9. When the material yields, the stresses must be adjusted to account for plastic strains. The total strain increments are assumed to be the superposition of elastic and plastic strain increments:

$$\Delta e_1 = \Delta e_1^e + \Delta e_1^p$$

$$\Delta e_2 = \Delta e_2^e + \Delta e_2^p \qquad (1.4\text{-}18)$$

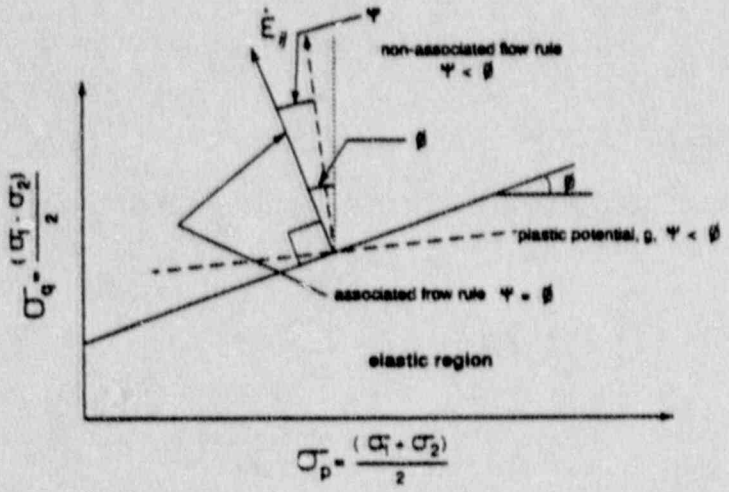

Fig. 1.4-9 Mohr-Coulomb Failure Criteria, f, Showing Tension Cut-Off, Plastic Potential Function, g, and Strain Rate Increments

The plastic strain rates are given by the non-associated flow rule:

$$\dot{e}_1^p = \lambda \frac{\partial g}{\partial \sigma_1} = \lambda$$

$$\dot{e}_2^p = \lambda \frac{\partial g}{\partial \sigma_2} = -\lambda N_\psi \qquad (1.4\text{-}19)$$

where λ is the scalar multiplier which accounts for the fact that incremental strains are being related to finite stress components. For stable, so-called perfectly-plastic, materials, the plastic potential function, g, is said to exist, and is identical to the yield surface, f, at yield. Derivation of the multiplier λ follows.

Multiplying the plastic strain rate [Eq. (1.4-19)] by Δt gives the plastic strain increments:

$$\Delta e_1^P = \lambda \, \Delta t$$

$$\Delta e_2^P = - \lambda N_\psi \, \Delta t \qquad (1.4\text{-}20)$$

Recall that, in FLAC, $\Delta t = 1.0$, but it is left here for clarity.

The incremental principal elastic stresses are given by:

$$\Delta \sigma_1 = \alpha_1 \, \Delta e_1^e + \alpha_2 \, \Delta e_2^e \qquad (1.4\text{-}21)$$

$$\Delta \sigma_2 = \alpha_2 \, \Delta e_1^e + \alpha_1 \, \Delta e_2^e \qquad (1.4\text{-}21)$$

where α_1 and α_2 are the elastic constants given in Eq. (1.4-2).

Substituting Eq. (1.4-18) for the elastic strain increments and Eq. (1.4-20) for the plastic strain increment into Eq. (1.4-21), the incremental principal stresses are expressed as

$$\Delta \sigma_1 = \alpha_1 \, (\Delta e1 - \lambda \Delta t) + \alpha_2 \, (\Delta e_2 + \lambda N_\psi \, \Delta t)$$

$$\Delta \sigma_2 = \alpha_1 \, (\Delta e_2 + \lambda N_\psi \, \Delta t) + \alpha_2 \, (\Delta e_1 - \lambda \Delta t)$$

From a numerical standpoint, an estimate of the stresses must be made at the beginning of the constitutive law. These estimated initial, or "trial", stresses may then be corrected before leaving the constitutive law if yield is indicated. It is convenient to estimate initial stresses based on elastic theory and the total strain (since we do not, as yet, know what portion of the total strain is plastic).

Denoting the initial principal stresses by σ_1^I and σ_2^I, the correction vector $\Delta\sigma_i^c$ can be written in two ways:

$$\Delta\sigma_i^c = \sigma_i - \sigma_i^I = \Delta\sigma_i - \Delta\sigma_i^I \tag{1.4-23}$$

Hence,

$$\sigma_i = \sigma_i^I - (\Delta\sigma_i^I - \Delta\sigma_i)$$

The initial principal stress increments are given by

$$\Delta\sigma_1^I = \alpha_1 \Delta e_1 + \alpha_2 \Delta e_2$$
$$\Delta\sigma_2^I = \alpha_2 \Delta e_1 + \alpha_1 \Delta e_2 \tag{1.4-24}$$

Substituting Eqs. (1.4-22) and (1.4-24) into Eq. (1.4-23) yields the corrected principal stresses in terms of the trial initial stress, the material constants, and the multiplier, λ:

$$\sigma_1 = \sigma_1^I - \lambda\Delta t\ (\alpha_1 - \alpha_2 N_\psi)$$
$$\sigma_2 = \sigma_2^I - \lambda\Delta t\ (\alpha_2 - \alpha_1 N_\psi) \tag{1.4-25}$$

The λ value can be found since σ_1 and σ_2 must lie on the yield surface (if a non-admissible stress state is detected). This is done by substituting Eq. (1.4-25) into the equation for the yield surface [Eq. (1.4-16)] and equating to zero:

$$\lambda\Delta t = \frac{\sigma_1^I - N_\phi \sigma_2^I + 2C (N_\phi)^{1/2}}{\alpha_1 (N_\phi + N_\psi) - \alpha_2 (1 + N_\phi N_\psi)} = \frac{f}{\gamma} \tag{1.4-26}$$

where $\gamma = \alpha_1 (N_\phi + N_\psi) - \alpha_1 (1 + N_\phi N_\psi)$, and

$$f = \sigma_1^I - N_\phi \sigma_2^I + 2C(N_\phi)^{1/2}. \tag{1.4-27}$$

The corrected principal stress components are obtained by simply substituting Eq. (1.4-27) into Eq. (1.4-25):

$$\sigma_1 = \sigma_1^I - (\alpha_1 - \alpha_2 N_\psi) \frac{f}{\gamma} \tag{1.4-28}$$

$$\sigma_2 = \sigma_2^I - (\alpha_2 - \alpha_1 N_\psi) \frac{f}{\gamma}$$

1.4.4.4.2 Inclusion of Out-of-Plane Stress Component

FLAC allows for two methods for consideration of the out-of-plane stress component in the Mohr-Coulomb to constitutive law. First, the user may simply define the out-of-plane stress, σ_{33}, and, second, axisymmetry may be assumed. The following derivation of the Mohr-Coulomb law follows closely that given previously, and is modified from Cundall and Shillabeer (1977):

The failure surface, f, and plastic potential function, g, in terms of principal stress in 3-D are given by

$$f = \sigma_1 - N_\phi \sigma_3 + 2c (N_\phi)^{1/2}$$
$$g = \sigma_1 - N_\psi \sigma_3 + 2c (N_\psi)^{1/2} \qquad (1.4\text{-}29)$$

where N_ϕ, N_ψ are defined as before.

The strain increments are composed of elastic and plastic parts:

$$\Delta e_1 = \Delta e_1^e + \Delta e_1^p$$
$$\Delta e_2 = \Delta e_2^e + \Delta e_2^p \qquad (1.4\text{-}30)$$
$$\Delta e_3 = \Delta e_3^e + \Delta e_3^p$$

The plastic strain increments are found from the non-associated flow rule:

$$\dot{e}_i^p = \lambda \frac{\partial g}{\partial \sigma_i} \qquad (1.4\text{-}31)$$

As before, multiplying each component of Eq. (1.4-31) by the timestep, Δt, yields the plastic strain increments

$$\Delta e_1^p = \lambda \Delta t$$
$$\Delta e_2^p = 0 \qquad (1.4\text{-}32)$$
$$\Delta e_3^p = - \lambda N_\psi \Delta t$$

where in FLAC, Δt is set to 1.0.

The stress increments can be described in terms of elastic constants and elastic strain increment:

$$\Delta\sigma_1 = \alpha_1 \Delta e_1^e + \alpha_2 \Delta e_2^e + \alpha_2 \Delta e_3^e$$

$$\Delta\sigma_2 = \alpha_1 \Delta e_2^e + \alpha_2 \Delta e_1^e + \alpha_2 \Delta e_3^e \qquad (1.4\text{-}33)$$

$$\Delta\sigma_3 = \alpha_1 \Delta e_3^e + \alpha_2 \Delta e_1^e + \alpha_2 \Delta e_2^e$$

where α_1 and α_2 are the elastic constants given in Eq. (1.4-2).

The above equations for elastic stress increments can be formulated in terms of the total strains (Eq. 1.4-30) and plastic strains (Eq. 1.4-32), such that Eq. (1.4-33) becomes

$$\Delta\sigma_1 = \alpha_1 (\Delta e_1 - \lambda) + \alpha_2 \Delta e_2 + \alpha_2 (\Delta e_3 + \lambda N_\psi)$$

$$\Delta\sigma_2 = \alpha_1 \Delta e_2 + \alpha_2 (\Delta e_1 - \lambda) + \alpha_2 (\Delta e_3 + \lambda N_\psi) \qquad (1.4\text{-}34)$$

$$\Delta\sigma_3 = \alpha_1 (\Delta e_3 + \lambda N_\psi) + \alpha_2 (\Delta e_1 - \lambda) + \alpha_2 \Delta e_2$$

The initial (or trial) stress increment, had yielding not occurred, is given as

$$\Delta\sigma_1^I = \alpha_1 \Delta e_1 + \alpha_2 \Delta e_2 + \alpha_2 \Delta e_3$$

$$\Delta\sigma_2^I = \alpha_1 \Delta e_2 + \alpha_2 \Delta e_1 + \alpha_2 \Delta e_3 \qquad (1.4\text{-}35)$$

$$\Delta\sigma_3^I = \alpha_1 \Delta e_3 + \alpha_2 \Delta e_1 + \alpha_2 \Delta e_2$$

where Δe_i are <u>total</u> strains.

Denoting the initial, trial principal stresses by σ_i^I, the correction vector, σ_i^c, can be written in two ways:

$$\Delta\sigma_1^c = \sigma_i - \sigma_i^I = \Delta\sigma_i - \Delta\sigma_i^I \qquad (1.4\text{-}36)$$

Hence, $\sigma_1 = \sigma_1^I - (\Delta\sigma_1^I - \Delta\sigma_i)$.

The corrected stress becomes

$$\begin{aligned} \sigma_1 &= \sigma_1{}^I - \lambda\ (\alpha_1 - N_\psi\ \alpha_2) \\ \sigma_2 &= \sigma_2{}^I - \lambda\ \alpha_2\ (1 - N_\psi) \\ \sigma_3 &= \sigma_3{}^I - \lambda\ (\alpha_2 - N_\psi\ \alpha_1) \end{aligned} \qquad (1.4\text{-}37)$$

The multiplier, λ, may be found by substituting these stresses in the equation for the yield surface, f:

$$f = 0 = \sigma_1 - N\phi\ \sigma_3 + 2C(N_\phi)^{1/2} \qquad (1.4\text{-}38)$$

Substituting and solving for λ yields

$$\lambda = \frac{\sigma_1{}^I - N_\phi\ \sigma_3{}^I + 2C(N_\phi)^{1/2}}{\alpha_1\ (1 + N_\phi\ N_\psi) - \alpha_2\ (N_\phi + N_\psi)}$$

$$= \frac{f}{\gamma}$$

where $\gamma = \alpha_1\ (1 + N_\phi\ N_\psi) - \alpha_2\ (N_\phi + N_\psi)$.

The corrected stresses may be found by substitution of λ into Eqs. (1.4-37).

For two-dimensional applications, two cases are possible: plane strain or plane stress. In plane strain, $\Delta e_{33} = 0$ (i.e., $\Delta e_{33}^e + \Delta e_{33}^P = 0$). However, σ_{33} may be σ_1, σ_2 or σ_3.

If $\sigma_{33} = \sigma_1$, then $\Delta e_1 = \Delta e_1^e + \Delta e_1^P = 0$,

$$-\Delta e_1^e = \Delta e_1^P = \lambda \text{ , and} \qquad (1.4\text{-}40)$$

$$\Delta e_3^P = -\lambda N_\psi \text{ .}$$

In plane stress, $\sigma_{33} = 0$, and the elastic strain component in the out-of-plane direction is given by

$$\Delta e_{33}^e = -\frac{\beta_2}{\beta_1}(\Delta e_{11}^e + \Delta e_{22}^e) \qquad (1.4\text{-}41)$$

where $\beta_1 = \alpha_1 - \alpha_2^2/\alpha_1$, and

$$\beta_2 = \alpha_2 - \alpha_2^2/\alpha_1 \text{ .}$$

The equations for stress correction (σ_1, α_2) are derived as in the general two-dimensional case, as given by Eq. (1.4-28).

1.4.4.5 Application

The Mohr-Coulomb method is applicable in rock or soil masses where isotropic yield occurs. In general, the model is applicable where the rock is heavily jointed: that is, where the ratio of joint spacing to opening radius, S/a, is about 0.25 or less.

1.4.4.6 Numerical Method Type

No new or unique numerical methods are used in this logic.

1.4.4.7 Numerical Method Derivation

Initial elastic trial stresses are determined first from incremental stress derived from gridpoint velocities:

$$\sigma_{11}^{I} = \sigma_{11} + \alpha_1 \Delta e_{11} + \alpha_2 (\Delta e_{22} + \Delta e_{33})$$

$$\sigma_{22}^{I} = \sigma_{22} + \alpha_2 (\Delta e_{11} + \Delta e_{33}) + \alpha_1 \Delta e_{22} \qquad (1.4\text{-}42)$$

$$\sigma_{12}^{I} = \sigma_{12} + 2G \Delta e_{12}$$

If out-of-plane stress components are to be included (at the user's discretion),

$$\sigma_{33}^{I} = \sigma_{33} + \alpha_1 \Delta e_{33} + \alpha_2 (\Delta e_{11} + \Delta e_{22}) \qquad (1.4\text{-}43)$$

where σ_{11}^{I}, σ_{22}^{I}, σ_{33}^{I}, σ_{12}^{I} = initial (trial) stresses, and

σ_{11}, σ_{22}, σ_{33}, σ_{12} = existing stresses.

Note that the user may wish to include the out-of-plane stress component into the formulation. The principal stresses are given by (compression is negative):

$$\sigma_1^{I} = \sigma_p^{I} - \sigma_q^{I}$$

$$\sigma_3^{I} = \sigma_p^{I} + \sigma_q^{I} \qquad (1.4\text{-}44)$$

where $\sigma_p^I = \dfrac{\sigma_1^I + \sigma_3^I}{2}$, and

$$\sigma_q^I = \frac{1}{2}\left[(\sigma_{11}^I - \sigma_{22}^I)^2 + 4\ (\sigma_{12}^I)^2 \right]^{1/2}$$

The stresses are checked against the tension cutoff, T_o, for the two conditions given below. It is essential tnat if the tensile strength is overcome, then the tensile stress immediately drops to zero for that zone, simulating failure:

(1) failure in general tension

If $\sigma_1^I > T_o$,

then $\sigma_{11}^I = \sigma_{22}^I = \sigma_{12}^I = \sigma_{33}^I = T_o = 0.$

(2) failure in uniaxial tension

If $\sigma_3^I > To_o$

then $\sigma_3^I = T_o = 0.$

The failure surface is given by:

$$f = \sigma_1^I - N\phi\ \sigma_3^I + 2C(N_\phi)^{1/2} \qquad (1.4\text{-}45)$$

IF $f > 0$, then the material is elastic, and the stresses are below the yield surface. No stress correction is necessary. However, if $f \leq 0$, then the material is plastic, and the stresses are above the yield surface. Corrections to stresses are made:

$$\sigma_1 = \sigma_1^I - \frac{f}{\gamma}(\alpha_1 - \alpha_2 N_\psi)$$

$$\sigma_2 = \sigma_2^I - \frac{f}{\gamma}(\alpha_2 - \alpha_2 N_\psi) \qquad (1.4\text{-}46)$$

$$\sigma_3 = \sigma_3^I - \frac{f}{\gamma}(\alpha_2 - \alpha_1 N_\psi)$$

where γ is given by Eq. (1.4-39).

σ_1, σ_2, σ_3 are then resolved back to global axes (x,y,z).

Thermal stress increments are the same as given previously for the elastic case:

$$\Delta\sigma_{ij} = -\delta_{ij}\, 3K\, \alpha\, \Delta T \qquad (1.4\text{-}47)$$

where α = linear expansion coefficient.

The thermal stresses are treated in the same manner as elastic stress increments. They are added to σ_{ij} prior to calling the constitutive law routine.

The large strain logic may be significant when the failure models are used. If active plastic flow (i.e., collapse) occurs, large deformations may result. The large strain logic updates grid-point coordinates and masses as well as corrects stresses for rotation of the zone. A check is made every ten timesteps for geometry of the zones. If the area of a triangular subelement is reduced by 20% of the original area, a "bad geometry" message is generated, the run is stopped, and control is transferred to the user via interactive mode. The run may be continued if the element is deleted.

1.4.4.8 Location

The Mohr-Coulomb plasticity is found in subroutine CL3, and is called from subroutine STRESS. The thermal stress increment is also calculated in CL3, but called from subroutine TSTRES.

1.4.4.9 Numerical Stability and Accuracy

The Mohr-Coulomb model is subject to the same stability constraints as described previously. The critical timestep is determined identically as in the elastic case.

A common problem in plasticity models is that of "mesh locking" as described in Section 3.1. FLAC uses the technique of mixed discretization to overcome this problem. Problems 1 and 2 in Volume 3, Example Problems, illustrate the ability of FLAC to adequately predict the standard plasticity solutions for a hole in a circular plate and the bearing capacity for a frictionless material. Simulations of direct shear and uniaxial compression for a material exhibiting dilation show that volumetric strains are calculated properly.

Again, it is impossible to rigorously provide analytic expressions for accuracy for general problems. Example Problem 1 in Volume 3 shows the effects of mesh density, boundary location and boundary condition on problem solution accuracy.

1.4.4.10 Alternatives

For situations where a quick indication of failure potential is needed, the elastic model can be used to calculate elastic stress concentrations. FLAC allows the user to plot "safety factors" of the Mohr-Coulomb and Hoek-Brown yield criteria as the ratio of elastic stresses to allowable yield stresses. No additional corrective calculations are made if the ratio is 1.0 or less. If extensive yield is indicated, the user should conduct a full plasticity analysis as the "empirical safety factor approach" may yield results which contain significant errors.

1.4.5 Ubiquitous Joint Plasticity Model

1.4.5.1 Purpose

Often, the response of the rock mass indicates anisotropic yield as a result of a set of distinct, continuous joints. The ubiquitous joint model provides the ability to model the yielding effects of the joints via a continuum Mohr-Coulomb model rather than explicitly modeling the joints themselves. In effect, this model is an anisotropic Mohr-Coulomb model.

1.4.5.2 Assumptions and Limitations

This model has the following assumptions and limitations:

(1) one joint set is modeled inclined at a constant dip angle from the horizontal;

(2) the spacing of the joints is not modeled explicitly, nor are the stiffnesses of the joints modeled (Only the shear behavior of the joints is modeled. The joints may be considered to be infinitely closely spaced.);

(3) The intact material is assumed to be Mohr-Coulomb;

(4) the joint shear behavior is assumed to conform to the Mohr-Coulomb slip condition; and

(5) the joint aperture change (or void strain) is assumed not to be affected by the shear stress change across the joints.

The ubiquitous joint model describes the behavior of a closely jointed material with one predominant joint set. The joint spacing is not modeled explicitly, but is assumed to be infinitely small and there is no stiffness ascribed to the joints. Therefore, there is no "load sharing" between the intact rock and joints as occurs where intact blocks are separated by fractures. The limitations of this type of model have been described by Blanford and Key (1987).

1.4.5.3 Notation

Table 1.4-4 presents the notation of variables used in this model.

Table 1.4-4

NOTATION USED IN THE UBIQUITOUS JOINT MODEL

Variable Notation			
Algebraic	Computer	Comment	Where Found
θ	zx(kj)	angle of joints anti-clockwise from the horizontal	zx( ) is a material properties array found in the main common block FLACOM.
C_j	zx(kjcoh)	cohesion of joints	
Φ_j	zx(kjf)	friction angle of joints	
T_j	zx(kjten)	tensile strength of joints	
ALL PARAMETERS DEFINED IN TABLE 1.4-3 FOR INTACT MATERIAL ALSO APPLY TO THE UBIQUITOUS JOINT MODEL.			

1.4.5.4 Derivation

Figure 1.4-10 illustrates the weak plane existing in a Mohr-Coulomb solid and the global (x-y) and local (x'-y') coordinate frame.

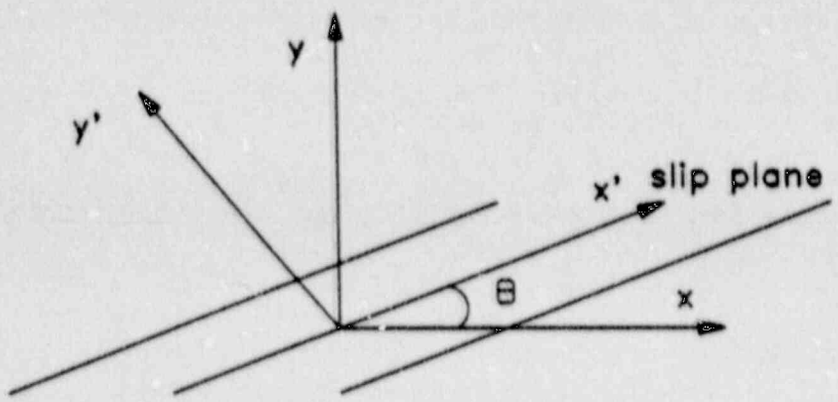

Fig. 1.4-10 A Slip Plane Oriented at an Angle θ to the Global Reference Frame

The Coulomb failure criteria for joints is given by (compression positive):

$$\tau > \sigma_n \tan\phi_j + C_j \qquad (1.4\text{-}48)$$

where τ = shear stress along the joint,

σ_n = normal stress on the joint plane,

ϕ_j = joint friction angle, and

C_j = joint cohesion.

The excess shearing stress along the joint is given by:

$$\Delta\sigma_{12}' = \text{sign}(|\tau|, \sigma_{12}') - \sigma_{12}' \qquad (1.4\text{-}49)$$

where σ_{12}' = shear stress along plane, and

$\Delta\sigma_{12}'$ = shear stress correction along plane.

This correction is added to the global stress state. Indicators are kept which provide a history of the joints for each zone.

1.4.5.5 Application

This model is best applied where a continuous, thinly-spaced joint set exists and controls yield behavior of the rock mass. Examples of applications include bedded deposits overlying excavations of wide expanse (e.g., a longwall coal mine), rock masses with sets of continuous, dominant joint planes, etc.).

1.4.5.6 Numerical Method Type

No new or unique numerical methods are required in this model.

1.4.5.7 Numerical Implementation

Consider the geometry of the slip plane shown in Fig. 1.4-10. The global stresses must be resolved parallel and perpendicular to the potential slip surface:

$$\sigma_{11}' = \sigma_{11}\cos^2\theta + 2\sigma_{12}\sin\theta\cos\theta + \sigma_{22}\sin^2\theta$$

$$\sigma_{22}' = \sigma_{11}\sin^2\theta - 2\sigma_{12}\sin\theta\cos\theta + \sigma_{22}\cos^2\theta \qquad (1.4\text{-}50)$$

$$\sigma_{12}' = -(\sigma_{11} - \sigma_{22})\sin\theta\cos\theta + \sigma_{12}(\cos^2\theta - \sin^2\theta)$$

where θ = joint angle counterclockwise from the x global axis,

σ_{22}' = normal stress on the joint, and

σ_{12}' = shearing stress.

The initial stress increments above (σ_{ij}) are found from the plasticity model presented in Section 1.4.4.4. If the matrix material is currently elastic, then σ_{ij} will simply be the elastic stress increments. If, however, the matrix is yielding, then σ_{ij} will be the stress increments corrected for plasticity. The stresses along the joint are examined for yield:

$$\sigma_{12}' < |\sigma_{22}' \tan\phi| + C \qquad (1.4\text{-}51)$$

where ϕ = joint friction angle, and

C = joint cohesion (positive sign).

If Eq. (1.4-51) is true, then no corrections to the stresses are necessary because slip is not taking place. If Eq. (1.4-51) is false, then slip is occurring, which requires stress corrections. The "excess" shearing stress along the joint is given by

$$\Delta\sigma_{12}' = \text{sign}(\tau, \sigma_{12}') - \sigma_{12}' \qquad (1.4\text{-}52)$$

where $\Delta\sigma_{12}'$ is the shearing correction, and

$\tau = |\sigma_{22}' \tan\phi| + C$.

The corrections to the global stresses can be computed as follows by using the reverse stress transformation:

$$\Delta\sigma_{11} = -2\Delta\sigma_{12}' \cos\theta \sin\theta$$

$$\Delta\sigma_{22} = 2\Delta\sigma_{12}' \cos\theta \sin\theta \qquad (1.4\text{-}53)$$

$$\Delta\sigma_{12} = \Delta\sigma_{12}' (\cos^2\theta - \sin^2\theta)$$

assuming that $\Delta\sigma_{22}' = \Delta\sigma_{11}' = 0$ (i.e., no joint dilation).

These stress corrections are added into the stresses to be used in for determination of gridpoint forces.

Thermal stress components are treated, as before, as elastic trial increments which are added into the existing stress state prior to calling the constitutive model.

1.4.5.8 Location

The ubiquitous joint model is found in subroutine CL5, and called from subroutine STRESS. The thermal stresses are calculated in CL5 and called from subroutine TSTRES.

1.4.5.9 Numerical Stability and Accuracy

The discussion in Section 1.4.4.9 regarding the Mohr-Coulomb model applies to the ubiquitous joint model. This model is experimental in nature and, therefore, no analytic solutions are available to check accuracy. It has been used in comparison to field displacements for a shaft construction in a thinly-bedded quartzite, and yielded reasonable results (Board and Beus, 1989).

1.4.5.10 Alternatives

Two alternatives exist for modeling of the effects of jointing in FLAC. First, if the effects can be considered elastic, the transversely-isotropic elastic model may provide an alternative approach. Second, discrete interfaces may be modeled using the interface logic available within the code.

1.4.6 General Strain Hardening/Softening

1.4.6.1 Purpose

The standard Mohr-Coulomb model described in Section 1.4.4 provides for a peak strength in shear for rock or soil, and assumes that the material exhibits perfectly-plastic response in the post-peak range. Laboratory compression tests of rock and soil may indicate two other forms of post-peak response. These include strain-hardening and strain-softening behavior (Fig. 1.4-11).

The purpose of the strain hardening/softening model is to provide the ability to examine various forms of post-peak response on the macroscopic yield behavior of the material being modeled.

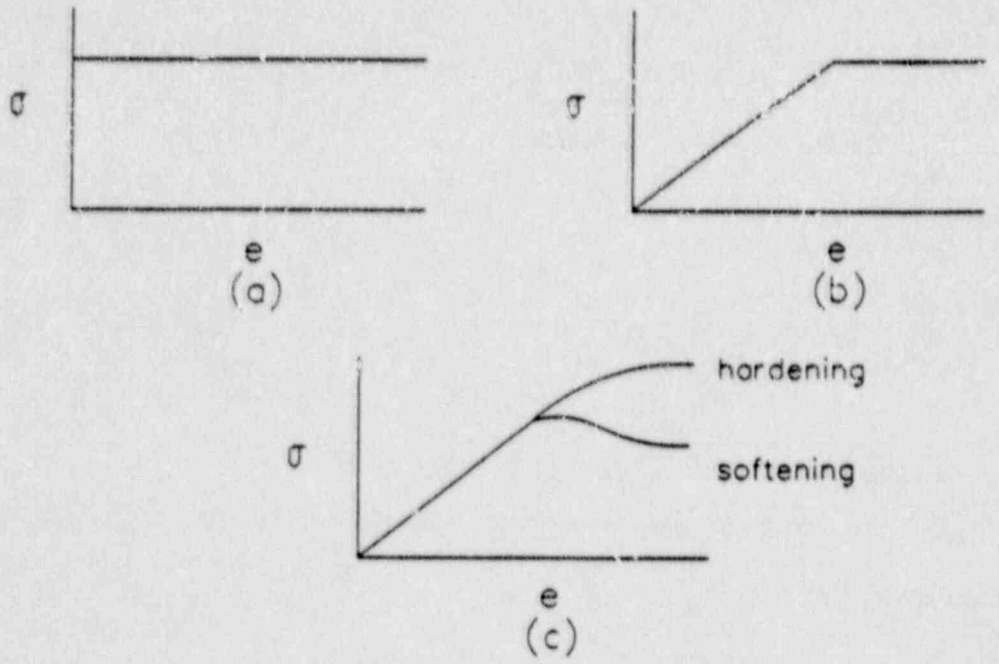

Fig. 1.4-11 Various Forms of Plasticity Illustrating Pre- and Post-Failure Response in Rock and Soil: (a) rigid-perfectly plastic; (b) elastic-perfectly plastic; and (c) strain hardening/softening

1.4.6.2 Assumptions and Limitations

The following assumptions and limitations are inherent to this model.

1. The failure surface is described by the standard Mohr-Coulomb criteria and non-associated flow rule.

2. Post-failure response can be described by the Mohr-Coulomb relation. Essentially, the model represents post-peak response through adjustment of the cohesion, friction and dilation angles as functions of plastic strain, thereby adjusting the location of the failure surface in stress space.

3. The model operates in large or small strain mode.

4. Although the model assumes yield is isotropic for each zone, depending on the plastic strain, the strength properties will change from location to location. As a result, yield may be geometrically highly anisotropic.

The greatest limitation of this model is that not all researchers accept softening behavior as being true constitutive behavior. Softening in the laboratory has been attributed to factors such as sample geometry and test apparatus stiffness effects. Additionally, softening behavior often involves formation of shearing fractures in the material. Localization of plastic strain in a shear band or shear fracture implies that these features have a width. For a given model geometry, this width should be independent of model element dimension. However, in doubling the size of an element, the displacement required for loss of cohesion is also doubled, even though a large portion of plastic strain is contained within the shear band. Maintaining a constant displacement for loss of cohesion in the shear band would require that the plastic strain for cohesion loss be reduced by a proper amount. Estimation of this amount may be very difficult, as the portion of localized strain is not a material constant and will depend on material and stress field inhomogeneity. These limitations are discussed by Whyatt and Board (1988). It is noted that Cundall (1988) and Hobbs and Ord (1989) have successfully produced hardening and softening behavior in FLAC using the standard Mohr-Coulomb model with large strain and random property variations through the body.

1.4.6.3 Notation

Notation for the strain-softening model is given in Table 1.4-5.

Table 1.4-4

NOTATION FOR THE STRAIN-SOFTENING MODEL

Variable Notation

Algebraic	Computer	Comment	Where Found
Δe^p	ep(i)	total plastic strain	subroutine CL6
ϕ	zx(kphi)	friction angle, now treated as a function of ep(i)	zx( ) material array found in the main common common block FIACOM.
c	zx(kcoh)	cohesion, now treated as a function of ep(i)	
ψ	zx(kpsi)	dilation angle, now treated as a function of ep(i)	

THE STRAIN-SOFTENING MODEL USES THE SAME BASIC NOTATION AS THE STANDARD MOHR-COULOMB MODEL, TABLE 1.4-4. THE ONLY DIFFERENCES ARE NOTED ABOVE.

1.4.6.4 Derivation

This constitutive model allows the user to represent arbitrary non-linear material hardening and softening behavior based on the variation of the cohesion, friction, and dilatancy with plastic strain. The model is based on Mohr-Coulomb elasto-plasticity with non-associated flow rule, as described earlier. The difference, however, lies in the ability of the cohesion, friction and dilation to harden or soften after the onset of plastic yield. Here, the user defines the cohesion, friction and dilation as piecewise linear functions of the plastic strain. The code determines the total plastic strain at each time increment and causes the cohesion, friction and dilation to conform to the user-defined functions.

The following derivation is made in terms of global coordinate stresses, σ_{ij}, and strains, e_{ij}, instead of principal stresses, σ_i, and strains, e_i, as described earlier. This is because the current strain level is required to determine the magnitude of the stress drop when calculating yield.

Determination of Plastic Strain Increments

Consider the Mohr-Coulomb yield surface in two dimensions, where stress space is defined by the mean and deviatoric stress components p and q. The principal stresses are given by

$$\sigma_1 = \sigma_p - \sigma_q$$
$$\sigma_2 = \sigma_p + \sigma_q \qquad (1.4\text{-}54)$$

where $\sigma_p = \frac{1}{2}(\sigma_{11} + \sigma_{22})$, and

$$q = \frac{1}{2}\left[(\sigma_{11} - \sigma_{22})^2 + 4\sigma_{12}^2\right]^{1/2}. \qquad (1.4\text{-}55)$$

The Mohr-Coulomb yield surface is given by (Fig. 1.4-12):

$$f = \sigma_1 - (\sigma_2 N_\phi) + 2C(N_\phi)^{1/2} \qquad (1.4\text{-}56)$$

or

$$f = (\sigma_p - \sigma_q) - (\sigma_p + \sigma_q)N_\phi + 2C(N_\phi)^{1/2}$$

where $N_\phi = \dfrac{1 + \sin\phi}{1 - \sin\phi}$,

ϕ = angle of internal friction, and

C = cohesion.

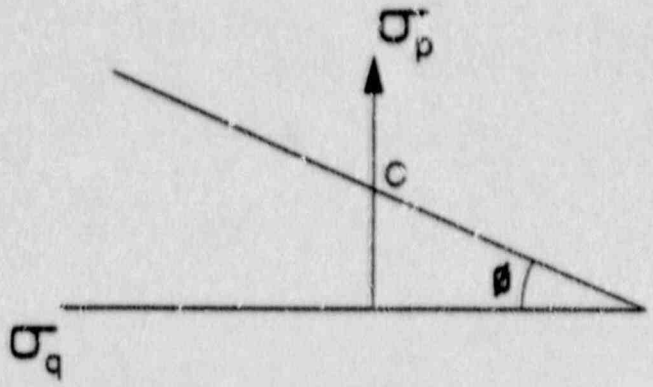

Fig. 1.4-12 Mohr-Coulomb Yield Surface in p-q Space, Compression Negative

The plastic potential function is given by:

$$g = (\sigma_p - \sigma_q) - (\sigma_p + \sigma_q)N_\psi + 2C(N_\psi)^{1/2} \qquad (1.4\text{-}57)$$

where $N_\psi = \dfrac{1 - \sin\psi}{1 + \sin\psi}$, and

ψ = dilation angle.

The plastic strain increments are given by the non-associated flow rule in terms of the plastic potential function and the scalar multiplier λ:

$$\Delta e^P_{11} = -\lambda \frac{\partial g}{\partial \sigma_{11}}$$

$$\Delta e^P_{22} = -\lambda \frac{\partial g}{\partial \sigma_{22}} \qquad (1.4\text{-}58)$$

$$\Delta e^P_{12} = -\lambda \frac{\partial g}{\partial \sigma_{12}}$$

Using the chain rule, the above derivatives may be expanded:

$$\frac{\partial g}{\partial \sigma_{11}} = \frac{\partial g}{\partial \sigma_p} \cdot \frac{\partial \sigma_p}{\partial \sigma_{11}} + \frac{\partial g}{\partial \sigma_q} \cdot \frac{\partial \sigma_q}{\partial \sigma_{11}}$$

$$\frac{\partial g}{\partial \sigma_{22}} = \frac{\partial g}{\partial p} \cdot \frac{\partial \sigma_p}{\partial \sigma_{22}} + \frac{\partial g}{\partial q} \cdot \frac{\partial \sigma_q}{\partial \sigma_{22}} \qquad (1.4\text{-}59)$$

$$\frac{\partial g}{\partial \sigma_{12}} = \frac{\partial g}{\partial \sigma_p} \cdot \frac{\partial \sigma_p}{\partial \sigma_{12}} + \frac{\partial g}{\partial \sigma_q} \cdot \frac{\partial \sigma_q}{\partial \sigma_{12}}$$

Taking the derivatives of Eq. (1.4-57) gives the following:

$$\frac{\partial g}{\partial \sigma_p} = (1 - N_\psi)$$

$$\frac{\partial g}{\partial \sigma_q} = - (1 - N_\psi)$$

$$\frac{\partial \sigma_p}{\partial \sigma_{11}} = \frac{1}{2} \; ; \; \frac{\partial \sigma_p}{\partial \sigma_{22}} = \frac{1}{2} \; ; \; \frac{\partial \sigma_p}{\partial \sigma_{12}} = 0 \qquad (1.4\text{-}60)$$

$$\frac{\partial \sigma_q}{\partial \sigma_{11}} = \frac{(\sigma_{11}-\sigma_{22})}{4\sigma_q} \; ; \; \frac{\partial \sigma_q}{\partial \sigma_{22}} = - \frac{(\sigma_{11}-\sigma_{22})}{4\sigma_q} \; ; \; \frac{\partial \sigma_q}{\partial \sigma_{12}} = \frac{\sigma_{12}}{\sigma_q}$$

Substitution of Eqs. (1.4-59 and 1.4-60) into Eq. (1.4-58) yields

$$\Delta e^P_{11} = - \lambda \left[\frac{1}{2} (1 - N_\psi) - (1 + N_\psi) \frac{(\sigma_{11} - \sigma_{22})}{4\sigma_q} \right]$$

$$\Delta e^P_{22} = - \lambda \left[\frac{1}{2} (1 - N_\psi) + (1 + N_\psi) \frac{(\sigma_{11} - \sigma_{22})}{4\sigma_q} \right] \qquad (1.4\text{-}61)$$

$$\Delta e^P_{12} = - \lambda \left[(1 + N_\psi) \frac{\sigma_{12}}{\sigma_q} \right]$$

An iterative method is used to determine the value of λ which places the stress state on the yield surface (see Section 1.4.6-7). The plastic strain components can then be determined. The cohesion, friction and dilation are defined as piecewise linear segments of a generally non-linear function of the total plastic strain. For example, assume the rock mass has a stress-strain curve which softens upon yield and attains some residual strength (Fig. 1.4-13):

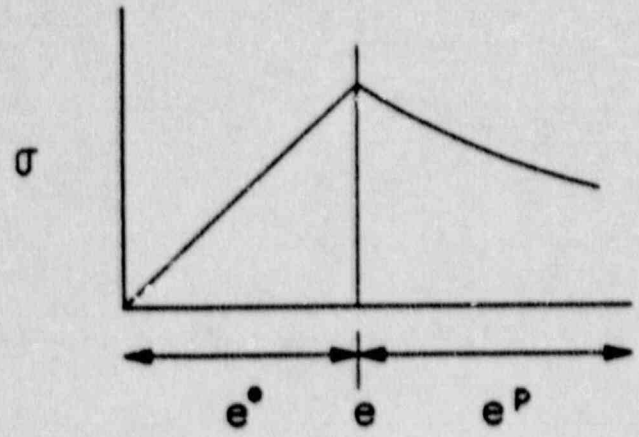

Fig. 1.4-13 General Form of Stress-Strain Curve Showing Elastic and Plastic Strain

The stress-strain curve is linear to the point of yield, therefore, the strain will be elastic only (e^e). After yield, the total strain will be composed of elastic and plastic parts. This model requires the user to define the cohesion, friction and dilation variance as a function of the plastic portion of the total strain. These functions are, in reality, most likely non-linear (Fig. 1.4-14):

However, they may be approximated for use in FLAC as a set of linear segments (Fig. 1.4-15):

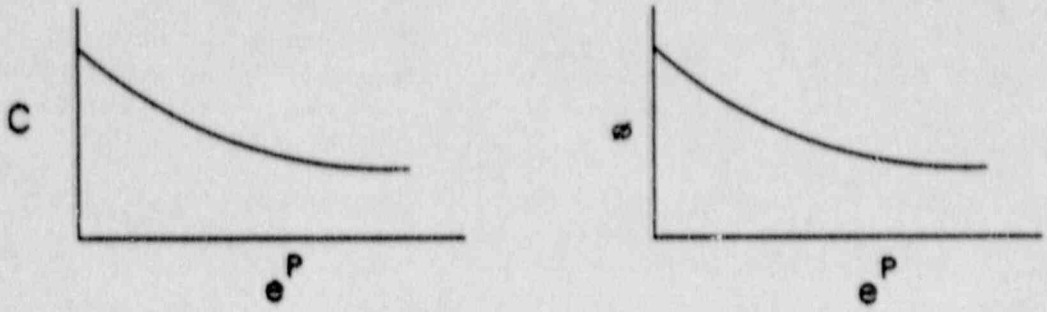

fig. 1.4-14 Cohesion and Friction Represented as Non-Linear Functions of Plastic Strain

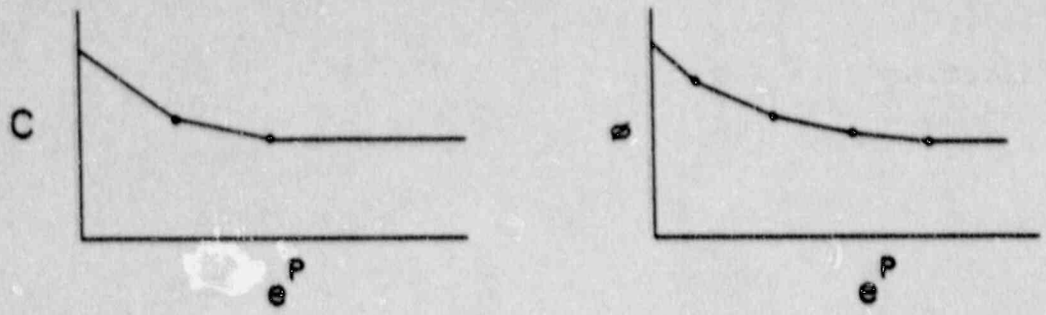

Fig. 1.4-15 Cohesion and Friction Idealized as Piecewise Linear Functions of Plastic Strain

1.4.6.5 Application

This model is considered experimental in nature and is particularly applicable to cases in which collapse or shear fracture occurs in initially-homogeneous materials.

1.4.6.6 Numerical Method Type

Newton's method is used for iteratively determining the stress location of the yield surface.

1.4.6.7 Derivation of Numerical Model

This routine performs the following tasks:

(1) sets up tables of C, Φ and Ψ values as functions of accumulated plastic strain;

(2) using trial initial elastic stresses, Newton's method is used to iteratively find the stress state on yield surface, based on the non-associated flow rule;

(3) determines plastic strain increments and keeps track of accumulated plastic strain; and

(4) adjusts properties, as necessary, based on accumulated plastic strain.

The incoming strain increments to the constitutive law are taken as initial elastic strain increments:

$$\Delta e_{ij}^{I} = \Delta e_{ij}^{e} = \Delta e_{ij} \qquad (1.4\text{-}62)$$

where Δe_{ij} are strains determined from gridpoint velocities.

Initially, it is assumed that there is no plastic strain increment

$$\Delta e_{11}^{P} = \Delta e_{22}^{P} = \Delta e_{12}^{P} = 0 \qquad (1.4\text{-}63)$$

Trial elastic stresses are calculated using Hooke's Law:

$$\begin{aligned} \sigma_{11}^{I} &= \overset{0}{\sigma}_{11} + \alpha_1 \Delta e_{11}^{e} + \alpha_2 \Delta e_{22}^{e} \\ \sigma_{22}^{I} &= \overset{0}{\sigma}_{22} + \alpha_2 \Delta e_{11}^{e} + \alpha_1 \Delta e_{22}^{e} \\ \sigma_{12}^{I} &= \overset{0}{\sigma}_{12} + 2G \Delta e_{11}^{e} + \alpha_1 \Delta e_{22}^{e} \end{aligned} \qquad (1.4\text{-}64)$$

where $\overset{0}{\sigma}_{ij}$ are old stresses, and

α_1, α_2 are the elastic constants given in Eq. (1.4-2).

The mean and deviatoric stresses are given by:

$$\sigma_p = \frac{1}{2} (\sigma_{11} + \sigma_{22}) \qquad (1.4\text{-}65)$$

$$\sigma_q = \frac{1}{2} \left[(\sigma_{11} - \sigma_{22})^2 + 4\sigma_{12}^2 \right]^{1/2}$$

The failure surface, f, and plastic potential, g, are given by:

$$f = (\sigma_p - \sigma_q) - (\sigma_p + \sigma_q) N_\phi + 2C (N_\phi)^{1/2}$$

$$g = (\sigma_p - \sigma_q) - (\sigma_p + \sigma_q) N_\psi + 2C (N_\psi)^{1/2} \qquad (1.4\text{-}66)$$

where N_ϕ, N_ψ are as defined previously.

If f is positive, then the elastic stresses are within the yield surface, and no adjustment to the stresses are required. If f is negative, the stresses must be adjusted.

The plastic strain increments are based on the gradients of the plastic potential, and are given by:

$$\Delta e_{11}^p = - \lambda \frac{\partial g}{\partial \sigma_{11}} = - \lambda (C_1 - C_2 S)$$

$$\Delta e_{22}^p = - \lambda \frac{\partial g}{\partial \sigma_{22}} = - \lambda (C_1 + C_2 S) \qquad (1.4\text{-}67)$$

$$\Delta e_{12}^p = - \lambda \frac{\partial g}{\partial \sigma_{12}} = - \lambda \left(C_3 \frac{\sigma_{12}}{2\sigma_q}\right)$$

$$S = \frac{\sigma_{11} - \sigma_{22}}{4\sigma_q}$$

where $C_1 = \frac{1}{2} (1 - N_\psi)$,

$$C_2 = \frac{1}{2}\,(1 + N_\psi), \text{ and}$$

$$C_3 = -\,2.0\,(1 + N_\psi).$$

Note that the gradients are based on values of stress at the start of the timestep.

The new elastic stresses are given by

$$\sigma_{11} = \sigma_{11}^{I} + \alpha_1\,\Delta e_{11}^{e} + \alpha_2\,\Delta e_{22}^{e}$$

$$\sigma_{22} = \sigma_{22}^{I} + \alpha_2\,\Delta e_{11}^{e} + \alpha_1\,\Delta e_{22}^{e} \qquad (1.4\text{-}68)$$

$$\sigma_{12} = \sigma_{12}^{I} + 2G\,\Delta e_{11}^{e} + \alpha_1\,\Delta e_{22}^{e}$$

The iteration scheme used to determine σ_{ij} and Δe_{ij}^{P} is performed as follows.

1. A tolerance of $\tau = 0.001 \times \max\,[|\sigma_p|, |\sigma_q|, |C|]$ is established for convergence to the yield surface.

2. The elastic stress increments are calculated via Eq. (1.4-2), and used to compute the yield function, f. If the absolute value of f is less than the tolerance, convergence is achieved, and the stresses lie on the yield surface. If the tolerance is not met, the plastic strains are determined from:

$$\Delta e_{ij}^{P} = -\,\lambda\,\frac{\partial g}{\partial \sigma_{ij}} \qquad (1.4\text{-}69)$$

The value of λ is varied by

$$\lambda^{n+1} = \lambda^n + \Delta\lambda^n \qquad (1.4\text{-}70)$$

where $\Delta\lambda^n = - \dfrac{f^n \, \Delta\lambda}{f^n - f^{n-1}}$, and

n denotes the iteration number.

At the start of the iteration process, λ is set to

$$\lambda^i = - \frac{\tau}{\max[\alpha_1, \alpha\sigma_2]} \qquad (1.4\text{-}71)$$

New elastic strains are determined from

$$\Delta e_{ij}^e = \Delta e_{ij} - \Delta e_{ij}^P \qquad (1.4\text{-}72)$$

These elastic increments are used to determine new elastic stresses, σ_{ij}^n and, hence, control returns to step 2. If convergence is not achieved in ten iterations, the final mean elastic stress values are chosen as the corrected stresses. The iteration also halts if ($|f^n - f^{n-1}| < 10^{-6} \max [|\sigma_p|, |\sigma_q|, |C|]$). In this case, the stress tensor is unchanged: $\sigma_{ij} = \sigma_{ij}^{n-1}$.

At the completion of the iteration process, the plastic strain increments, Δe_{ij}^P, and the corrected stresses, σ_{ij}, are available. Recall that FLAC divides each quadrilateral element into four overlapping triangular subelement zones. Subroutine STRESS (which calls the constitutive laws) invokes the constitutive laws one triangle at a time (as described in Section 3.1). Because these triangles overlap in a quadrilateral, the plastic strain for the quadrilateral during this timestep is averaged from the four subelement triangles:

$$e^{p}_{avg} = \frac{1}{4} \sum_{i=1}^{4} e^{p}_{i} \qquad (1.4\text{-}73)$$

The accumulated strain is the sum of all values from previous timesteps:

$$e^{p}_{tot} = \sum_{n=1}^{\#\ timesteps} e^{p}_{avg} \qquad (1.4\text{-}74)$$

Prior to exiting the routine, the values of C, ϕ and ψ are updated, depending on the value of e^{p}_{tot}.

Thermal stress is added to the total stress state as an elastic increment prior to entering the constitutive law. This is the same as that given in Section 1.4.2.

1.4.5.8 Location

This routine is located in subroutine CL6, and called from subroutine STRESS. The thermal stress calculation is also located in CL6, and is called from subroutine TSTRES.

1.4.6.9 Numerical Stability and Accuracy

The numerical stability is governed by the overall critical timestep for a gridpoint (as described before) as well as the convergence of the iterations to locate the stress state on the yield criterion. The convergence characteristics of Newton's method are discussed by Gerald (1980). It can be mathematically shown that this method is quadratically convergent for monotonic functions, which is the case here. Typically, less than 5 iterations are necessary for convergence.

1.4.6.10 Alternatives

No alternative methods are available in the present FLAC code.

1.4.7 Null Model

1.4.7.1 Purpose

The purpose of the null model is to represent excavations or removed material.

1.4.7.2 Assumptions and Limitations

This model assumes that the components of the stress tensor, σ_{ij}, are identically 0.0 within excavated areas.

1.4.7.3 Notation

Not applicable.

1.4.7.4 Derivation

The stresses within nulled zones or regions are set to 0.0 within nulled zones:

$$\sigma_{ij} = 0.0 \qquad (1.4\text{-}75)$$

1.4.7.5 Application

This model is used to represent excavations within a rock or soil mass (e.g., a tunnel) or can be used to remove material at the ground surface (e.g., to form a slope). This model, similar to the other models, may be assigned to any zone or region at any time.

1.4.7.6 Numerical Method Type

Not applicable.

1.4.7.7 Derivation of Numerical Model

Not applicable.

1.4.7.8 Location

Reference to the null model is found in many routines, particularly in subroutine CYCLE, where the constitutive model is passed if the null model is encountered for a zone.

1.4.7.9 Numerical Stability and Accuracy

Not applicable.

1.4.7.10 Alternatives

No alternatives exist within FLAC for representing the excavation of elements.

1.4.8 Viscoelastic Models

1.4.8.1 Purpose

An important class of rocks such as salt, potash, etc. exhibit rate-dependent material behavior. FLAC provides three standard viscoelastic laws which may be used to model this behavior.

1.4.8.2 Assumptions and Limitations

The following assumptions and limitations apply to the viscoelastic models:

(1) deformation is isotropic; and

(2) although the models may be run in large-strain mode, no material rupture is possible.

The constitutive laws for rate-dependent materials are developed primarily from simple uniaxial compression experiments in the laboratory conducted using constant stress or strain rate tests. A great amount of controversy presently exists over how well these laws truly represent the actual deformation mechanisms. In general, the WIPP and Norton Power constitutive laws are simple curve fits to laboratory data based on fundamental deformation mechanisms. A mathematical formulation is developed which predicts this fit. The solution procedure is quasi-static, in that inertial terms are ignored in the solution procedure.

1.4.8.3 Notation

Table 1.4-5 gives the relevant material property notation for the viscoelastic models.

Table 1.4-5

NOTATION FOR VISCOELASTIC MODELS

Variable Notation			
Algebraic	Computer	Comment	Where Found
G	zx(kg)	shear modulus	z(x) is a material property array.
K	zx(kk)	bulk modulus	
η	zx(kvis)	dynamic viscosity, Kelvin	
$e_{11}^{(d)}$	de11d	deviatoric xx strain	CL7, CL8, CL9
$e_{22}^{(d)}$	de22d	deviatoric yy strain	
$e_{33}^{(d)}$	de33d	deviatoric zz strain	
$\sigma_{11}^{(d)}$	dS11d	deviatoric xx stress	
$\sigma_{22}^{(d)}$	dS22d	deviatoric yy stress	
$\sigma_{33}^{(d)}$	dS33d	deviatoric zz stress	

Table 1.4-5

NOTATION FOR VISCOELASTIC MODELS
(continued)

Variable Notation

Algebraic	Computer	Comment	Where Found
A	zx(kawip)	A parameter, WIPP Law	CL9
Q	zx(kqwip)	Q parameter, WIPP Law	
B	zx(kbwip)	B parameter, WIPP law	
$\dot{\varepsilon}^{*}_{ss}$	zx(kedwip)	critical steady-state creep rate, WIPP Law	
R	zx(krwip)	Universal Gas Constant, WIPP Law	
$\dot{\varepsilon}_{p}$	zx(kepwip)	primary creep strain, WIPP Law	
n	zx(knwip)	n parameter, WIPP Law	
D	zx(kdwip)	D parameter, WIPP Law	
n_1	zx(kn1)	n_1 exponent, Norton Law	CL8
n_2	zx(kn2)	n_2 exponent, Norton Law	
A_1	zx(kac1)	A_1 parameter, Norton Law	
A_2	zx(kac2)	A_2 parameter, Norton Law	

Table 1.4-5

NOTATION FOR VISCOELASTIC MODELS
(continued)

Variable Notation			
Algebraic	Computer	Comment	Where Found
σ_1^{ref}	zx(krs1)	σ_1 reference stress, Norton Law	CL9
σ_2^{ref}	zx(krs2)	σ_2 reference stress, Norton Law	

1.4.8.4 Derivation

Three creep models have been implemented in FLAC. These are:

(1) a classical visco-elastic model;

(2) an exponential-time creep model; and

(3) a two-component Norton power law.

The second model is commonly used in thermomechanical analyses associated with studies for the underground isolation of nuclear waste in salt, and the third can be used for mining applications. A description of these models and their implementation is provided in this section.

1.4.8.4.1 Classical Visco-Elasticity (Kelvin Substance)

The classical description of Newtonian viscosity is that the rate of strain is proportional to stress. Stress-strain relationships can be developed for viscous flow in exactly the same way as those developed for the theory of elasticity. The derivation of the equations in three dimensions can be found, for example, in Jaeger (1969).

Visco-elastic materials exhibit both viscous and elastic behavior. One such material is the Kelvin material, which can be represented in one dimension by a spring and dashpot in parallel, as shown in Fig. 1.4-16.

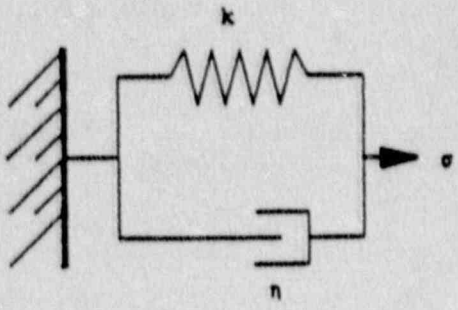

Fig. 1.4-16 One-Dimensional Kelvin Model

The stress-strain law for this material can be written as

$$\sigma_{ij} = \sigma_{ij}^{(e)} + \sigma_{ij}^{(v)} \tag{1.4-76}$$

where $\sigma_{ij}^{(e)} = 2\,G e_{ij}^{(d)} + K\delta_{ij}\, e_{kk}$,

$\sigma_{ij}^{(v)} = 2\eta\, \dot{e}_{ij}^{(d)}\, \delta_{ij}$,

G = shear modulus,

K = bulk modulus,

η = dynamic viscosity,

$e_{ij}^{(d)}$ = deviatoric strain = $e_{ij} - \frac{1}{3} e_{kk}\, \delta_{ij}$,

$\dot{e}_{ij}^{(d)}$ = deviatoric strain rate = $\dot{e}_{ij} - \frac{1}{3} \dot{e}_{kk}\, \delta_{ij}$,

e_{ij} = ij strain component,

$\sigma_{ij}^{(e)}$ = elastic part of stress, and

$\sigma_{ij}^{(v)}$ = viscous part of stress.

The material properties required for this model are the shear and bulk moduli (for the elastic behavior) and the viscosity.

1.4.8.4.2 Exponential-Time Creep Law for Nuclear Waste Isolation Studies

An empirical law has been developed (Senseny, 1985) to describe the time- and temperature-dependent creep of natural rock salt. In addition to the elastic component, the material is assumed to undergo creep, based on the equation

$$\frac{d\dot{\varepsilon}}{dt} = -\zeta\ (\dot{\varepsilon} - \dot{\varepsilon}_{ss})$$

—that is, the strain rate is the superposition of a steady-state strain rate and a time-decaying strain rate:

$$\dot{\varepsilon} = \dot{\varepsilon}_{ss} + e_a\ \zeta\ \exp(-\zeta t) \qquad (1.4\text{-}77)$$

where $\dot{\varepsilon}$ = creep rate,

$\dot{\varepsilon}_{ss}$ = steady-state creep rate,

ζ = a rate parameter,

e_a = an integration constant, and

t = time.

Based on experiments, Senseny observed two regimes. For steady-state creep rates above a critical value $\dot{\varepsilon}^{\star}_{ss}$, e_a is a constant $\dot{\varepsilon}_a$, and $\zeta = B\dot{\varepsilon}_{ss}$, where B is a constant.

For steady-state creep rates below $\dot{\varepsilon}^{\star}_{ss}$,

$$e_a = \left[\frac{\dot{\varepsilon}_{ss}}{\dot{\varepsilon}^{\star}_{ss}}\right] \varepsilon_a \qquad \text{and} \qquad \zeta = B\,\dot{\varepsilon}^{\star}_{ss} \tag{1.4-78}$$

Thus, Eq. (1.4-77) can be written as

$$\dot{\varepsilon} = \begin{cases} \dot{\varepsilon}_{ss} + \varepsilon_a B\dot{\varepsilon}_{ss} \exp(-B\dot{\varepsilon}_{ss}t) & \dot{\varepsilon}_{ss} \geq \dot{\varepsilon}^{\star}_{ss} \\ \dot{\varepsilon}_{ss} + \varepsilon_a B\dot{\varepsilon}_{ss} \exp(-B\dot{\varepsilon}^{\star}_{ss}t) & \dot{\varepsilon}_{ss} \leq \dot{\varepsilon}^{\star}_{ss} \end{cases}$$

Also, the steady-state strain rate is assumed to be given by

$$\dot{\varepsilon}_{ss} = A\sigma^n \exp(-Q/RT) \tag{1.4-79}$$

where σ = applied stress,

A, n, Q = parameters of the model,

R = universal gas constant, and

T = temperature (in Kelvin).

This formulation of the creep law is known as the RE/SPEC baseline exponential-time creep law for the high-level nuclear waste program.

Another formulation of this law, known as the WIPP reference exponential-time creep law, can be written as

$$\dot{\varepsilon} = \dot{\varepsilon}_s + \dot{\varepsilon}_p \qquad (1.4\text{-}80)$$

where

$$\dot{\varepsilon}_p = \begin{cases} (A - B\varepsilon_p)\ \dot{\varepsilon}_s & \dot{\varepsilon}_s \geq \dot{\varepsilon}^*_{ss} \\ (A - B\ (\dot{\varepsilon}^*_{ss}/\dot{\varepsilon}_s) - \dot{\varepsilon}_p)\ \dot{\varepsilon}_s & \dot{\varepsilon}^*_{ss} < \varepsilon \end{cases}$$

$$\dot{\varepsilon}_s = D(\bar{\sigma})^n \exp(-Q/RT)$$

where ε_p = primary creep strain,

ε_s = secondary creep strain,

$\dot{\varepsilon}$ = rate used to calculate the strain-rate components using

$$\dot{\varepsilon}_{ij} = (3/2)^{1/2} \left[\frac{\sigma^d_{ij}}{\bar{\sigma}} \right] \dot{\varepsilon} \qquad (1.4\text{-}81)$$

n, A, B, D, Q = parameters of the model,

R = universal gas constant,

$\bar{\sigma}$ = deviatoric stress, calculated as

$$(3/2)^{1/2} \left[\sigma^d_{ij}\ \sigma^d_{ij} \right]^{1/2} \qquad (1.4\text{-}82)$$

where σ^d_{ij} = ij-component of deviatoric stress; and

T = temperature (in Kelvin).

The WIPP and RE/SPEC formulations are different expressions of the same law, using slightly different notations. The WIPP formulation has been implemented in FLAC because it is better-suited for implementation in explicit computer codes since the effect of temperature and stress histories is automatically built into the formulation. The RE/SPEC formulation is only valid for constant stresses and temperatures, although it can be modified to account for stress and temperature histories. The relationship between the notations used in the two laws is given in Table 1.4-6.

Table 1.4-6

NOTATION FOR WIPP AND RE/SPEC FORMULATIONS

WIPP Notation	RE/SPEC Notation	Units	Typical Value
A	$B\sigma^{a}$	—	4.56
B	B	—	127
D	A	$Pa^{-n}\ s^{-1}$	5.79×10^{-36}
n	n	—	4.9
Q	Q	cal/mol	1200
R	R	cal/mol K	1.987
$\dot{\varepsilon}^{\star}_{ss}$	$\dot{\varepsilon}^{\star}_{ss}$	—	5.39×10^{-8}

1.4.8.4.3 The Two-Component Norton Power Law

The Norton power law (Norton, 1929) is commonly used to model the isothermal creep behavior of salt. The standard form of this law is:

$$\dot{\varepsilon}_{cr} = A\,\bar{\sigma}^{\,n} \qquad (1.4\text{-}83)$$

where $\bar{\sigma} = \dfrac{(3)^{1/2}}{2}\,(\sigma^d_{ij}\ \sigma^d_{ij})^{1/2}$,

σ^d_{ij} = deviatoric part of σ_{ij}, and

$$\dot{\varepsilon}_{ij} = \frac{(3)^{1/2}}{2}\ \dot{\varepsilon}_{cr}\ (\sigma^d_{ij}/\bar{\sigma})\ .$$

Usually, the amount of data available does not justify adding any more parameters to the creep law. There are cases, however, where it is justifiable to use a law based on multiple creep mechanisms. FLAC, therefore, includes an option to use a two-component law of the form

$$\dot{\varepsilon}_{cr} = \dot{\varepsilon}_1 + \dot{\varepsilon}_2 \qquad (1.4\text{-}84)$$

where

$$\dot{\varepsilon}_1 = \begin{cases} A_1\bar{\sigma}^{n_1} & \bar{\sigma} \geq \sigma_1^{ref} \\ 0 & \bar{\sigma} < \sigma_1^{ref} \end{cases}$$

$$\dot{\varepsilon}_2 = \begin{cases} A_2\bar{\sigma}^{n_2} & \bar{\sigma} \leq \sigma_2^{ref} \\ 0 & \bar{\sigma} > \sigma_2^{ref} \end{cases}$$

With these two terms, several options, described below, are possible.

1. The Default Option

$$\sigma_1^{ref} = \sigma_2^{ref} = 0$$

$\bar{\sigma}$ is always positive, so this is the one-component law with

$$\dot{\varepsilon}_{cr} = A_1 \bar{\sigma}^{n_1}$$

2. Both Components Active

$$\sigma_1^{ref} = 0$$

$$\sigma_2^{ref} = \text{"large"}$$

$$\dot{\varepsilon}_{cr} = A_1 \bar{\sigma}^{r_1} + A_2 \bar{\sigma}^{n_2}$$

3. Different Law for Different Stress Regimes

(a) $$\sigma_1^{ref} = \sigma_2^{ref} = \sigma^{ref} > 0$$

$$\dot{\varepsilon}_{cr} = \begin{cases} A_2 \bar{\sigma}^{n_2} & \bar{\sigma} < \sigma_{ref} \\ A_1 \bar{\sigma}^{n_1} & \bar{\sigma} > \sigma_{ref} \end{cases}$$

(b) $\sigma_1^{ref} < \sigma_2^{ref}$

$$\dot{\varepsilon}_{cr} = \begin{cases} A_2 \, \bar{\sigma}^{n_2} & \bar{\sigma} < \sigma_1^{ref} \\ A_1 \, \bar{\sigma}^{n_1} + A_2 \, \bar{\sigma}^{n_2} & \sigma_1^{ref} < \bar{\sigma} < \sigma_2^{ref} \\ A_1 \, \bar{\sigma}^{n_1} & \bar{\sigma} > \sigma_2^{ref} \end{cases}$$

(c) $\sigma_2^{ref} > \sigma_1^{ref}$

This option is not used because it implies that creep occurs for $\bar{\sigma} < \sigma_1^{ref}$ and for $\bar{\sigma} > \bar{\sigma}_2^{ref}$, but not for $\sigma_1^{ref} < \bar{\sigma} < \sigma_2^{ref}$.

1.4.8.5 Application

These models are applicable to materials which exhibit rate-dependent behavior within the assumptions and limitations given in Section 1.4.8.2. These models are applicable in analysis of mining or waste disposal operations in salt or other evaporite deposits. Because transient laws are not included, all analyses are steady-state in nature.

1.4.8.6 Numerical Method Type

No new or unique numerical methods are used.

1.4.8.7 Derivation of Numerical Method

The new stresses at the end of the timestep are calculated from the initial stresses and strain increments as follows.

First, the mean and deviatoric parts of the stress and strain are calculated from

$$\sigma_v^{curr} = \frac{1}{3}(\sigma_{11} + \sigma_{22} + \sigma_{33})$$

$$\sigma'^{curr}_{ij} = (\sigma^{curr}_{ij} - \delta_{ij} + \sigma^{curr}_{v}) \qquad (1.4\text{-}85)$$

$$\Delta\varepsilon^v = \frac{1}{3}(\Delta\varepsilon_{11} + \Delta\varepsilon_{22} + \Delta\varepsilon_{33})$$

$$\Delta\varepsilon'_{ij} = \Delta\varepsilon_{ij} - \delta_{ij}\,\Delta\varepsilon^v \qquad (1.4\text{-}86)$$

The deviatoric strain increments $\Delta\varepsilon'_{ij}$ is defined as the sum of elastic and creep strain. The elastic strain increments is

$$\Delta\varepsilon'^{(e)}_{ij} = \Delta\varepsilon'_{ij} - \Delta\varepsilon'^{(cr)}_{ij} \qquad (1.4\text{-}87)$$

The creep strain increment, $\Delta\varepsilon'^{(e)}_{ij}$, is a function of the current stress, but the stress is calculated from the elastic stain increment. Therefore, an iterative method is used to calculate the stresses as follows.

1. Assume $\overline{\sigma'_{ij}} = \sigma'^{curr}_{ij}$

   where $\overline{\sigma'_{ij}}$ = average stress during timestep.

2. Calculate $\dot{\varepsilon}_{ij}^{(cr)} = f(\overline{\sigma'}_{kl}\ \overline{\sigma'}_{kP})$.

3. Calculate $\Delta\varepsilon_{ij}^{(cr)} = \dot{\varepsilon}_{ij}^{(cr)}\ \Delta t$.

4. Calculate $\Delta\varepsilon_{ij}^{\prime(e)} = \Delta\varepsilon_{ij}^{\prime} - \Delta\varepsilon_{ij}^{(cr)}$.

5. Calculate $\sigma_{ij}^{\prime(new)} = \sigma_{ij}^{\prime} + 2G\ \Delta\varepsilon_{ij}^{(e)}$.

6. Calculate $\overline{\sigma'}_{ij} = \frac{1}{2}\ (\sigma_{ij}^{\prime(new)} + \sigma_{ij}^{\prime})$.

7. Repeat Steps 2 through 6 four (4) times to ensure convergence.

8. Calculate $\sigma_{ij} = \sigma_{ij}^{\prime(new)} + \delta_{ij}^{\prime}\ (\sigma^{v} + K\ \Delta\varepsilon^{v})$.

1.4.8.8 Location

The classical Kelvin viscoelastic model is found in subroutine CL7, the Norton Power Law in subroutine CL8, and the WIPP Baseline Law in CL9. These models are called from the STRESS subroutine. The thermoelastic stress increments for each law are determined in each subroutine, but called from TSTRES.

1.4.8.9 Numerical Stability

The stability of the solution is dependent on the choice of Δt. If Δt is too large, the creep rate calculation may be sufficiently inaccurate that the average deviatoric stress σ_{ij} is incorrect. The effect of a large timestep may be sufficient to cause numerical instability, as well as inaccuracy. FLAC presently requires the user to define the critical timestep, and allows a schedule where the timestep may be changed as a function of the maximum out-of-balance force. However, a timestep which

is too large will generally result in numerical instability which is obvious from the code results. It has been found that, in general, if the code provides stable response, the accuracy of the problem solution is good, provided the mesh discretization is sufficient.

1.4.8.10 Alternatives

No specific models presently exist within FLAC to replace the viscoelastic models.

1.5 EXPERIENCE

The FLAC code is a commercially-available program and, as such, is routinely applied to a wide variety of problems in soil, rock and solid body mechanics, as well as to heat transfer and fluid flow problems. At the time of writing, there are roughly 300 users of the FLAC code in the mining, civil construction, oil and nuclear industries, as well as in government-sponsored research in approximately 20 countries worldwide. This group of users includes those who are quite sophisticated in their ability as well as those who have little training in numerical modeling. The FLAC code can provide excellent results provided it is used properly. Although the code traps common errors, the user necessarily must define the problem and translate it into the problem geometry, boundary conditions, and solution procedure. Additionally, the user must analyze the results with his or her knowledge and experience. The ability to obtain meaningful solutions from any numerical model varies widely from user to user, and is based primarily on knowledge and experience.

In general, "poor" results from the FLAC code may be traced to the following causes:

(1) erroneous or unrealistic input data with which it can pre-analyze input for correctness;

(2) poor specification of the finite difference mesh, in particular, insufficiently detailed discretization around complex geometries and boundaries which are placed too close to the excavations;

(3) improperly specified boundary and initial conditions; and

(4) insufficient number of timesteps to bring the problem to equilibrium or a steady condition.

The primary point to keep in mind when using FLAC is that, due to the explicit solution procedure, it should be treated like a physical model. A run should be set up such that it mirrors the physical stages which occur in reality. For example, modeling of the excavation of a near surface tunnel subjected to internal water pressure might involve the following steps.

1. Set initial grid and boundary conditions, apply gravity, timestep problem until the body consolidates under gravity, inducing vertical and lateral stresses, judge equilibrium by sampling histories of displacements and stresses at critical locations in the grid. When the change in these parameters is less than about 1% of the total, the system is more-or-less at equilibrium. (Models the physical reality of development of initial gravity stresses in the body).

2. Excavate the tunnel by nulling proper zones or regions within the grid, timestep again until equilibrium or steady condition occurs. (Models the physical reality of excavating a tunnel and the resulting equilibrium.)

3. Apply fluid pressure to the interior of the excavation and timestep to equilibrium or until a steady condition occurs. (Models the physical reality of the diversion of water to the tunnel and application of fluid pressure to the excavation periphery.)

For each step of the analysis, a perturbation to the unbalanced forces occurs which damps with time as equilibrium is attained. The following suggestions and advice regarding the code have been developed from user experience.

- FLAC uses constant-strain zones. If the strain gradient is high, you need many zones to represent the non-uniform strain distribution. Try running the same problem with more zones, to check. Constant-strain zones are used because, for plastic flow, it is better to use many low-order elements than a few high-order elements.

- Try to keep zoning as uniform as possible. Avoid long, thin zones or very distorted zones. A maximum aspect ratio of about 10:1 should be used.

- For a new problem, always do a trial run with a few zones to get a quick feel for the response and possible difficulties. When you understand the trial results, increase the number of zones to obtain better accuracy.

- FLAC will take a longer time to converge if:

  (a) there are big contrasts in stiffnesses; or

  (b) there are big contrasts in zone sizes.

- A very stiff loading plate often can be replaced by a series of fixed gridpoints which are given constant velocity.

- In order to determine a collapse load, it often is better to do it under "strain-controlled" conditions rather than "stress-controlled" conditions (i.e., apply a constant velocity and measure the reaction forces rather than applying forces and measuring displacements). A system that collapses becomes difficult to control as the applied load approaches the collapse load. (This is true of a real system as well as a model system.)

- Use symmetry conditions, whenever possible, to save computer memory and run time. For example, if a system is symmetrical about a vertical axis, you can represent the symmetry line as a vertical boundary with the gridpoints fixed in the x-direction (but free in the y-direction).

- Make frequent use of save files. For example, save intermediate states when doing parameter studies. If the run stops for any reason, you will have the intermediate states.

- Treat a FLAC model just like a physical model. Try to reproduce in a FLAC run the stages that actually would occur in nature. Keep in mind that there is no unique equilibrium state for an inelastic system. There may be many possible states that satisfy equilibrium; the one you get depends on the history.

- FLAC shows how a system behaves. Make frequent, simple tests to check that you are doing what you think you are doing. For example, if a loading condition and geometry is symmetrical, check that the response is symmetrical or, after making a loading change or other change, execute a few steps initially (e.g., 5) to verify that the initial response is of the correct sign and in the correct location. You might also do back-of-the-envelope estimates of the expected order of magnitude of stress or displacements and compare them to FLAC output.

- If you apply a violent shock to a system, you will get a violent response. If you do non-physically reasonable things to the system, you must expect strange results.

- Critically examine the output before proceeding with the simulations. If, for example, everything is ok except for large velocities in one corner zone, do not go on until you understand the reason. In this case, you might have left a "fixed" grid point free.

- FLAC does not give a "Factor of Safety" directly. If you need a factor of safety, it can be defined for any parameter that you consider important by taking the ratio of the actual value to the value which causes failure. For example,

$$F_w = \frac{\text{water level to cause collapse}}{\text{actual water level}}$$

$$F_\phi = \frac{\tan\ (\text{actual friction angle})}{\tan\ (\text{friction angle to cause failure})}$$

$$F_L = \frac{\text{load to cause failure}}{\text{design load}}$$

Note that the larger value is always divided by the smaller value (assuming that the system does not fail under the actual conditions).

- Use history plots of displacement or stress at critical locations to determine when a model is in equilibrium.

1.6 REFERENCES

Blanford, Mark L., and Samuel W. Key. "An Example of Continuum versus Quasi-Discrete Modeling of a Jointed Rock Mass," in Constitutive Laws for Engineering Materials: Theory and Practice, pp. 1003-1010. C. S. Desai et al., Eds. New York: Elsevier Science Publishing, Inc., 1987.

Board, M. P., and M. J. Beus. "In-Situ Measurements and Preliminary Design Analysis for Deep Mine Shafts in Highly Stressed Rock," USBM Report of Investigations, RI-9231, 1989.

Brady, B.H.G., and E. T. Brown. Rock Mechanics for Underground Mining. London: George Allen and Unwin, 1985.

Chajes, A. Structural Analysis. Englewood Cliffs, New Jersey: Prentice Hall, 1983.

Cundall, P. A. "Explicit Finite Difference Methods in Geomechanics," in Numerical Methods in Engineering (Proceedings of the EF Conference on Numerical Methods in Geomechanics, Blacksburg, VA, 1976), Vol. 1, pp. 132-150.

Cundall, P. A. "UDEC - A Generalized Distinct Element Program for Modelling Jointed Rock," Peter Cundall Associates, Report PCAR-1-80; U.S. Army, European Research Office, Contract DAJA37-79-C-0548, March 1980.

Cundall, P. A. "Adaptive Density-Scaling for Time-Explicit Calculations," in Proceedings of the 4th International Conference on Numerical Methods in Geomechanics (Edmonton, 1982), pp. 23-26.

Cundall, P. A. "Distinct Element Models of Rock and Soil Structure," Chapter 4, in Analytical and Computational Methods in Engineering Rock Mechanics, pp. 129-163. E. T. Brown, Ed. London: George Allen and Unwin, 1987.

Cundall, P. A. "Formulation of a Three-Dimensional Distinct Element Model — Part I: A Scheme to Detect and Represent Contacts in a System Composed of Many Polyhedral Blocks," Int. J. Rock Mech., Min. Sci. & Geomech. Abstr., 25, 107-116 (1988).

Cundall, P. A., and J. H. Shillabeer. "Program LS3 - A Computer Model to Predict the Free-Standing Height of Backfill in Pillar Recovery Operation," Dames and Moore, London, Report to CANMET, Contract OSQ76-00113, 1977.

Desai, C. S., and J. T. Christian. Numerical Methods in Geomechanics. New York: McGraw-Hill, 1977.

Donovan, K., W. E. Pariseau, and M. Cepak. "Finite Element Approach to Cable Bolting in Steeply Dipping VCR Stopes," in Geomechanics Applications in Underground Hardrock Mining. New York: AIME, 1984.

Fossum, A. F. "Qualification of SPECTROM-32 to Sandia/WIPP Benchmark II Specifications," ReSpec Report, RSI-0249, 1984.

Gerald, A. F. Applied Numerical Analysis, 2nd Ed. Reading, Mass.: Addison-Wesley, 1980.

Hart, Roger Dale. "A Fully Coupled Thermal-Mechanical-Fluid Flow Model for Nonlinear Geologic Systems," Ph.D. Thesis, University of Minnesota, March 1981.

Hobbs, B. E., and A. Ord. "Validation of an Explicit Code for Shear Band Formation in Frictional-Dilatant Materials," Ingenieur-Archiv, 59 (1989).

Itasca Consulting Group, Inc. FLAC (Fast Lagrangian Analysis of Continua), Version 2.2 User Manual. Minneapolis: ICG, 1989.

Jaeger, J. C. Elasticity, Fracture and Flow with Engineering and Geological Applications, 3rd ed. London: Methuen & Co. Ltd., 1969.

Karlekar, B. V., and R. M. Desmond. Heat Transfer, 2nd Ed. St. Paul, Minnesota: West Publishing Company, 1982.

Lekhnitskii, S. G. Theory of Elasticity of an Anisotropic Body. Moscow: Mir Publishers, 1981.

Malvern, L. E. "Introduction," to the Mechanics of a Continuous Medium. Englewood Cliffs, New Jersey: Prentice Hall, 1969.

Marti, J., and P. A. Cundall. "Mixed Discretisation Procedure for Accurate Solution of Plasticity Problems," Int. J. Num. Methods in Eng., 6, 129-139 (1982).

Morgan, H. S. "MARC Calculations for the Second WIPP Structural Benchmark Problem," Sandia National Laboratories, SAND81-0925, May 1981.

Nagtegaal, J. C., D. M. Parks and J. R. Rice. "On Numerically Accurate Finite Element Solutions in the Fully Plastic Range," Comp. Mech. in Appl. Mech. & Eng., 4, 153-177 (1974).

Norton, F. H. Creep of Steel at High Temperatures. New York: McGraw-Hill Book Company, 1929.

Otter, J.R.H., A. C. Cassell and R. E. Hobbs. "Dynamic Relaxation," Proc. Inst. Civil Eng., 35, 633-665 (1966).

Senseny, Paul, E. "Determination of a Constitutive Law for Salt at Elevated Temperature and Pressure," American Society for Testing and Materials Reprint 869, 1985.

St. John, C. M., and D. E. Van Dillen. "Rockbolts: A New Numerical Representation and Its Application in Tunnel Design," in Rock Mechanics — Theory - Experiment - Practice (Proceedings of the 24th U.S. Symposium on Rock Mechanics (Texas A&M University, June 1983), pp. 13-26. New York: Association of Engineering Geologists, 1983.

Wardle, L. J. "Stress Analysis of Multilayered Anisotropic Elastic Systems Subject to Rectangular Loads," CSIRO Division of Geomechanics, Melbourne, Australia, Technical Paper No. 33, 1980.

Whyatt, Jeff, and Mark Board. "A Strain-Softening Model for Representing Shear Fracture in Continuous Rock Masses," 2nd International Symposium on Rockbursts and Seismicity in Mines (University of Minnesota, June 1988).

Wilkins, M. L. "Calculation of Elastic-Plastic Flow," University of California, Lawrence Radiation Laboratory, Report UCRL 7322, 1963.

NRC FORM 335 (2-89) NRCM 1102 3201, 3202

U.S. NUCLEAR REGULATORY COMMISSION

BIBLIOGRAPHIC DATA SHEET

(See instructions on the reverse)

1. REPORT NUMBER (Assigned by NRC, Add Vol., Supp., Rev., and Addendum Numbers, if any.)

NUREG/CR-5430
Vol. 1

2. TITLE AND SUBTITLE

FLAC (Fast Lagrangian Analysis of Continua)
Version 2.20

Software Summary

3. DATE REPORT PUBLISHED

MONTH	YEAR
October	1989

4. FIN OR GRANT NUMBER

FIN D1016

5. AUTHOR(S)

Mark Board

6. TYPE OF REPORT

Formal

7. PERIOD COVERED (Inclusive Dates)

8. PERFORMING ORGANIZATION – NAME AND ADDRESS (If NRC, provide Division, Office or Region, U.S. Nuclear Regulatory Commission, and mailing address; if contractor, provide name and mailing address.)

Itasca Consulting Group, Inc.
1313 5th Street, SE, Suite 210
Minneapolis, MN 55414

9. SPONSORING ORGANIZATION – NAME AND ADDRESS (If NRC, type "Same as above"; if contractor, provide NRC Division, Office or Region, U.S. Nuclear Regulatory Commission, and mailing address.)

Division of High-Level Waste Management
Office of Nuclear Material Safety and Safeguards
U.S. Nuclear Regulatory Commission
Washington, DC 20555

10. SUPPLEMENTARY NOTES

11. ABSTRACT (200 words or less)

FLAC, Version 2.20, is a two-dimensional, large-strain, explicit finite difference program for analysis of problems in geotechnical engineering. Principal features of the code include various mechanical constitutive models, heat transfer analysis, fluid flow analysis, structural element coupling and frictional and cohesive interfaces. The thermal and fluid flow analyses may be coupled to the mechanical portion of the code. The following report presents the documentation of FLAC in compliance with NUREG-0856, Documentation of Computer Codes for High Level Waste Management. The report is in three volumes: the first presents the mathematical formulation of the various portions of the code; the second, a user's manual; and the third, assessment of the code and support.

12. KEY WORDS/DESCRIPTORS (List words or phrases that will assist researchers in locating the report.)

FLAC, Version 2.20
large-strain
finite difference
computer program
geotechnical
mechanical
thermal
fluid flow
coupled
interfaces
structural elements
NUREG-0856
documentation
code assessment

13. AVAILABILITY STATEMENT

Unlimited

14. SECURITY CLASSIFICATION

(This Page)
Unclassified

(This Report)
Unclassified

15. NUMBER OF PAGES

16. PRICE

UNITED STATES
NUCLEAR REGULATORY COMMISSION
WASHINGTON, D.C. 20555

OFFICIAL BUSINESS
PENALTY FOR PRIVATE USE, $300

SPECIAL FOURTH-CLASS RATE
POSTAGE & FEES PAID
USNRC
PERMIT No. G-67